UNIVERZITA KARLOVA V PRAZE

Přírodovědecká fakulta

Ústav geochemie, mineralogie a nerostných zdrojů

Studijní program: Geologie
Studijní obor: Mineralogie a krystalografie

Bc. Róbert Pánik

Určení geologické provenience katodoluminiscenční spektroskopií apatitů a karbonátů

Determination of geological provenance by cathodoluminescence spectroscopy of apatites and carbonates

Diplomová práce

Vedoucí diplomové práce: RNDr. Dobroslav Matějka, CSc.

Konzultant diplomové práce: doc. RNDr. Jiří Zachariáš, Ph.D.

Praha, 2015

Prohlášení:

Prohlašuji, že jsem závěrečnou práci zpracoval samostatně a že jsem uvedl všechny použité informační zdroje a literaturu. Tato práce ani její podstatná část nebyla předložena k získání jiného nebo stejného akademického titulu.

V Praze, dne 28. 4. 2015

Podpis

Poděkování:

Děkuji svému školiteli, RNDr. Dobroslavu Matějkovi, Csc. za vedení této práce a doc. RNDr. Jiřímu Zachariášovi, Ph.D. za cenné konzultace a pomoc při analýze vzorků. Dále bych chtěl poděkovat Mgr. Anetě Kuchařové, Ph.D. za zapůjčení vzorků mramorů a Mgr. Václavu Procházkovi, Ph.D. za provedení analýz apatitů. Za spolupráci při tvorbě této práce děkuji také Kriminalistickému ústavu Praha. Práce byla financována z projektu Ministerstva vnitra ČR VG20102015065.

ABSTRAKT

Tato práce představuje novou metodu pro určování geologické provenience pomocí statistické analýzy katodoluminiscenčních spekter mramorů a karbonátových hornin z různých lokalit Českého masivu. Analýza je založena na kombinaci dat ze sedmi různých způsobů určování podobnosti spekter a poskytuje robustnější výsledky než přístup založený pouze na jedné metodě. Tyto výsledky je možné dále vylepšit pomocí metaanalýzy, která vyhodnocuje chování spekter v průběhu jednotlivých kroků analýzy.
Analýza byla provedena jak na původních katodoluminiscenčních spektrech, tak na reziduálních spektrech u kterých byla zvýšena relativní variabilita odstraněním Gaussovského trendu přítomného ve všech spektrech karbonátů. Kombinací výsledků analýz a metaanalýz originálních i reziduálních spekter bylo možné téměř jednoznačně určit provenienci vzorků ze všech studovaných lokalit.
Jako doplňková metoda pro klasifikaci spekter bylo použito aglomerativní hierarchické shlukování. Ze 72 různých způsobů výpočtu shlukování byl na základě počtu správně klasifikovaných spekter vybrán nejvhodnější způsob pro originální i reziduální data.
Druhá část této práce představuje analýzu katodoluminiscenčních spekter apatitů z různých hornin zahrnujících granit, gabro, durbachit, ryolit, pararulu, kvarcit a granulit. Další analyzované vzorky apatitů jsou zastoupeny biogenními apatity z fosilních kostí a zubů zvířat.
Byly definovány dva typy katodoluminiscenčních spekter - spektra s dominancí luminiscence Mn (charakteristická pro všechny vzorky granitu, pararuly a část vzorků gabra) a spektra s dominancí luminiscence lanthanidů (charakteristická pro všechny ostatní horniny a biogenní apatity).
Analýza vzorků s dominancí luminiscence Mn odhalila velkou variabilitu jejich reziduálních spekter s pozorovaným trendem této variability, který je připisován vlivu různé krystalografické orientace analyzovaných apatitů. Emisní čáry lanthanidů pozorované v druhé skupině spekter byly přiřazeny odpovídajícím aktivátorům a trendy variability těchto spekter byly diskutovány ve spojitosti s geologií a chemismem studovaných lokalit.

SUMMARY

This work presents new method for determination of geological provenance based on the statistical analysis of cathodoluminescence spectra of marbles and carbonate rocks from various localities in the Bohemian Massif. Analysis is based on the combination of data from seven different measures of spectral similarity and provides results that are more robust than those obtained by approach based only on a single measure of similarity. These results may be further improved by employing meta-analysis that evaluates behaviour of spectra during the individual steps of analysis.
Analysis was performed on the original cathodoluminescence spectra, as well as on the residual spectra in which relative variability was amplified by the subtraction of Gaussian trend present in all spectra of carbonates. By combining results from analysis and meta-analysis of both original and residual spectra it was possible to almost unambiguously determine provenance of samples from all studied localities.
Agglomerative hierarchical clustering was employed as a supplementary method for classification of spectra. Out of 72 different methods for clustering, one was selected for both original and residual data based on the number of correctly classified spectra.
Second part of this work presents analysis of cathodoluminescence spectra obtained from apatites in various rock types including granite, gabbro, durbachite, rhyolite, paragneiss, quartzite, and granulite. Additional analysed samples of apatites were represented by biogenic apatites from fossil bones and teeth of animals.
Two types of cathodoluminescence spectra were defined - those dominated by the luminescence of Mn (characteristic for all samples of granite, paragneiss, and some samples of gabbro) and those dominated by the luminescence of lanthanides (characteristic for all the other rock types, as well as biogenic apatites).
Analysis of Mn-dominated samples revealed high variability of their residual spectra with observed trend of this variability that is ascribed to effects induced by the variable crystallographic orientation of analysed apatites. Emission bands of lanthanides observed in the second group of spectra were assigned to corresponding activators and trends of variability in these spectra were discussed in relation to geology and chemism of studied localities.

Contents

Figures

Abbreviations

BSE - back-scattered electrons
CFSE - crystal field splitting energy
CL - cathodoluminescence
DB - database
EDS - energy-dispersive X-ray spectroscopy
EMPA - electron microprobe analysis
FWHM - full width at half maximum
IR - infrared
P-T - pressure-temperature
PC - principal component
PCA - principal component analysis
OM-CL - optical microscopy cathodoluminescence
SE - secondary electrons
SEM-CL - scanning electron microscopy cathodoluminescence
UV - ultraviolet
WDS - wavelength-dispersive X-ray spectroscopy

Appendices

Appendix A - Comparison of results from the first two principal components
Appendix B - Complete results of meta-analysis for locality Bohdaneč (227)
Appendix C - Hierarchical clustering of marbles

1. INTRODUCTION

1.1 Definition of cathodoluminescence

Cathodoluminescence is defined as an emission of photons induced in emitting material by incident electron radiation from an external source (cathode). Incident electron rays used for excitation have high energies usually in the range of 5-15 kV. Resulting photon emission is polychromatic, spanning from high-energy UV to the low-energy IR range of electro-magnetic spectrum, encompassing the whole range of visible light. Emission of visible light is indisputably the most widely utilized cathodoluminescence feature employed in various fields of scientific research. Since the first observations of cathodoluminescence in combination with petrographic optical microscope half a century ago (Sippel, 1965), optical microscopy-cathodoluminescence (OM-CL) and later scanning electron microscopy-cathodoluminescence (SEM-CL) have become simple and fast tools widely applied both by geoscientists and forensic scientists (various works employing cathodoluminescence analysis will be discussed in section 2.1). These two types of cathodoluminescence systems may each offer quite different information based on the luminescence emission of a sample. Advantage of OM-CL systems lies in the fact that the observation of cathodoluminescence can be readily alternated with observation in polarized light, thus enabling fast identification of accessory minerals that would be otherwise difficult to discern with optical microscopy alone, either due to the small size of accessory mineral grains or other limitations of optical system used. Optical microscope allows direct observation of emitted cathodoluminescence in the visible range and comparison of cathodoluminescence colours with colours observed in polarized light. Disadvantage of OM-based systems lies in lower overall intensities of cathodoluminescence emission due to the lower energy of used electron radiation. This may prove to be a great difficulty especially with geological samples which often show very weak luminescence. Hot-cathode SEM-based cathodo-luminescence systems overcome this problem by using higher-energy electron sources. Electron beam in SEM is focused and thus allows much better spatial resolution. Further, it is possible to readily compare observed cathodomicrofacies with SE/BSE imaging and with data from WDS, EDS or EMPA. Higher energies of incident electrons and focused beam however also imply greater risk of sample heating, damage and resulting interference from associated processes (further discussed in section 2.2). Even though processes of cathodoluminescence have been extensively studied during the past decades, we still lack complete understanding of all the processes taking part in the production of luminescence, their interactions and relative contributions. In the following part we will attempt to outline some general principles of luminescence emission in order to better understand and evaluate its limitations and potential to reveal deeper information about the genesis, history, and composition of studied samples.

1.2 Principles of cathodoluminescence

Principles of cathodoluminescence generation imply that this emission is produced only in insulators and semiconductors that are characterized by an energy gap between the valence shells of their atoms and so-

called conduction band. This energy gap is also commonly referred to as a forbidden zone. High-energy electrons from the incident ray colliding with the surface of a sample transfer part of their energy to the electrons in outer electron shells of atoms and these can thus overcome energy barrier between the valence and conduction band. This process of electron excitation creates an unstable state and electrons therefore tend to regain their pre-excitation ground states. They achieve this either by releasing energy surplus in the form of photons with wavelengths in UV, visible, and IR range of electro-magnetic spectrum or alternatively by emissionless transition where energy surplus is transferred from excited electron via non-radiative pathways (e.g. absorption or resonance). Pure minerals often show very weak luminescence. This is given by the fact that the energy difference separating electrons in conduction band and valence band is often so high that the probability of radiative de-excitation of electron from conduction to valence band is quite low. Thus, most of the surplus energy in pure minerals is released through non-radiative relaxation. In natural samples, however, pure mineral phases are rare. Apart from some biologically precipitated minerals, majority of naturally occurring mineral phases contain in their crystal structures various impurities. These can be either atoms of accessory elements, molecules, and/or organic compounds. Impurities on one hand promote physical defects of lattice that enhance luminescence of mineral and on the other hand provide an additional energy levels laying in the forbidden zone that increase probability of emissive electron de-excitation. Most important for enhancement of cathodoluminescence emission in natural mineral phases are ions of transition metals (e.g. Mn^{2+}, Cr^{3+}, Pb^{2+}) and trivalent lanthanide ions, providing energy levels in the forbidden zone resulting from their unfilled *d* and *f* orbitals, respectively. They further promote structural defects in the crystal lattice as it has to accommodate substituting ions of varying radii and/or valence state. Elements acting in a way described above are commonly referred to as *activators* of luminescence. Apart from activators, other ions entering the structure may also play role in the formation of observed mineral luminescence. Some ions contribute to the luminescence indirectly by transferring absorbed excitation energy to the activator ions, thus increasing overall luminescence intensity. These are referred to as luminescence *sensitizers* and comprise of two major groups:

- ions that sensitize transition metals - characterized by absorption bands in the UV region
- ions that sensitize trivalent lanthanides - ions of transition metals and other divalent or trivalent lanthanide ions (Götze & Kempe, 2009).

Apart from activating and sensitizing effects of impurities in crystal lattice, substituting ions can also act against the production of luminescence in a mineral. This is the case especially with ions having electron shell energy levels near the Fermi level (e.g. ions of Fe, Ni, Co), allowing effective transfer of absorbed excitation energy throughout the crystal lattice. Ions diminishing luminescence intensity in this way are referred to as luminescence *quenchers*. Quenching of luminescence can be further induced by high degree of lattice defects or even by activator ions self-quenching when present in sufficiently high concentrations. Additionally, long detection times and high voltage of used electron beam can cause heating of the sample, resulting in decrease of luminescence intensity due to thermal quenching (further

discussed below).

Combined effects of activators, sensitizers, and quenchers give rise to luminescence that often outshines *intrinsic* luminescence produced by electron-hole recombinations in pure mineral domains. This *extrinsic* luminescence shows quite different spectrum of emitted wavelengths (i.e. colour) from that of intrinsic luminescence and is usually dominant type of luminescence observed in natural samples.

While shapes of the cathodoluminescence spectra are to a great extent controlled by the presence of activators, sensitizers, and quenchers, overall intensity of luminescent emission is highly dependent on the current and voltage of used electron beam. Electrons colliding with the surface of a sample interact not only with the outer layer of atoms but penetrate further into the material. Penetration depth is usally in the order of first micrometers and apart from the energy of colliding electrons depends also on the density of analysed material and the critical energy of electron transition. In both cases, penetration depth decreases with increasing values of these variables (Reed, 2005). Equation for the intensity of observed luminescence is then given as:

$$I = N_a . E_{ab} . A_{ab} \quad (1)$$

N_a being number of ions that are in an excited state, E_{ab} being energy of electron transition between the levels a,b and A_{ab} being probability of emission (Götze & Kempe, 2009). As we discussed above, not all energy received from electron beam is emitted back in the form of luminescence or other types of radiation. Part of the energy is absorbed in the form of lattice resonance or transformed into heat. This implies that the energy of emitted radiation will be lower than that of incident electron beam. Thus, with increasing absorption in studied material, luminescent emission will tend to shift towards higher wavelengths of emitted photons. This process is known as *Stokes shift*. Heating of a sample causes changes in the relative proximities of energy levels in atoms until the point of their intersection. This lowers probability of emissive transition (term A_{ab} in Eq. 1) and results in lower intensity of observed luminescence. Long exposures to electron beam may also accelerate some physical processes in a sample such as defect migration, annealing, shift of ligands, and other modes of lattice equilibration. As in previous case, this results in the diminishing of luminescence with time. To overcome obstacles outlined above, analysis should be carried out with an appropriate type of detection system depending on the type of data we wish to obtain.

In this respect, existing detection systems can be divided into three groups - panchromatic, multiband, and hyperspectral systems (MacRae et al., 2013). Panchromatic systems, being the simplest of the three, perform no classification of detected photons and provide us only with total yields (counts). With multiband systems we are able to detect only a few specific emission lines at a time, meaning that detection times - and thus chance of sample damage - increases with each new set of wavelengths being analysed. Best choice for analysis of complete cathodoluminescence spectra are therefore hyperspectral systems using large CCD detectors allowing analysis of the whole electromagnetic spectrum from UV to IR range in a single step (Mason et al., 2005). This greatly reduces time of exposure to electron

bombardment and thus lowers the risk of sample damage.

In this work we present statistical approach to analysis of data from optical microscopy cathodoluminescence (OM-CL) equipment with hyperspectral detection system in order to evaluate potential of complete luminescence spectra to provide clues for fast identification and provenance determination of natural rock samples. For this analysis, two groups of minerals were chosen:

- carbonates, commonly encountered by geologists, forensic scientists and archaeologists as the main constituents of sedimentary rocks, building materials, statues, stone tools, and other artifacts
- apatites, apart from being major constituent of bones and teeth, they are also present as an accessory in majority of igneous and many metamorphic as well as sedimentary rocks. Thus, they have potential of being universal tool for provenance determination of geological and forensic samples.

Cathodoluminescence characteristics of these two major groups will be discussed more closely in the following section.

1.3 Cathodoluminescence of carbonates and apatites

1.3.1 Cathodoluminescence of carbonate minerals

Trigonal and orthorombic polymorphs of $CaCO_3$, calcite and aragonite, along with trigonal double carbonate dolomite, $CaMg(CO_3)_2$ are the most commonly occurring carbonate minerals in nature. Calcite and dolomite are the main constituents of limestones, dolostones, and marbles, while aragonite - metastable at ambient conditions - is typically precipitated through biological action as shells of molluscs and corals or additionally forms along with calcite in cave environments as a constituent of speleothems.

Structure of calcite is based on alternating layers of calcium cations and negatively charged carbonate groups, analogous to some cubic structures such as that of halite. Great difference in the size of Ca^{2+} and $(CO_3)^{2-}$ however distorts this symmetry into a rhombohedron. Each atom of Ca is coordinated by six oxygen atoms forming an irregular octahedron. Each oxygen in this structure binds to two Ca cations.

Structure of dolomite is analogous to that of calcite with the exception that every other cation layer is made up of Mg. In ideal dolomite structure Ca and Mg do not mix within the layer as the difference in their ionic radii makes this arrangement thermodynamically unstable. Difference in thickness of these layers lowers the trigonal symmetry of calcite ($\bar{3}$ 2/m) to trigonal rhombohedral symmetry ($\bar{3}$) of dolomite.

Crystal structure of aragonite is also similar to that of calcite - each Ca is coordinated by six O forming irregular octahedron and each O binding to two atoms of Ca. Difference is in the arrangement of carbonate ions that lie in two distinct layers pointing in opposite direction. Resulting structure is more compact than that of calcite and its symmetry is orthorombic (2/m 2/m 2/m).

As discussed above, these carbonate minerals show both intrinsic and extrinsic luminescence. Intrinsic cathodoluminescence is usually very faint, produced by low-probability electron-hole recombinations in natural structural defects. Energy of this emission is given by energy difference of conduction band

and valence band, i.e. depends on width of forbidden zone (Palenik & Buscaglia, 2007).

Two emission bands of intrinsic carbonate cathodoluminescence are shared by all three minerals and lie at approximately 440 and 520 *nm*, with their intensity ratios differing in each mineral (Götte & Richter, 2009). Band at 440 *nm* is dominant in aragonite and thus this mineral exhibits faint greenish luminescence with lower contribution of 520 *nm* band characterized by blue colour. In calcite and dolomite second band is dominant and this gives rise to their typical blue intrinsic luminescence. This kind of luminescence is quite rare in natural rock samples and can be usually observed only in specimens of biogenic carbonates with low degree of post-genetic alteration (Habermann et al., 1998). Carbonates precipitated without biological control and biogenic carbonates modified by later processes show dominance of extrinsic luminescence due to the presence of impurities in crystal lattice that serve as activators of this extrinsic luminescence. Most important of these activators in carbonate minerals is Mn^{2+} that substitutes for Ca^{2+} in calcite and aragonite structures and for Ca^{2+} or Mg^{2+} in dolomite structure. To better understand how cathodoluminescence of these minerals is produced, we will need to investigate principles of crystal field theory underlying processes of luminescence generation in their extrinsic luminescence centres.

Activation of luminescence by Mn^{2+} is induced due to its *d* electron orbitals being only partially occupied by electrons. Each of the five *d* orbitals can hold two electrons with opposite spin, i.e. ten electrons in total. These orbitals can be divided into two groups depending on their wave function symmetry (Putnis, 1992):

- t_{2g} containing d_{xy}, d_{yz}, and d_{xz} orbitals,
- e_g containing d_z^2 and $d_{x^2-y^2}$ orbitals (Fig. 1a).

Electronic configuration of Mn^{2+} is $(t_{2g})^3(e_g)^2$ with one electron in each orbital, obeying second Hund's rule to ensure minimal electron repulsion. Mn^{2+} entering the structures of aragonite, calcite, or dolomite is coordinated by six oxygen atoms in the crystal lattice and this induces changes in the energies of *d* orbitals depending on their orientation relative to coordinating anions. Distribution probabilities of orbitals d_z^2 and $d_{x^2-y^2}$ (e_g) point in the direction of axes x, y, and z, i.e. directions in which lie coordinating anions. Electrons in these two orbitals are being repelled by electrons in the shells of oxygen atoms and thus their energy is increased. Consequently, energy of other three *d* orbitals (t_{2g}) is lowered in order to maintain the average energy of all *d* orbitals (Fig. 1b). This process is referred to as splitting of the crystal field and its magnitude varies depending on the configuration of ion and the way it is bound in crystal lattice. For Mn^{2+} there is no reduction of energy during this process, i.e. it has zero crystal field splitting energy - CFSE (Burns, 1993).

When incident electron transfers its energy to the Mn^{2+} ion, it is excited from a ground state $^6A_{1g}(^6S)$ to excited state $^4T_{1g}(^4G)$ and subsequently returns to its ground state by transition $^4T_{1g}(^4G) \rightarrow {}^6A_{1g}(^6S)$ resulting in radiation of excess energy in the form of luminescence (Cazenave et al., 2003). Even though this type of transition is shared by aragonite, calcite, and dolomite, resulting cathodoluminescence spectra

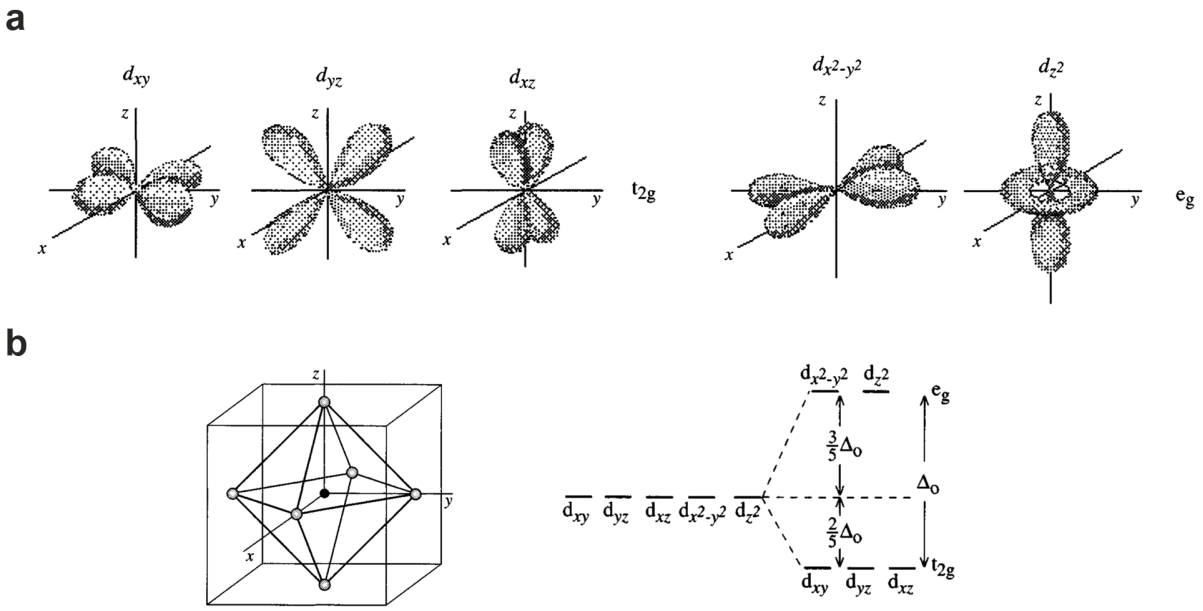

Fig. 1. a - shapes and orientations of the five *d* electron orbitals and their classification; b - geometry of octahedral coordination and its orientation relative to axes *x, y,* and *z* (left) and resulting splitting of the crystal field where Δ_0 denotes energy difference between orbitals e_g and t_{2g} (right). Modified after Putnis (1992).

show variable emission bands due to the difference in the crystal fields of these minerals (Fig. 2a). Magnitude of energy splitting between orbitals increases with decreasing interatomic distances in octahedral site (Waychunas, 2014). Resulting energy of emission band thus depends on the surrounding crystal field, with lowering of luminescence energy as a function of increasing degree of splitting. In aragonite, octahedral site is largest of the three minerals and luminescence emission band has its maximum at 575 - 580 *nm* corresponding to the green colour of observed luminescence (Richter et al., 2003; Götte & Richter, 2009). Emission band of calcite lies in the lower energy region with amplitude at around 570 - 620 *nm,* producing yellow-orange luminescence (Palenik & Buscaglia, 2007; Götze, 2012). This emission band is observed also in dolomite as half of its octahedral sites are similar in size to those of calcite. Other half of these sites, occupied in pure dolomite by smaller Mg^{2+} ions, produce still lower-energy luminescence upon the activation by manganese ions. Thus, cathodoluminescence spectra of dolomites show second emission band corresponding to red colour with wavelengths in the range of 630 - 670 *nm* (Gillhaus et al., 2001; Palenik & Buscaglia, 2007). It is apparent from Fig. 2a that the character of this extrinsic luminescence is far from the quasi-monochromatic emission that would be expected when only one type of transition occurs in the crystal. Emission bands in these minerals are broad pseudo-Gaussian curves - or convolution of two such curves in case of dolomite - with values of FWHM ranging between 80 to 90 *nm* (Götte & Richter, 2009). This is a result of various factors that influence characteristics of observed spectrum - its intensity, width (given by FWHM), and the position of its maximum. *3d* orbitals of Mn^{2+} activator ions form the outermost shell that is not shielded by any other orbitals against the influence of local crystal field (Götze, 2012). Part of the excitation energy is

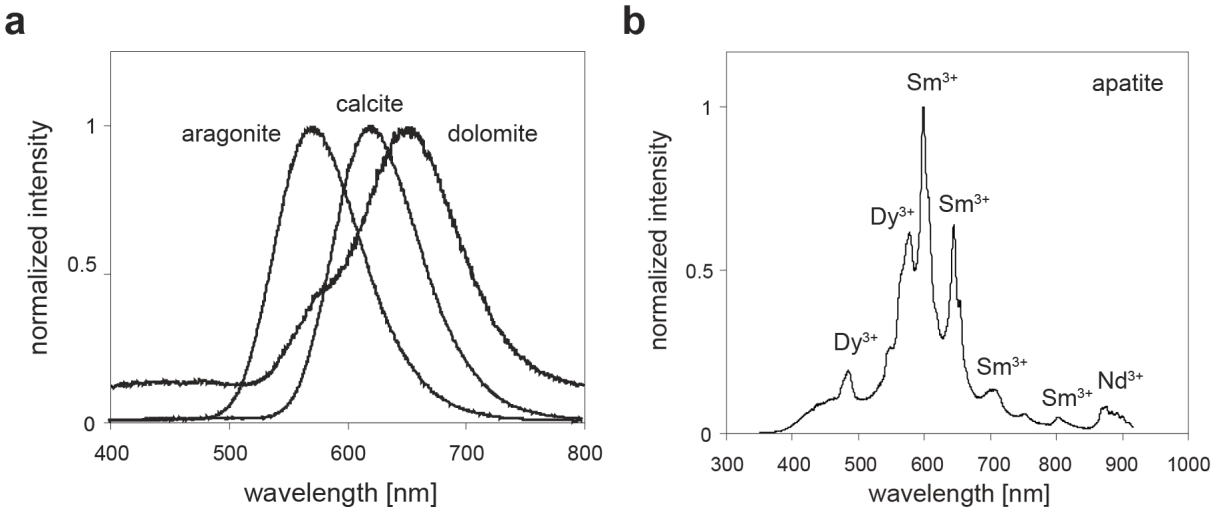

Fig. 2. a - typical cathodoluminescence spectra of carbonate minerals aragonite, calcite, and dolomite. Position of emission maximum is influenced by the mineral structure and emission bands broaden due to effects of the local crystal field; b - typical cathodoluminescence spectrum of apatite where *f* orbitals of lanthanide activators Dy^{3+}, Sm^{3+}, and Nd^{3+} are shielded against the influence of local crystal field, producing sharp emission bands. Modified after Götze (2012).

thus lost in the form of crystal lattice vibrations (phonons) and consequently, luminescence energy shifts towards lower values. Magnitude of this shift - referred to as Stokes shift - will vary depending on the type and strength of crystal field in a given mineral structure (Götze & Kempe, 2009). This means that the shapes of cathodoluminescence spectra are also affected by the physical effects in mineral such as stress or strain (MacRae et al., 2013). However, knowledge of chemical effects induced by the presence of luminescence quenchers in crystal lattice are also necessary for understanding characteristics of observed cathodoluminescence emission. Fe^{2+} is the most important quencher of Mn-activated luminescence in carbonates. Observations show that the intensity of luminescence in carbonates diminishes with increasing amounts of Fe^{2+} in the structure, with lower limit for this effect being at Fe concentration of about 2000 ppm (Gillhaus et al., 2001; Götte & Richter, 2009).

Quenching can however occur also when the concentration of activator Mn^{2+} reaches certain critical level. At low concentrations, there is a linear correlation between amount of Mn and luminescence intensity. Self-quenching induced by the interaction of luminescence centres then becomes apparent when concentration of Mn exceeds approximately 1000-1500 ppm, causing decrease in the intensity of luminescence (Habermann et al., 2000; Götte & Richter, 2009). Some workers report much higher concentration limits for self-quenching of Mn between 3500 and 50000 ppm (Cazenave et al., 2003). Another effect of increasing concentrations of Mn is broadening of resulting emission band and shift of its maximum towards slightly higher energies (Habermann, 2002).

Apart from these main factors there are still other processes taking place in the mineral that may influence its final luminescence. These include adsorption of activator and quencher ions on residual

organic matter, presence of other activators such as trivalent lanthanides, partitioning of Mn and Fe depending on the redox conditions during the process of diagenesis, and many others (Boggs & Krinsley, 2006; Götte & Richter, 2009).

1.3.2 Cathodoluminescence of apatites

Apatite, $Ca_5(PO_4)_3(F, Cl, OH)$ is hexagonal phosphate mineral of variable composition. It is the most common phosphate and accessory mineral found in the majority of igneous, metamorphic and sedimentary rocks. Additionally, apatites represent main constituents of bones and teeth in most animals, including humans.

Structure of apatite is very complex as it allows myriad of substitutions, vacancies, charge compensations, and their numerous combinations. Therefore, structural characteristics will be discussed only very briefly with details sufficient for our present study.

Tetrahedrally coordinated phosphorus in complex phosphate anions PO_4^{3-} may be substituted by others such as SO_4^{2-} or AsO_4^{3-}, while Ca^{2+} is generally replaced by wide range of cations with differing valence state (e.g. Mn, Fe, Pb, Y, or trivalent lanthanides; Hughes and Rakovan, 2002). Atoms of Ca in the apatite structure fall into two groups depending on their crystallographic position in the holes created by hexagonally packed structures of complex anions:

- Ca1 is bonded by six O atoms forming trigonal prism. Through the faces of this prism are bonded another three O atoms, thus forming $Ca1O_9$ coordination polyhedron corresponding to tricapped trigonal prism.
- Ca2 is also coordinated by six atoms of O and further by one of the column anions (F, Cl, or OH), creating coordination polyhedron $Ca2O_6X$. Geometry of this polyhedron shows highest degree of variation as it accommodates to column anions of quite different properties (Elliott et al., 2002). Space group of resulting apatite structure is $P6_3/m$.

As in carbonates, intrinsic luminescence of apatites due to natural defects in crystal lattice is usually very faint with various unresolved emission bands in the range of approximately 340-430 *nm,* producing visible blue emission (Barbarand & Pagel, 2001; Götze et al., 2001). This is usually obscured by more intense extrinsic luminescence induced by various activators. Most important activator ions substituting for Ca^{2+} in the apatite structure are trivalent lanthanides, Eu^{2+}, and Mn^{2+}. Higher charge of substituting lanthanides must be compensated by other substitutions in order to maintain charge balance of mineral. These include substitutions such as $lanthanide^{3+} + Na^{+} \leftrightarrow Ca^{2+} + Ca^{2+}$, or $lanthanide^{3+} + Si^{4+} \leftrightarrow Ca^{2+} + P^{5+}$ (Roeder et al., 1987).

Mn-activated extrinsic luminescence in apatites follows the same principles as in carbonates, resulting in broad pseudo-Gaussian emission bands corresponding to yellow colour. However, as the crystallographic positions and effects of local crystal field are different to those in carbonates, this emission shows specific variations in width, intensity, and degree of Stokes shift with band maxima lying between 560-580 *nm*. Luminescence activated by lanthanides is characterized by quite dissimilar types

of emission due to different set of principles underlying its generation in these ions. Emissive transitions during electron bombardment of lanthanide activator occur in its *4f* orbitals. In contrast to outer *3d* orbitals in Mn^{2+} easily influenced by local crystal field, electrons of *f* orbitals are not involved in bonding to coordinating anions and are protected against the effects of crystal field by electrons in *s* and *p* orbitals (Götze & Kempe, 2009). This means that the energy levels of *f* orbitals don't split as in the *d* orbitals of Mn^{2+}. Observed emission lines of individual lanthanides (Fig. 2b) are relatively sharp - quasi-Lorentzian curves - and their position, i.e. energy, is mostly independent of the structure incorporating given ion (Götze, 2012; MacRae et al., 2013). Assignment of particular emission band to specific transition is not as straightforward as in the case of Mn^{2+} owing to the fact that there is myriad of possible emissive transitions that can occur in electron shells of lanthanides (Götze et al., 2001). For purposes of this study it is sufficient to point out that each lanthanide shows several characteristic emission bands in its luminescence spectra. Table 1 lists positions of these lines and associated visible colours for most important lanthanide activators - Ce^{3+}, Pr^{3+}, Sm^{3+}, Eu^{2+}, Eu^{3+}, Tb^{3+}, Dy^{3+} - as reported by various workers since 1969 to 2005. It is apparent that wavelengths reported in different papers are not always in accordance with each other. This can be partly attributed to different means of excitation and detection used by different workers. Complications arising when comparing cathodoluminescence data obtained by different equipment and consequent need for normalization will be further discussed in section 2.2. As in carbonates, quenching of luminescence in apatites can be induced by the presence of Fe^{2+} substituting for Ca^{2+} and additionally by As^{5+} replacing P^{5+} in complex phosphate anions (Perseil et al., 2000). Self-quenching can also take place for both Mn^{2+} and lanthanides. This effect is most apparent for Ce^{3+} that is believed to promote formation of lattice defects when present in higher concentrations (Dempster et al., 2003).

Interesting feature of apatite luminescence in natural rocks is that the type of activator - Mn vs. lanthanides - depends on the genetic type of rock in which these apatites occur. In granites, pegmatites, and related felsic rocks, Mn^{2+} is the dominant activator inducing characteristic yellow or yellow-green luminescence, while apatites from alkaline rocks show activation by lanthanides with luminescence colour ranging from blue to violet (Kempe & Götze, 2002). In both of these rock types, apatites show relative enrichment of light lanthanides over the heavy lanthanides (Mitchell et al., 1997; Dempster et al., 2003).

Tab. 1. Emission bands [*nm*] and associated luminescence colours of most important lanthanide activators and Mn in apatite as reported by different workers.

	Portnov & Gorobets (1969)	**Mariano & King (1975)**	**Roeder et al. (1987)**	**Marshall (1988)**	**Gaft et al. (1998)**	**Barbarand & Pagel (2001)**	**Kempe & Götze (2002)**	**Gaft et al. (2005)**	**observed colour**
Ce^{3+}	365	-	-	-	365	350, 380, 458	365	360, 430	light blue
Pr^{3+}	-	-	-	-	600, 650	-	-	485, 607	red
Sm^{3+}	560, 600, 648	-	595, 645	560, 600, 645, 710	565, 599, 607, 645, 654	566, 599, 649	420, 600, 640, 690, 800	598, 604, 645, 652, 654, 734	orange-red
Eu^{2+}	450	410, 450, 460	-	450	430 - 450	451	410 - 445	450	light blue
Eu^{3+}	-	590, 617, 695, 700	585, 615, 645, 690	590, 615, 695	579, 590, 618, 653, 700	-	-	574, 589, 601, 617, 623, 630, 651, 695, 696	
Tb^{3+}	-	-	540	545	380	381, 416, 438, 490, 546	-	380, 414, 436, 487, 545	-
Dy^{3+}	480, 580	-	480, 568	480, 575	480, 575, 663, 750	482, 577, 667	470, 570	481, 485, 570, 575, 578, 579	yellow
Mn^{2+}	576	565, 595	560	562, 565, 570	575	577	565	569, 583	green-yellow

2. APPLICATION OF CATHODOLUMINESCENCE FOR PROVENANCE STUDIES

2.1 Cathodoluminescence as provenance indicator

Cathodoluminescence analysis is often employed as a supplementary method in provenance studies of geomaterials due to its ability to reveal presence of elements - activators or quenchers - and textural features - such as zoning or defects - that are commonly beyond detection capabilities of other analytical methods. While spectroscopy as discussed above is common tool for analysis of cathodoluminescence data, use of luminescence as a provenance indicator was traditionally done through visual inspection of cathodomicrofacies and identification of their features characteristic for particular locality.

Julig et al. (1998) used observations from cathodoluminescence microscopy as a supplementary method for archaeological provenance study of lithic tools. They report that many of visually indistinguishable sandstone and quartzite artifacts may be easily classified based on cathodoluminescence properties of either quartz grains or SiO_2-rich cements and rims present between these grains. Use of cathodoluminescence is of particular interest for archaeologists as it represents non-destructive method that may be readily performed on unaltered artifact without any observable damage.

Akridge & Benoit (2001) investigated further potential of cathodoluminescence obtained from SiO_2-rich materials as an archaeological provenance tool and found that chert samples may be in most cases clearly sorted based on the textures and overall abundance of luminescing components they contain.

Lapuente et al. (2000) studied marbles from classical Mediterranean quarries and possibilities for their fingerprinting with combined data from stable isotope analysis, cathodoluminescence, and petrography. They conclude that characterization of cathodomicrofacies is a useful supplementary method when data from other analyses overlap and further that when distinction between particular cathodomicrofacies is not possible, quantitative cathodoluminescence data may reveal differing provenance. For this quantitative analysis, intensities of emission bands at 360 *nm* and 620-650 *nm* were used.

In a series of works, Šťastná & Přikryl (2009; 2010) and Šťastná et al. (2009; 2011) studied provenance indicators for marbles from Bohemian Massif by combination of analytical methods such as X-ray diffraction analysis, petrographic image analysis, optical microscopy and cathodoluminescence. They report effectivity of cathodoluminescence observations for identification of accessory minerals in these marbles and further suggest that in cases when observation of cathodomicrofacies are insufficient for unambiguous provenance identification, application of quantitative luminescence analysis may help discriminate between samples from different quarries.

Bernet & Bassett (2005) combined optical microscopy with SEM-CL analysis of cathodomicrofacies for individual grains of quartz in samples of sand and sandstone. This technique allowed them to distinguish between textures of plutonic, volcanic, and metamorphic quartz. Quartz is by far the most widely studied luminescent provenance indicator as textures and colour of its emission closely depend on its origin. Thus, number of workers (Walderhaug & Rykkje, 2000; Boggs & Krinsley, 2006; Augustsson & Reker, 2012) define following connections between genetic type of quartz, its cathodoluminescence, and

observed textural features:

- *plutonic quartz* - blue to violet cathodoluminescence of low intensity in heterogeneous patches and fillings of healed cracks.
- *volcanic quartz* - usually red cathodoluminescence - but occasionally also blue - with well-developed oscillatory zoning.
- *metamorphic quartz* - cathodoluminescence colour similar as in plutonic quartz with brownish tones indicating regional metamorphism. Distribution of luminescence is heterogeneous, often forming mottles.
- *hydrothermal quartz* - green-blue cathodoluminescence that rapidly fades with time. Commonly observed zoning typical for hydrothermal formations and healed cracks.
- *authigenic quartz* - usually without visible cathodoluminescence emission.

More recently, Hunt (2013) investigated whether this genetic signature of quartz prevails in ceramic materials that were subjected to high temperature. Experiments demonstrated that genetic information of cathodomicrofacies was preserved up to the temperature of 1100°C, thus confirming potential of catohodoluminescence-based provenance studies of quartz in archaeological ceramic artifacts.

In another recent study, Bajnóczi et al. (2013) used cathodoluminescence analysis to distinguish between archaeological artifacts made of recent and fossil aragonite shells. Even though these artifacts were indistinguishable by traditional methods such as stable isotope analysis, cathodoluminescence microscopy revealed small amounts of diagenetic calcite in fossilised aragonitic shells.

In studies such as those presented above, characterization of cathodoluminescence and cathodo-microfacies is based on purely subjective consideration of observed phenomena. As this may lead to inconsistencies and disagreement between subjectively perceived cathodoluminescence properties by individual workers, it is desirable to employ quantitative tools for analysis of luminescence in order to obtain data that can be objectively compared with others. Some of the works that apply quantitative cathodoluminescence analysis for study of provenance are briefly presented below.

Picouet et al. (1999) studied samples of Neolithic ceramic artifacts and showed that their provenance can be deciphered from SEM-induced cathodoluminescence spectra of quartz grains. This was done by comparison of relative intensities of two emission bands of quartz in red and blue regions of visible spectra.

Boggs et al. (2002) obtained SEM-CL images of quartz with various optical filters in order to estimate contribution of red, green, and blue component to overall intensity of luminescence in various genetic types. Further, by subtraction of these partial intensities from overall cathodoluminescence spectra it was possible to quantify contribution of UV emission, which was found to be important particularly in plutonic quartz samples.

Another provenance study of detrital quartz by Augustsson & Bahlburg (2003) employed analysis of peak and trough positions in cathodoluminescence spectra, as well as relative ratios of red and blue emission bands as a criteria for sample classification.

Commonly observed phenomenon during irradiation of quartz is shift of luminescence colour with time.

Several authors hypothesized that type of this shift - i.e. relationship of initial and final luminescence colour - may also serve as a tool for identification of genetic types in quartz. Götte & Richter (2006) explored this phenomenon with the use of cathodoluminescence spectroscopy and concluded that the nature of colour shift is controlled by the type of defect structure in quartz grains and thus may potentially reveal information about conditions and processes that prevailed during their crystallization and subsequent alteration.

Potential use of cathodoluminescence spectroscopy in forensic science was demonstrated by Bell et al. (2009) who analyzed samples of glass and converted data contained in cathodoluminescence spectra into three variables representing coordinates of CIE Lab colour space, i.e. *L* - lightness of the colour, *a* - coordinate of position between red and green colour, and *b* - coordinate of position between yellow and blue. These were then plotted in 3D scatter plot and apparent clustering of related glass samples was observed.

Provenance study by Ebert et al. (2010) examined luminescence properties of marbles from Naxos island in Aegean sea. Average intensities of cathodoluminescence emission defined for each locality were shown to form trend along the sampled profile running through the island. When luminosity data were combined with grain size characteristics from quantitative microstructural analysis, distinct data clusters for each locality were obtained.

Different approach to cathodoluminescence study was demonstrated by Lisitsyn et al. (2012) who used pulsed cathodoluminescence equipment for study of various genetic types of calcite. After a short pulse of excitation beam, two components were observed in emitted luminescence - fast, with broad band in near-UV/visible range and slow, with emission band at approximately 610-620 *nm*. Properties of fast component were found to be more representative of genetic type of calcite than those of slow component. However, slow components showed variable times of decay after excitation and thus, their evolution with time combined with characterization of fast component provided additional data for sample identification.

Most recent study by Lapuente et al. (2014) analysed colour, intensity, and spatial distribution of cathodoluminescence in 51 white marble sculptures and based on these data were able to divide analysed marbles into five different groups. Consequently, by combination of cathodoluminescence data with optical microscopy, stable isotope analysis, and X-ray diffraction analysis they were able to characterize various types of marble used in these statues.

Apart from quantitative studies utilizing characteristics of cathodoluminescence spectra as presented above, several workers attempted to use these spectra for quantitative and semi-quantitative analysis of activator contents in luminescent minerals. This may be of particular interest especially because detectable luminescence emission is often induced by activator in concentrations lower than detection limits of other methods such as EDS or WDS.

Gillhaus et al. (2001) measured areas of emission bands of Mn^{2+} in diagenetic and hydrothermal dolomites and found linear correlation of this area with Mn content when concentrations of quenching

Fe were under 2000 ppm. Extrapolation of this linear trend allowed them to spectroscopically detect Mn concentrations of approximately 1 ppm.

Similar linear trend for Mn in calcite and feldspar was observed by Habermann (2002) at Mn concentrations below approximately 1000 ppm. Additionally, comparable linear trend was found for Sm^{3+} and Eu^{3+} activators at concentrations below 500 ppm.

Finally, Götte & Richter (2009) report analogous positive linear relation for Mn in aragonite when concentrations for both Mn and Fe do not exceed 2000 ppm.

Now that we reviewed possibilities of qualitative and quantitative cathodoluminescence microscopy and spectroscopy, it is important to consider difficulties and limitations associated with these methods. This topic will be briefly treated in the next section.

2.2 Limitations of cathodoluminescence spectroscopy

When analysing cathodoluminescence data obtained either from optical (OM-CL) or scanning electron microscope (SEM-CL) systems it is important to understand possibilities and limitations of these systems and the data they provide. As we discussed in section 1.1, both types of data acquisition have their specific features and consequently specific limitations arising from their architecture. Some of the key issues of cathodoluminescence spectroscopy originating from excitation source, detector, or the sample itself are discussed below.

Type of used electron beam and its characteristics are first variable that greatly influences final cathodoluminescence emission. Both SEM-CL and OM-CL electron beams use similar range of accelerating voltage usually between 5-15 kV. In each system, however, this beam interacts with analysed sample in quite a different way. OM-CL systems use defocused beam whose energy is spread across relatively large area of irradiated surface. In contrast, electron beam in SEM is focused in order to minimize its radius at the point of interaction with the sample. This means that the spatial resolution of SEM systems can be several orders higher than that of optical microscopes and that with SEM we have greater control over the beam energy actually reaching analysed point. Beam electrons that collide with the surface have energies sufficient for further penetration into the interior of sample, thus creating interaction volume that extends several μm under the surface depending on voltage, current, and type of material analysed. When beam properties at the surface cannot be fully controlled as in the case of OM-CL, variations in the degree of material excitation will lead to different overall intensity and changes in relative intensities of emission bands even in spectra obtained from the same portion of the sample (Polikreti & Maniatis, 2002). Spot focusing of electron beam in SEM also means higher degree of sample heating, damage, and defect annealing which results in fading of luminescence intensity with time. This is caused by the combination of thermal quenching, promotion of structural defects in crystal lattice, migration of interstitial ions to new equilibrium positions, and other processes taking place in excited and heated interaction volume (Götze et al., 2005; England et al., 2006).

Another issue with SEM-based systems is occurrence of phosphorescence interfering with the

luminescence emission. Phosphorescence is in principle identical to luminescence, only difference between the two being that phosphorescence occurs only after the electron irradiation of sample is terminated. In order for emission to be classified as phosphorescence it has to occur at least 10^{-8} seconds after irradiation ceases. This is an issue exclusive for SEM as its non-stationary electron beam constantly scans across the analysed area with only short irradiation and subsequent detection for each spot, thus promoting production of phosphorescence interfering with detected cathodoluminescence spectra (Götze & Kempe, 2008).

As shown in section 1.2.2 on the example of emission bands found in lanthanide-induced spectra, there can be considerable discrepancies between spectra collected by different CL-systems, even when the same sample is analysed. Apart from the properties of electron beam such as acceleration voltage or current density discussed above, other factors must also be considered when evaluating obtained cathodoluminescence data:

- *detector resolution* - when the smallest change of energy (wavelength) that detector is capable to discriminate is greater than energy difference between two close emission bands, signal from these two lines will be summed into one data point and thus part of the information is lost. When these low resolution data are compared with data from detectors with higher resolution, positions and relative intensities of some emission bands will not correspond.

- *system response* - each CL-equipment shows different efficiency of detection for various wavelengths of electro-magnetic spectrum. This is given both by the construction of detector itself and by light attenuation in optical fibre that transmits signal into the detector. Light attenuation - or loss of intensity during transmission - is a consequence of variable efficiency in transmission of certain wavelengths in the medium of optical fibre. Response curves for both detectors and fibre optics are usually provided by the manufacturer. Calibration for this system response is performed using reference calibration lamps with well-defined narrow emission bands and corresponding ratios of their relative intensities. Most commonly used calibration standards are mercury vapour lamp and quartz-iodine lamp (Polikreti & Maniatis, 2002).

Another issue that affects system response in OM-based systems is strong absorption of wavelengths in the UV range by glass elements in optical microscope. This means that with OM-CL systems, lower limit of wavelength detection lies at approximately 380 *nm* (Götze & Kempe, 2008). On the other hand, upper limit of detection varies with different detectors and this may be an issue especially when analysed material contains activators with important emission bands in near-IR and IR range (e.g. Nd^{3+}). Thus, while some systems will detect presence of this activators, others with narrow detection range may fail to do so and therefore provide incomplete cathodoluminescence information.

However, even with properly controlled voltage of electron beam, acquisition times, and calibration for system response, issues due to inherent properties of analysed sample may still prevail (Edwards et al., 2012). For example, when performing quantitative or semi-quantitative analysis, crystallographic orientation of analysed mineral may influence cathodoluminescence signal and therefore also estimated

concentration of a given element (Polikreti & Maniatis, 2002). Further, when obtaining spectra of weakly luminescing minerals surrounded by minerals with more intense emission, these may interfere with spectrum of analysed mineral, contributing to its spectrum additional emission bands of activators not present in this mineral (Götze & Kempe, 2008). This interference must be considered especially with the use of OM-CL.

Finally, from what has been discussed in section 1 and further above it is clear that properties of luminescence emission in any sample are the result of complicated interplay between many factors. This presents considerable difficulty for study of provenance as concentrations of activators and quenchers can greatly vary among the samples from same locality and at the same time samples from different localities may exhibit similar cathodoluminescence signatures due to convergence of their compositions. In such cases it is advisable to analyse wider array of samples from one locality and perform subsequent provenance study with average spectra for individual localities.

3. MATERIALS AND METHODS

3.1 Materials

Two major mineral groups selected for our present study - carbonates and apatites - were chosen due to their good luminescence properties and also because each of this groups can be found in types of geological and non-geological samples often subjected to provenance studies. Carbonates are major constituents of limestones, marbles, and other sedimentary rocks used as a building materials or materials for stone tools. Apatites are present as an accessory in vast majority of igneous and metamorphic rocks and thus have potential of being indicators for a wide range of samples encompassing provenance studies in geology, archaeology, forensic science, and others.

3.1.1 Carbonates

Carbonates studied in this work comprise of white calcitic or calcite-dolomitic marbles and hydrothermal calcite-dolomite veins. For each of the localities presented below 1-8 polished thin sections were analysed.

Samples of marbles analysed in this work were previously studied by Šťastná & Přikryl (2009; 2010) and Šťastná et al. (2009; 2011) and represent four major areas of Bohemian Massif (Fig. 3):

- Lugicum (Krkonoše-Jizera Terrane, Orlice-Sněžník Crystalline Unit) represented by white calcite-dolomitic marbles from locality Raspenava (174).
- Silesicum (Branná Group) represented by white calcitic marbles from locality Lipová - Na Pomezí (234).
- Moravicum (Svratka Crystalline Complex) represented by white calcitic marbles from locality Nedvědice (288).
- Kutná Hora Crystalline Complex represented by white calcite-dolomitic marbles from locality Bohdaneč (227).

Carbonates from these localities were modified by different degrees of regional metamorphism corresponding to greenschist to amphibolite metamorphic facies and occur as marble lenses encased in surrounding metasedimentary rocks. Petrographic characterization, mineral assemblages, fabric characteristics, cathodomicrofacies, and stable isotope data of these samples may be found in cited works by Šťastná et al. For easier orientation and comparison, numbering of samples used in this work is identical to that used in previous studies by these workers.

Second group of analysed carbonates represents hydrothermal calcite-dolomitic veins from limestone quarry Čertovy Schody in northern border of Devonian Koněprusy Limestone in the zone of Očkov Fault. In contrast to samples of marbles that show mostly homogeneous structure, carbonate veins from Čertovy Schody show marked structural dichotomy with relatively large euhedral crystals of dolomite encased in fine-grained matrix of calcite. These samples were chosen in order to ascertain importance of consistent sampling for meaningful results of provenance studies as cathodoluminescence data obtained

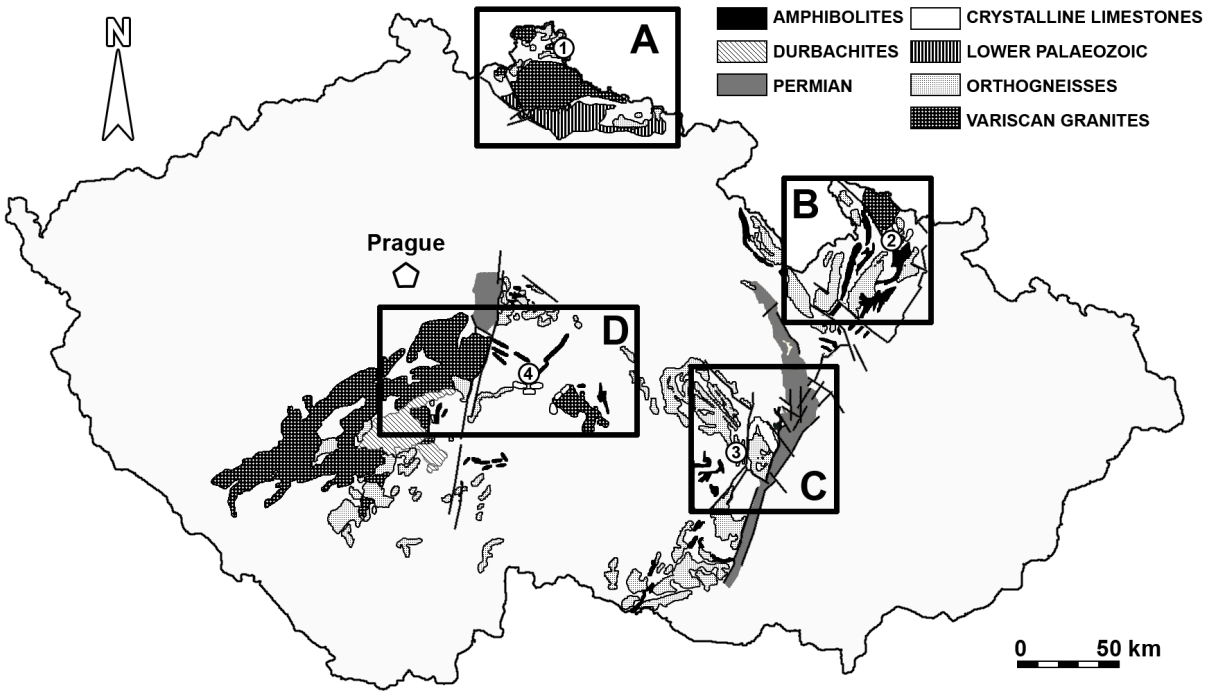

Fig. 3. Geological map showing localities of studied marbles. 1 - Raspenava (Lugicum, Krkonoše-Jizera Terrane); 2 - Lipová - Na Pomezí (Silesicum, Branná Group); 3 - Nedvědice (Moravicum, Svratka Crystalline Complex); 4 - Bohdaneč (Kutná Hora Crystalline Complex). Geological features were simplified for easier orientation. Modified after Šťastná et al. (2011).

from different structural features in heterogeneous sample may be impossible to match against each other when statistical approach of spectral analysis is employed.

3.1.2 Apatites

Analysis of apatites was performed on samples from a wide range of rock types including intrusive and extrusive igneous rocks such as granite, durbachite, gabbro, and rhyolite, as well as metamorphic rocks represented by paragneiss, quartzite, and granulite (Fig. 4). Additionally, apatites of biogenic origin including bones and teeth were analysed. Geology of each studied rock type is briefly presented below. For more detailed information refer to sources cited for individual localities.

All samples of studied granites present Eisgarn type of granites and belong to northern part of Moldanubian Pluton in the NE portion of Moldanubian Zone in Bohemian Massif. First group includes three types of Variscan granites that form the Melechov Massif in the northernmost part of Moldanubian Pluton. These are Melechov granite, Lipnice granite, and Kouty granite. Fourth type - Stvořidla granite - that occurs as a small - approximately 3 km wide - intrusion in the core of the Melechov granite was not included in our study.

Granites of Melechov Massif present P-rich peraluminous two-mica granites of variable degree of fractionation and crystallinity. Due to high content of P, fluorapatite is the most commonly observed

accessory mineral, accompanied by other phosphates such as monazite and xenotime (Procházka & Matějka, 2006).

Melechov granite (albite granite) is the coarsest of the three types and shows highest degree of fractionation. Apatites form relatively large - 100-600 μm - accessory grains with numerous inclusions of phosphates and zircon. Crystallization of inclusions preceded or was simultaneous with the crystallization of fluorapatite and these were later enclosed inside the growing apatite crystals (Harlov et al., 2008). This resulted in fractionation of lanthanides between these phases, with enrichment of monazite in light lanthanides relative to the whole rock chemistry and subsequent depletion of these elements in apatite (Procházka, 2010a). Apatites in this type thus concentrate only considerable portions of Sm, Gd, Dy, and Yb. Samples of Melechov granite analysed in this study are represented by the locality Melechov (MM1) approximately 3 km east of Kamenná Lhota.

Kouty granite (monzogranite to granodiorite) presents medium-grained variety with lower degree of fractionation. Fluorapatites in this type show highly variable content of inclusions of zircon with lower portion of monazite inclusions (Harlov et al., 2008). Studied samples of Kouty granite are represented

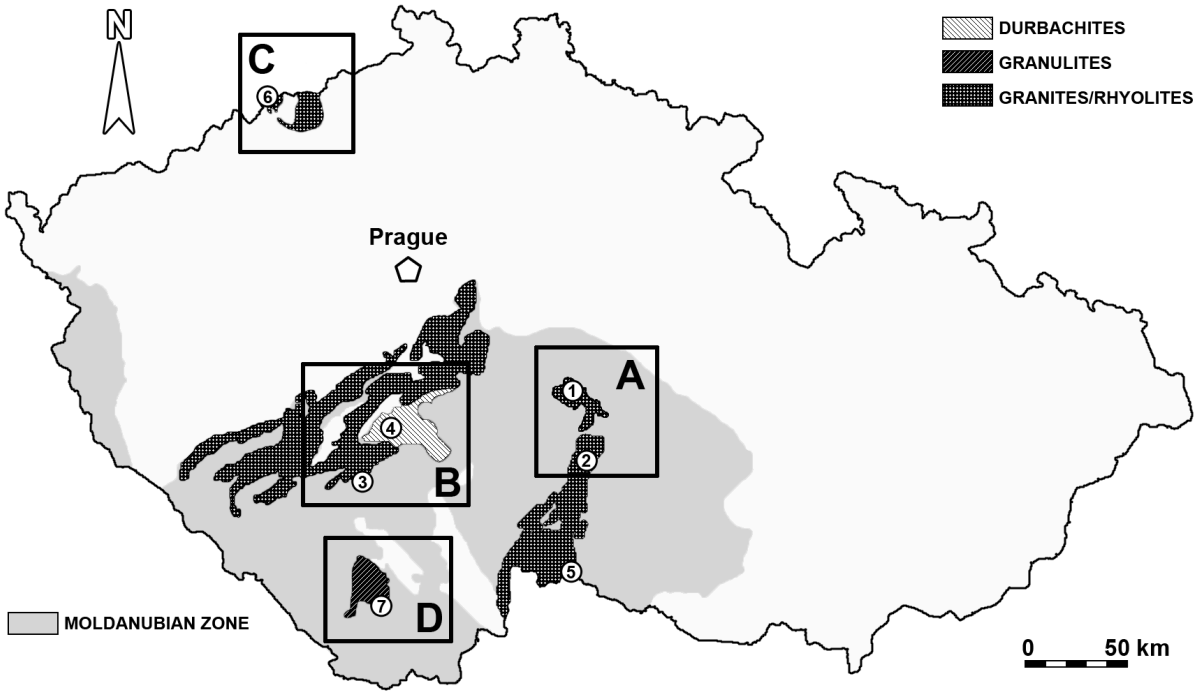

Fig. 4. Simplified geological map showing major localities of different rock types studied in this work. 1 - granite and paragneiss from the area of Melechov Massif (Moldanubian Pluton); 2 - granite and paragneiss from the area of Čeřínek intrusion (Moldanubian Pluton); 3 - durbachite from Kamenné Doly (Central Bohemian Pluton); 4 - durbachite from Vepice (Čertovo Břemeno intrusion, Central Bohemian Pluton); 5 - gabbro from Mařiž (Moldanubian Monotonous Unit); 6 - rhyolite from Fláje (Altenberg-Teplice Caldera); 7 - granulite from Plešovice (Blanský les Massif). For additional localities see text.

by localities from eastern part of Melechov Massif. These include locality Hurtova Lhota (MM6) and locality Kojkovice (MM7) on the endocontact of Kouty granite with surrounding paragneiss.

Lipnice granite (monzogranite to granodiorite) is most fine-grained of the three types with the lowest degree of fractionation (Procházka & Matějka, 2006). Crystals of fluorapatites in this type have low amount of inclusions with vast majority of them being zircon (Harlov et al., 2008). As in Melechov granites, light lanthanides are concentrated in monazite while apatites show depletion of these elements in comparison to the whole rock chemistry. Lanthanides mostly concentrated in apatites of Lipnice granite are Tb, Dy, Ho, Er, and Yb (Procházka, 2010a). Samples representing Lipnice granite include localities Kopaniny (MM2), Žebrákov (MM3), Dolní Město (MM4), and borehole Mel-5 near Žebrákov (MM5).

Second group of analysed Eisgarn type two-mica granites belong to the area of Čeřínek approximately 20 km south of Melechov Massif. Granites of Čeřínek type are chemically similar to Melechov granites, with the same and possibly higher degree of fractionation (Matějka & Janoušek, 1998). This area is in our study represented by localities Dolní Cerekev (CE1), Horní Hutě (CE2), and Čertův Hrádek (CE3). Other types of granites that occur in this area - Bílý Kámen and Boršov granites - were not included in present study.

Another group of rocks studied are durbachites represented by localities Kamenné Doly (DU1) and Vepice (DU2) on the western border of Moldanubian Zone of Bohemian Massif. Durbachite (K-rich melagranite to melasyenite) from Kamenné Doly north-east of Písek on the southern border of Central Bohemian Pluton occurs in the zone of contact between granitoids and marble in migmatites and orthogneisses accompanied by numerous dykes of pegmatites and leucogranites intruding this metamorphic complex (Houzar et al., 2008). Porphyritic durbachite from Vepice approximately 25 km north-east of Kamenné Doly belongs to Variscan Čertovo Břemeno intrusion of amphibole-biotite melasyenites and melagranites in the central part of Central Bohemian Massif (Holub, 1997; Janoušek et al., 2000).

Samples of gabbro are represented by locality Maříž (MA1, MA2) on the southern border of Czech Republic. These gabbros (gabbronorites) form layered intrusions in the northern part of Monotonous Unit of Moldanubicum - consisting of migmatitic paragneiss - along the Přibyslav mylonite zone and are bordered from the west by the Moldanubian Pluton (Ulrych et al., 2010).

Volcanites analysed in this study include rhyolite from locality Fláje (RH1) in the western part of Altenberg-Teplice Caldera where rhyolite and granite porphyry dykes intrude into monzogranites of Fláje Massif (Štemprok et al., 2003; Mlčoch & Skácelová et al., 2010).

Samples of metamorphic rocks represent three major rock types - paragneiss, quartzite, and granulite. First group of paragneiss samples comprises of localities Kojkovice (PMM1), Orlík (PMM2), Žebrákov (PMM3), and Lipnice (PMM4) in the area of Melechov Massif. Sample from locality Kojkovice represents exocontact of gneiss with Kouty granite (as described for sample MM7 from the endocontact in this area). Locality Orlík is situated on the southern border of Melechov Massif in the zone of

Humpolec magnetic anomaly and is characterized by paragneiss rich in cordierite (Procházka et al., 2010b). Sample from Žebrákov is a paragneiss core of borehole Mel-6 - from depth of approximately 50 m - on the northern border of Melechov Massif. Locality Lipnice in the south-eastern part presents fine-grained paragneiss with alternation of microcline bands (Procházka et al., 2011).

Second type of analysed gneiss is biotitic paragneiss from the western exocontact of Čeřínek intrusion represented by locality Rohozná (PCE1). Last type of gneiss is from locality Sudoměřice (PCB1) and is described as a migmatitic breccia-type rock with paragneiss paleosome of high Th content (Procházka, 2010a).

Quartzites from two localities were analysed - Rozkoš (Q1) south-east of Orlík hill, and Těchobuz (Q2) approximately 35 km to the east of this locality in a series formed by quartzitic paragneiss and amphibolite-interlayered paragneiss (Šťastná et al., 2014).

Granulites from locality Plešovice (PL1) in the east of Blanský les Massif in Moldanubian Zone represent garnet-bearing K-rich granulites - Plešovice type - hosting apatites with low contents of Mn (Janoušek et al., 2007).

Finally, samples of biogenic apatites analysed in this study include shell of Miocene turtle (B1) and teeth of fossil Pliocene rodent (B2) from Měňany east of Koněprusy caves and Čertovy Schody quarry.

3.2 Methods

Cathodoluminescence spectra of all studied samples were obtained by cold-cathode OM-CL equipment consisting of Leica DMLP optical microscope, CLmk4 cathodoluminescence for optical microscope (Cambridge Image Technology Ltd.), and thermo-electric cooled spectrometer Avantes SensLine AvaSpec-ULS2048L-TEC-USB2 with 2048 pixel CCD detector, resolution 0.27 *nm* per pixel, 100 μm slit, and diffraction grating of 600 lines per *mm*.

In order to minimize possible drift or fluctuations of system response, all carbonate samples were analysed in single session and operational parameters were kept constant. These include: beam voltage - 13 kV, beam current - 300 μA, acquisition time 15 *s* with 2x time averaging - i.e. overall acquisition time of 30 *s* - and single lens with 10x magnification. Twenty cathodoluminescence spectra were collected from each polished thin section and these were further corrected for background with dark baseline acquired before measurement of each thin section and after acquisition of every four spectra.

Operational parameters during the collection of apatite spectral data were not as strictly controlled as these generally show much higher intensities of luminescence emission and thus are less prone to interference from background noise and other phenomena. Additionally, analysis of apatite spectra will not be conducted as a complete provenance study with matching of spectra from individual localities as in the case of carbonates. Our analysis will rather attempt to identify trends and characteristics of apatite cathodoluminescence in different rock types and investigate some of the difficulties connected with analysis of these cathodoluminescence data (further described in section 4.2).

4.1 Analysis of carbonates

4.1.1 Data preparation

Before similarity of obtained spectra can be analysed, it is necessary to normalize and smooth raw data in order to allow meaningful comparison of cathodoluminescence spectra. It is apparent from Fig. 5a that due to structural inhomogeneities, maximum intensity of luminescence emission may greatly vary even in samples from the same locality. Thus, prior to analysis all spectra were normalized to maximum intensity and further smoothed by recursive moving average method with region of averaging 7 data points meaning that the given point was averaged with 3 neighbouring data points on each side. Due to the low intensities - i.e. high noise-to-signal ratios - of cathodoluminescence spectra in marginal parts of detection range, only spectral region of 500-750 *nm* (931 data points) was chosen for further analysis. Fig. 5b shows histogram of wavelengths at which spectra reach their intensity maxima. Two distinct groups can be observed with modes of maximum intensities at approximately 613 and 645 *nm* with gap between these groups between 621-630 *nm* where none of 338 analysed spectra reach their peak intensity. Group with maxima at lower wavelengths represents samples where calcite is the dominant component and group with maxima occurring at higher wavelengths corresponds with dolomite-rich samples. Clear distinction between these two groups is of great interest for our following provenance study as classification of unknown sample into one of these groups automatically excludes database entries that fall into the other group as a potential matches. This greatly reduces portion of spectra from database that

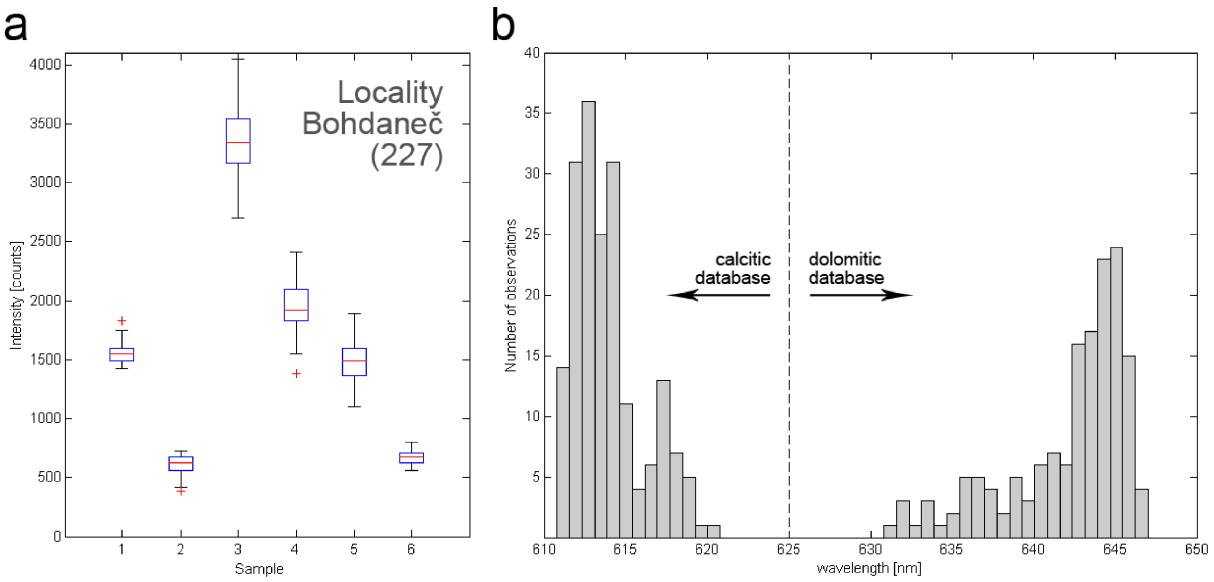

Fig. 5. a - variability of maximum intensities observed in spectra obtained by analysis of six different thin sections from locality Bohdaneč (227). Each box plot represents variability of 20 spectra with whiskers corresponding to 1.5 interquartile range; b - distribution of all 338 carbonate spectra based on the position of their peak intensity.

must be analysed and thus speeds up the whole process of provenance determination.

Fig. 6a shows average cathodoluminescence spectra representing each of the two groups. Our data are in accordance with those reviewed in sections 1 and 2, showing pseudo-Gaussian shape of cathodoluminescence spectra for both calcitic and dolomitic samples. This characteristic shape of luminescence emission bands may be used to obtain further information from carbonate cathodoluminescence signatures and thus further simplify process of provenance determination. For this purpose we employed Gaussian one-term model that fits whole normalized and smoothed spectra with function:

$$y = a.e^{\left[-\left(\frac{x-b}{c}\right)^2\right]} \tag{2}$$

where *a* represents amplitude of fitted curve, *b* is the location of this amplitude (centroid), and *c* corresponds to width of the curve (coefficient that influences its FWHM). Fitting is achieved by non-linear method of least-squares curve fitting with maximum number of iterations available for convergence set at 4000 and initial values of refined parameters at 0.5 - i.e. half of the maximum intensity of normalized spectra - for coefficient *a*, and median of wavelength range for both coefficient *b* and *c*.

Coefficients *a, b,* and *c* obtained for individual spectra are stored in a database and may be used either as a simple tool for reducing size of dataset necessary for analysis or may allow us to transform original data in order to reveal and amplify characteristic features - and thus information - in analysed spectra. While coefficients *a* and *c* are expected to be similar for various localities due to the effects of normalization, parameter *b* - i.e. centroid of fitted curve - is unaffected by this normalization. Position of curve centroid will depend on variations in chemical composition such as concentration of activators or quenchers. These variations are expected to be smallest in spectra of samples from the same locality as their physico-chemical properties should in theory converge. Thus, when matching an unknown sample against spectra in either calcitic of dolomitic part of database it is preferable to further reduce dataset being analysed by selecting only spectra with closest match of their *b* coefficients to *b* coefficient of unknown sample. This is easily achieved by calculating absolute value of difference between *b* of each database entry and *b* of analysed unknown sample. By sorting these values in ascending order it is possible to select appropriate cut-off value and analyse only database entries with differences of *b* coefficient lower than this value. This is a crucial step as it determines size of the dataset and overall speed of analysis. Therefore, cut-off value must be chosen with special care in order to achieve fast analysis while maintaining chosen dataset sufficiently large so that its analysis may provide representative results (further discussed in section 5.1).

It is apparent from Fig. 6a that even though shapes of spectra follow general trend of fitted Gaussian curves, they also show additional features in the form of fluctuations around the ideal Gaussian shape. In order to evaluate whether some of these features may be helpful as indicators of provenance, it is necessary to amplify information they bear. Our method for this amplification is based on subtraction

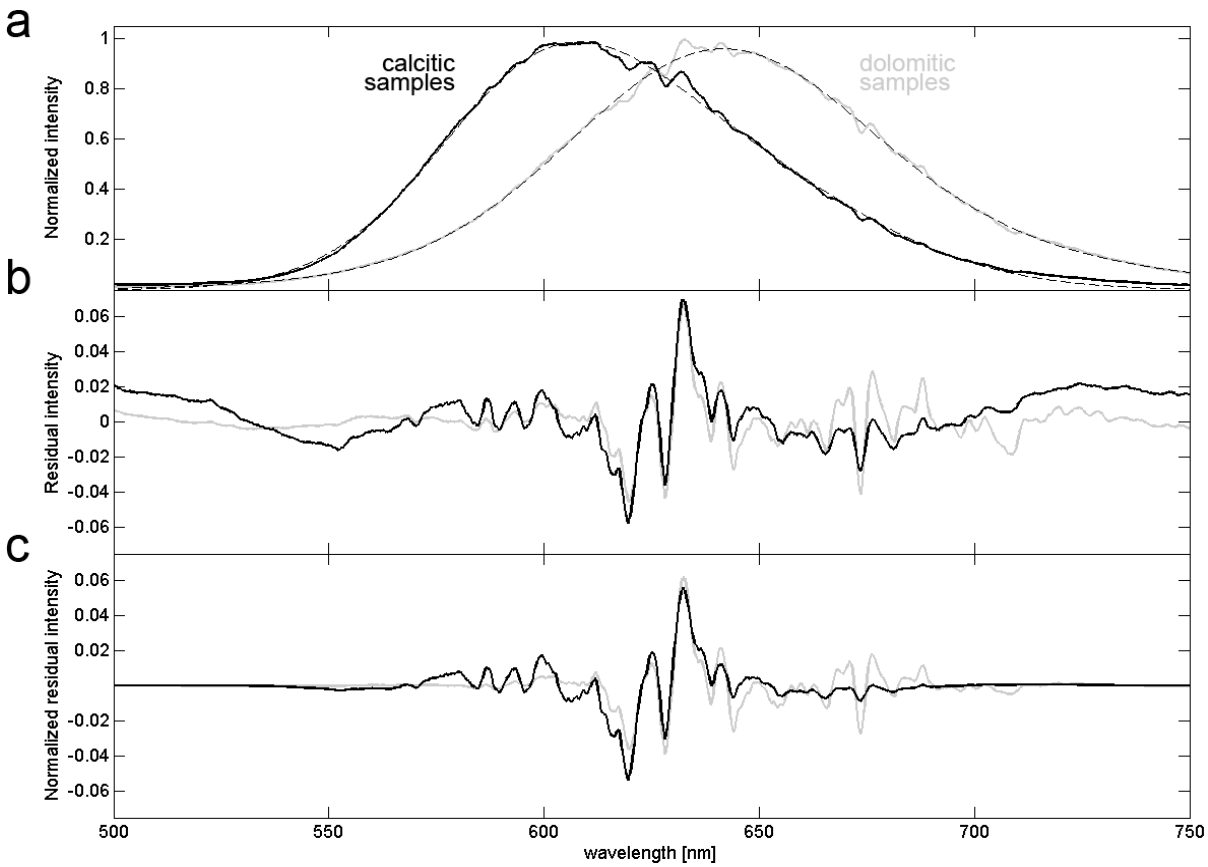

Fig. 6. Average normalized cathodoluminescence spectra, residual spectra, and normalized residual spectra of calcitic and dolomitic samples. a - average cathodoluminescence data from 185 calcitic and 153 dolomitic spectra with corresponding Gaussian fits (dashed line); b - residual spectra obtained by subtraction of Gaussian fit from each spectrum; c - residual spectra normalized by values of Gaussian curve in order to suppress marginal ranges with high noise-to-signal ratios.

of fitted curve from the original normalized spectrum, producing residual spectra for all samples that may be compared against each other by various similarity measures in analogy to normalized spectra. Prior to analysis, however, these residual spectra must be normalized. Residual data without normalization as shown in Fig. 6b exhibit high variability at the edges of detection range due to the fact that fitted Gaussian curve shows greatest degree of diversion from experimental data in these peripheral parts of spectra with high noise-to-signal ratio. As we are concerned primarily with high-intensity part of the spectrum containing more information due to lower noise-to-signal ratio, it is appropriate to normalize these residual spectra in a way that will suppress their low-intensity parts and amplify high-intensity part in the middle of analysed range. Simple way to achieve this is by multiplying each element of residual spectrum with corresponding value of Gaussian curve fit of original data. In this way, values of curve fit laying between 0 and 1 serve as weights for individual data points in accordance with relative intensity detected at that particular wavelength. Thus, we obtain normalized residual spectra (Fig. 6c).

While one Gaussian curve represents sufficiently close fit of experimental data, structural properties and theory of luminescence generation as discussed in section 1 imply that it should be possible to perform deconvolution of spectra into two components corresponding to Mn^{2+} luminescence bands in Ca^{2+} and Mg^{2+} octahedral sites of carbonate structure. In order to evaluate this, we employed a non-linear least-squares curve-fitting using two-term Gaussian model that fits spectra with function:

$$y = a_1 . e^{\left[-\left(\frac{x-b_1}{c_1}\right)^2\right]} + a_2 . e^{\left[-\left(\frac{x-b_2}{c_2}\right)^2\right]} \quad (3)$$

with coefficients a_1, b_1, c_1, and a_2, b_2, c_2 characterizing first and second fitted curve, respectively. As two-term fitting is more computationally complex and time-consuming than simple one-term fit, maximum number of iterations was in this case set to 500. All spectra in calcitic group were successfully deconvoluted into two components with variable relative normalized intensities ranging between 0.25 and 0.75 with centroids at 595-603 *nm* and 617-637 *nm* which may be attributed to luminescence centres in Ca^{2+} and Mg^{2+} sites, respectively. Band at higher wavelengths is broader for all samples, with values of coefficient *c* between 51 and 60 *nm* as opposed to the range of 26-37 *nm* for band at 595-603 *nm*. Same curve-fitting method applied to dolomitic group, however, failed to produce meaningful results as fitted curves always converged to a result where one of the curves was strongly dominant with relative maximum intensity higher than 0.9 and the second fitted curve with very low intensity served only as a fine shape refinement of the dominant curve. This may be explained with the help of results from calcitic samples clearly showing that emission bands from centres in Mg^{2+} sites are generally broader than those produced by centres in Ca^{2+} sites. Thus, when amount of Mg^{2+} sites becomes sufficiently high as in the case of dolomitic samples, this broad emission band extends with its tail to the range of emission from Ca^{2+} sites and conceals information from these narrower lower-intensity bands. This effect can be further proven by analysing skewness (third central moment) of spectra given by:

$$y = \frac{n}{(n-1)(n-2)} \sum_{i=1}^{n} \left(\frac{x_i - \bar{x}}{s}\right)^3 \quad (4)$$

where *n* is the number of data points, $\bar{x}$ is the mean of spectrum, x_i is the *i*th data point of spectrum, and *s* its standard deviation. Box plots in Fig. 7 show variation of skewness in both groups of carbonate samples. All spectra show positive skew which indicates that majority of values lies below the mean, i.e. at lower wavelengths. More importantly, it is apparent that skewness of dolomitic samples is systematically lower than that of calcitic samples, meaning that dolomitic spectra are more symmetrical. This further points to the fact that emission centres in Mg^{2+} sites dominate cathodoluminescence spectra of dolomitic samples and conceal emission band from Ca^{2+} sites. Thus, single Gaussian curve is more appropriate fitting model for this group of spectra.

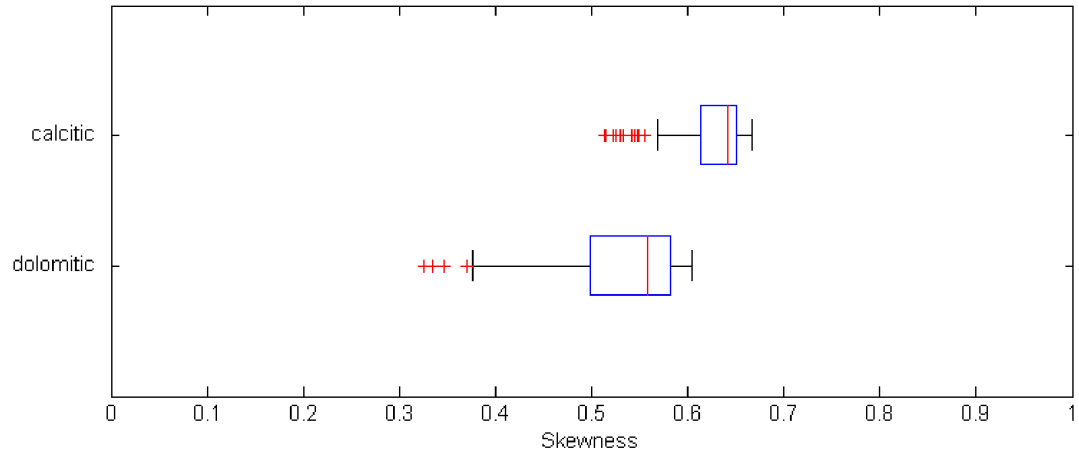

Fig. 7. Variation of skewness in spectra of calcitic and dolomitic samples of marble. Positive values for both groups indicate asymmetry of distribution towards the lower wavelengths. Whiskers correspond to 1.5 interquartile range.

New set of coefficients obtained for calcitic group of samples may be used for dataset reduction in a similar way as b coefficient from single curve fitting. Along with coefficients b_1 and b_2, it is possible in this case to also employ coefficients a_1, a_2, c_1, and c_2 as their relative values are unaffected by data normalization. One way to achieve this is analogous to single-curve method and consists of finding absolute values of differences between each of the six coefficients of unknown analysed sample and samples from the database. Each of these values must then be normalized in order to preserve same scaling of relative differences. This can be done for example by dividing every absolute value of difference by value of corresponding coefficient of an unknown sample. After this normalization, all six values may be summed into one single value representing each spectrum.

These results can be further connected with data from comparison of single-curve centroids described previously and this will provide still better results of data selection from spectral database. Before these two types of values can be combined, however, vectors containing values for all database entries must be scaled so that the minimal value will correspond to 0 and maximum to 1. When both vectors are scaled in this way, it is possible to combine corresponding values of coefficient differences and perform data selection from database by defining cut-off value in a same way as described for single-curve fitting.

In a similar manner it is further possible to use ratios of coefficients a_1/a_2, b_1/b_2, and c_1/c_2 as a measure of spectral similarity. This method - along with many others - will be discussed in section 4.1.2.

4.1.2 Measures of spectral similarity

Once we selected appropriate spectra from the database through operations described above and thus created dataset for matching with an unknown sample, it is possible to perform analysis of spectral similarity. This can be done by employing various types of similarity measures. Therefore, it must be

assessed which of these measures are appropriate when dealing with spectral data of mineral cathodoluminescence. Our analysis will employ all of the similarity measures presented below and consequently, discrimination ability of each of these measures will be evaluated.

Easiest way to express similarity between two vectors (spectra) is to calculate correlation of their values, i. e. degree of their association. *Pearson product-moment correlation coefficient* (often referred to simply as the *correlation coefficient* or *Pearson's r*) is one of the simplest tools for evaluation of linear correlation between two variables. It is defined as:

$$r = \frac{\sum_{i=1}^{n}(x_i - \bar{x})(y_i - \bar{y})}{\sqrt{\sum_{i=1}^{n}(x_i - \bar{x})^2}\sqrt{\sum_{i=1}^{n}(y_i - \bar{y})^2}} \tag{5}$$

where x and y are two vectors representing analysed unknown sample and sample from the database, x_i and y_i represent ith elements of these vectors and $\bar{x}$, $\bar{y}$ being mean values of each vector. This equation shows that Pearson product-moment correlation coefficient is given by the division of covariance between the two spectra and product of their respective standard deviations. As all of the analysed spectra show very similar general trends, expected values of correlation coefficients should be positive and close to the value 1. In order to overcome difficulties arising from narrow distribution of obtained correlation coefficients, these data are transformed so that the resulting values of matrix containing correlation coefficients for each pair of spectra in analysed dataset range between 0 and 1. This is achieved by assigning value 1 to the highest value in matrix and value 0 to the lowest matrix value, with corresponding scaling of all values that lay in-between.

More sophisticated method for evaluating how values of one spectrum correspond to the values of other spectrum is *Spearman's rank correlation coefficient*. This correlation coefficient goes beyond the simple assessment of correlation and defines degree of monotonous relationship between the ranked values of the two spectra. It is given as:

$$\rho = 1 - \frac{6}{n(n^2 - 1)}\sum_{i=1}^{n} d_i^2 \tag{6}$$

where n is the number of data points in each spectrum and d_i is the difference between the ranks of elements x_i and y_i of the two spectra. As a consequence of using transformed ranked values, this correlation coefficient is less sensitive to outliers which may otherwise cause overestimation or underestimation of correlation between the two variables. When relationship between ranked values of both vectors (spectra) is perfectly monotonous, Spearman's ρ is equal to 1. As in the case of Pearson product-moment correlation coefficient, values of ρ for our spectral data are expected to lie close to 1 and thus must be scaled in a same way to normalize their distribution between the values 0 and 1.

Additional method that can be employed for calcitic samples of marbles is determination of their similarity based on the coefficients of fitted curves. Ratios a_1/a_2, b_1/b_2, and c_1/c_2 can be calculated for

each sample and these are then compared between each pair of samples through absolute values of their differences, in analogy to the comparison of coefficients during the selection of appropriate samples from the database described in section 4.1.1. Each absolute value is normalized by corresponding ratio of analysed unknown sample which then allows us to add all three values and obtain single number for each pair of spectra from the dataset. However, these values act in an opposite way to those of correlation coefficients - similarity between the samples is highest when their sum of differences is smallest. In order to obtain data that can be compared with other similarity measures, each of these values x_{ij} is transformed to (1- x_{ij}). This results in a matrix with values 1 along the diagonal and values lower than 1 in the remaining cells and can be further scaled to range between 0 and 1 as in the previous cases.

Apart from similarity measures based on pair-wise correlation and association between pairs of spectra, it is also possible to utilize properties of the dataset as a whole. One of this methods is a modification of traditional 2D correlation spectroscopy analysis called *sample-sample correlation analysis* (Šašić et al. 2000). This method is based on the construction of 2D correlation coefficient maps (matrices) having two sample axes and showing correlation between each pair of samples from dataset. First step in the construction of 2D correlation map is scaling of the data to ensure consistent variance of analysed spectra. In order to achieve this it is necessary to calculate average spectrum from all spectra in a given dataset and standard deviation at each corresponding value of wavelength for all samples (Šašić & Ozaki, 2001). Scaling for spectra arranged in columns of the matrix is then given as:

$$x'_{ij} = \frac{(x_{ij} - \bar{x}_i)}{s_i} \tag{7}$$

where x'_{ij} is scaled *i*th element of *j*th spectrum, x_{ij} is original value of this element, $\bar{x}_i$ is dataset average at wavelength in *i*th row, and s_i is the standard deviation of dataset in this row. Resulting mean-centered data normalized by standard deviations are referred to as the *dynamic spectra*. Matrix X containing dynamic spectra can be now used for calculation of sample-sample correlation coefficient map given as:

$$\Phi = \frac{1}{k-1} X^T X \tag{8}$$

where k is the number of samples (columns of X), and X^T is transposed form of the matrix X. Φ thus presents symmetric k-by-k matrix with two sample axes where each matrix element shows relationship (correlation) between particular pair of spectral samples.

Similarity or dissimilarity of samples expressed by the values of matrix Φ may be further amplified by performing disrelation analysis of these data (Noda & Ozaki, 2005). This is achieved by transforming 2D correlation map Φ into *sample-sample disrelation matrix Λ* defined as:

$$\Lambda_{ij} = \sqrt{\Phi_{ii}\Phi_{jj} - \Phi_{ij}^{2}} \tag{9}$$

where Λ_{ij} is element of disrelation matrix corresponding to *i*th row and *j*th column. Disrelation matrix Λ is symmetric *k*-by-*k* matrix and its values increase with increasing dissimilarity between given pair of samples. Therefore, after scaling matrix to values between 0 and 1, each element Λ_{ij} must be transformed to the value (1 - Λ_{ij}) in order to obtain coefficients that behave in the same way as values of other similarity measures employed.

Another method for the examination of spectral similarity that utilizes properties of the whole analytical dataset is *principal component analysis* (PCA). This statistical method allows evaluation of similarity between variables in a dataset by their transformation into orthogonal variables called principal components. Each component represents an axis in *n*-dimensional space that is chosen in such a way that it accounts for the maximum variance in dataset unexplained by other components. Thus, first principal component can be thought of as the main axis of an ellipsoid enclosing all analysed data and consequently, second principal component as an axis accounting for maximum of remaining variance in dataset while satisfying condition of orthogonality. Principal components of higher order are then constructed in a similar way.

Calculation of PCA is traditionally done by constructing variance-covariance matrix (C) of mean-centered and scaled data, which is subsequently decomposed into eigenvectors (V) and eigenvalues (W) so that:

$$V^{T}CV = W \tag{10}$$

We propose modification of this method where covariance matrix C is replaced by sample-sample correlation matrix Φ. This then allows us to compare coefficients - i.e. loadings - of individual principal components for each pair of spectra and further, to evaluate which of the obtained principal components is the most appropriate for provenance determination of an unknown sample. Our study will assess sensitivity and performance of first three principal components that generally account for more than 90% of variability observed in analysed cathodoluminescence data.

Last method for determination of spectral similarity employed in this study is *agglomerative hierarchical clustering*. It is based on the construction of data clusters by agglomeration of individual spectra through evaluation of their mutual similarity which is in this case determined by calculating pair-wise distance between the corresponding values of spectral vectors. This distance can be calculated by a variety of different methods and so it is necessary to assess which of these will be the most appropriate for the analysis of our type of spectral data. Three of the most frequently used distance metrics in hierarchical clustering are *Euclidean, City block, and Minkowski distance*.

Euclidean distance between the two spectra x_a and x_b, each consisting of *n* elements, is given by the

expression:

$$d_E(a,b) = \sqrt{\sum_{i=1}^{n} (x_{ai} - x_{bi})^2} \tag{11}$$

which represents sum of the smallest distances (lengths of straight lines) between corresponding data points of spectra *a* and *b*.

City block distance (alternatively Manhattan distance or taxicab geometry) is calculated by summation of absolute difference between corresponding spectral points which represents lengths of the projections of their Euclidean distance onto the axes of used coordinate system (Fig. 8) and is given as:

$$d_C(a,b) = \sum_{i=1}^{n} |x_{ai} - x_{bi}| \tag{12}$$

In other words, it calculates absolute difference of coordinates between each pair of points in Cartesian coordinate system and subsequently sums these values for all *n* elements of analysed spectra.

Both Euclidean and City block distances are just a special cases of Minkowski distance defined as:

$$d_M(a,b) = \left[\sum_{i=1}^{n} |x_{ai} - x_{bi}|^p \right]^{1/p} \tag{13}$$

where parameter *p* defines order of the difference. City block distance corresponds to Minkowski distance with $p = 1$ and Euclidean distance is obtained when $p = 2$. Aim of our analysis is to determine which value of parameter *p* is the most appropriate for correct clustering of spectral cathodoluminescence data. Our present analysis will evaluate values of *p* between 1 and 3.

Second step of hierarchical clustering is agglomeration based on obtained distance data in order to create cluster tree that determines relationship between all spectra in a given dataset. As with the distance metrics between the individual samples, measurement of distance between different clusters can be also carried out by various methods. Most commonly used linkage methods are *average, single, complete,* and *Ward's.*

Average linkage method is based on the calculation of average value from the distances of all possible pairs of objects between the two clusters A and B:

$$D(A,B) = \frac{1}{n_A n_B} \sum_{i=1}^{n_A} \sum_{j=1}^{n_B} d(x_{Ai}, x_{Bj}) \tag{14}$$

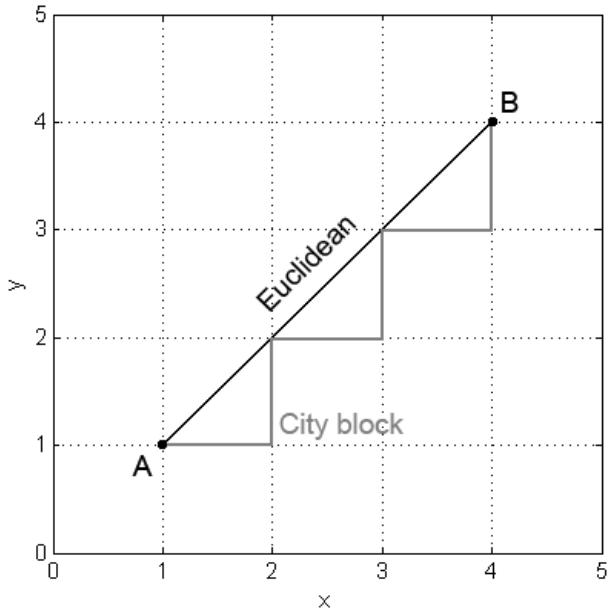

Fig. 8. Different distances between points A and B as calculated by Euclidean and City block methods.

where n_A and n_B is the number of objects in clusters A and B, and $d(x_{Ai}, x_{Bj})$ is the distance between the elements of each cluster calculated by one of the methods discussed above. One of the advantages of this method lies in the fact that it is not sensitive to outliers in analysed dataset.

Single linkage method connects data clusters based on the minimal distance between the pair of objects belonging to these clusters, i.e. it searches for the nearest neighbouring objects of the two groups. Disadvantage of this method is its sensitivity to outliers that produce false associations in resulting cluster tree.

Complete linkage overcomes this issue by calculating distance between the farthest objects of the two clusters and subsequently merging pairs with the lowest values of this distance.

Finally, Ward's linkage is based on the determination of within-cluster sum of squares and subsequent merging of clusters in order to minimize increase of this value. Sum of squares for cluster A is defined as:

$$S(A) = \sum_{i=1}^{n_A} (x_i - \frac{1}{n_A} \sum_{j=1}^{n_A} x_j)^2 \tag{15}$$

and represents the deviation of clustered data from the cluster centroid. Thus, Ward's linkage merges clusters A and B for which value of D(A, B) = S(A, B) - [S(A) + S(B)] is lower than values for all other possible combinations of clusters in the dataset. While this method is more complex and therefore more time-consuming than the previous methods, it is very efficient at detecting outliers in analysed data.

Once that we obtained values of distances and linkages between samples and clusters, it is possible to construct graphic representation of hierarchical cluster tree in the form of a dendrogram which allows

immediate visual inspection of obtained results. One of the dendrogram axes shows indices of individual spectra arranged based on their proximity in the cluster tree and the other axis shows distances between these clusters as calculated by one of the linkage methods. From the relative heights of links in the dendrogram it is possible to evaluate relative significance of each agglomerative step. When two links stemming from one node show great relative length, distance between the two clusters defined by these links is significant and it is said that links show high degree of inconsistency. When clusters are joined by very short links, it is an indication of small difference between these clusters and this means that the links are consistent. Thus, when inspecting obtained dendrogram it is important to consider that consistent divisions are less important for data classification than inconsistent ones.

4.1.3 Overview of algorithms

In the previous sections were presented means of selection and preparation of data for the analysis as well as similarity measures employed for this analysis. This section will briefly summarize architecture of used algorithms and individual steps undertaken in the course of similarity analysis for both calcitic and dolomitic samples.

Database of carbonate spectra is divided into two parts corresponding to calcitic and dolomitic samples based on the position of centroid (coefficient b) obtained by the method described in section 4.1.1. All spectra for which $b < 625$ *nm* are classified as calcitic and spectra with $b > 625$ *nm* as dolomitic. Raw spectra along with the corresponding coefficients are stored as column vectors in Excel spreadsheet database. Additionally, calcitic part of the database also contains coefficients obtained by two-term Gaussian curve fitting described in section 4.1.1. Complete algorithm of employed analysis is for easier orientation briefly summarized below.

1. Import raw spectrum - or more spectra - for analysis.
2. Normalize imported spectra by their maximum intensity and perform smoothing by the recursive moving average along the window of 7 data points.
3. Fit spectra by single Gaussian curve and determine value of coefficient b.
4. Sort spectra into individual matrices for calcitic and dolomitic samples.
5. If calcitic spectra were found between imported samples, start sub-procedure for analysis of these spectra. If only dolomitic samples were found, start sub-procedure for analysis of dolomitic spectra. If both types of samples were identified, analyse calcitic samples first and dolomitic samples afterwards.

(All steps described below are common for analysis of both calcitic and dolomitic samples, unless stated otherwise. These are performed in individual cycles for each imported spectrum.)

6. Load coefficients of single-curve fitting from the database.
7. Determine number of samples (N) from the database that will be selected for comparison with analysed sample.

8. (only for calcitic samples) Determine coefficients of two-term Gaussian fit for analysed spectra.
9. Search database for N closest matches to imported spectrum based on absolute differences of coefficient *b* (for dolomitic samples) and sum of a) normalized absolute differences of coefficient *b* and b) sum of normalized absolute differences for all six coefficients of two-term Gaussian fit (for calcitic samples).
10. Load N closest spectral matches, normalize them by their maximum intensities and perform smoothing by recursive moving average along the window of 7 data points.
11. Connect imported spectrum with the matrix of selected spectra from the database.
12. (only for calcitic samples) Calculate ratios of coefficients a_1/a_2, b_1/b_2, and c_1/c_2 for all samples in selected dataset.
13. Subtract values of fitted curve (or two curves for calcitic samples) from spectra and create new matrix containing residual values of this subtraction.
14. Normalize each residual spectrum via multiplication by corresponding values of fitted curve(s).

(Following steps apply both for original and residual values of calcitic and dolomitic samples, unless stated otherwise.)

15. Normalize and scale the whole dataset by subtracting average value of each row from every element in this row and by subsequent division of each row element by standard deviation of this row.
16. Calculate sample-sample correlation matrix Φ and sample-sample disrelation matrix Λ from the whole dataset. Scale elements of disrelation matrix and transform them into values $(1 - \Lambda_{ij})$. Resulting matrix will be referred to as matrix G.
17. Calculate principal component analysis based on sample-sample correlation matrix Φ as described in section 4.2.
18. Calculate absolute differences between coefficients of individual principal components and create matrix of these differences (matrix F). Scale and transform as data in step 16.
19. (only for calcitic samples) Determine absolute differences of ratios a_1/a_2, b_1/b_2, and c_1/c_2 for each pair of spectra. Normalize each value by corresponding ratio of analysed imported spectrum and sum these normalized values for all three ratios into one value representing each possible pair of spectra from the dataset. Transform elements of resulting matrix into values $(1 - R_{ij})$. This results in a matrix with ones along the diagonal and values lower than one in other cells (matrix E).
20. Calculate Pearson product-moment correlation coefficient and Spearman's rank correlation coefficient for each pair of spectra in the original normalized and smoothed dataset, obtaining matrices A and B. Determine the same coefficients for matrices of mean-centered and normalized values used for the calculation of sample-sample correlation - thus obtaining matrices C and D.
21. Scale all of the obtained matrices A-G to values ranging between 0 and 1, add them together -

i. e. sum values for each corresponding matrix element - and divide each element by the number of matrices combined.

22. Select row (or column) of the resulting matrix that corresponds to imported spectrum and sort values - along with connected sample indices - in the descending order. Sample with the highest value represents best match for analysed unknown sample, with other samples - showing progressively lower values - being less probable matches.
23. Combine results obtained from the original and residual spectra and calculate average of these results.
24. Perform cluster analysis with pre-defined type of distance metric and method of linkage. Create dendrogram based on these results.
25. Perform meta-analysis to further improve obtained results (described in section 4.1.4 below).

4.1.4 Meta-analysis of results

Method of our analysis based on addition of partial results from various similarity measures stored in the matrices A-G into one final matrix with overall results allows us to perform meta-analysis, i.e. an analysis of how each of the analysed spectra responds to individual methods of similarity assessment. This can be easily done by evaluating how coefficients of each sample behave during the process of addition.

For cells that represent auto-correlation of analysed unknown sample, coefficient is equal to 1 in all of the seven matrices A-G. Thus, final value of this cell after addition of all matrices will be 7. Gradual increase of this value can be illustrated as a linear function $y = x$ ranging between values [1,1] and [7,7], where axis x represents number of added matrices (Fig. 9).

Slope of this function can be calculated as:

$$m = \frac{\Delta y}{\Delta x} \tag{16}$$

where Δx and Δy denote change in the coordinates of x and y, respectively.

In the case of autocorrelation, slope is equal to 1. Values of m for all the other analysed samples that do not show perfect correlation with unknown spectrum will be lower than 1 as their Δy, corresponding to the addition of one value of correlation coefficient between two steps ($\Delta x = 1$) will always be less than one. Our method is to calculate slope of linear function defined by the initial cell value - i.e. value in matrix A - and the final value after addition of all seven matrices. Obtained slopes are subsequently scaled to range between 0 and 1. In this way, slope behaves similar to traditional correlation coefficients where value of 0 indicates no correlation and values closer to 1 indicate higher degree of association. Advantage of this method lies in the fact that it does not use actual spectral data from the dataset but evaluates their association based on the pattern of their behaviour during analysis. Thus, it provides an additional information that is not present in these spectra inherently but is actually generated in the course of the analysis.

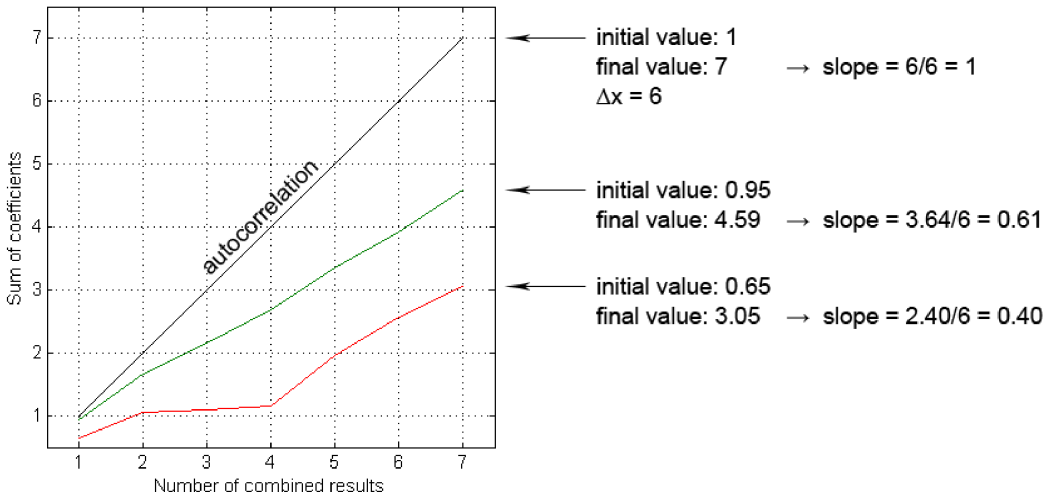

Fig. 9. Values of slope for spectra of various degree of correlation with unknown analysed spectrum. Autocorrelation of sample with itself is defined by the slope equal to 1. Spectrum from database showing better correlation with analysed sample acquires greater final sum of coefficients and thus its slope is closer to 1 as compared to less-correlated spectrum.

4.2 Analysis of apatites

As mentioned in section 3.2, scope of our analysis of apatite spectral data will not include complete process of similarity determination and subsequent spectral matching as in the case of carbonates described above. Our study will rather attempt to identify major activators in apatites from various types of rocks, assess trends and characteristics of luminescence in these rocks and evaluate possibilities and limitations of apatite cathodoluminescence spectroscopy applied to the provenance studies of igneous and metamorphic rocks, as well as the study of biogenic apatites from bones and teeth of animals. This is of particular interest as the number of studies employing cathodoluminescence spectroscopy of apatites is much smaller than that of studies concerned with cathodoluminescence of carbonates or quartz (discussed in section 2.1). Therefore, in order to perform complete study of provenance based on the spectroscopy of apatites, it is first necessary to evaluate advantages and constraints of this method as will be discussed below.

Similar to the case of carbonates, luminescence of apatites from different samples shows high degree of variability in intensity and thus as a first step of our analysis it is necessary to normalize all spectra to maximum intensity in order to obtain data that may be compared with each other. In contrast to carbonates, however, spectra of apatites were not smoothed by method of moving average as these generally show much higher intensities - i.e. lower noise-to-signal ratio - as compared to faintly luminescing carbonates. Wavelength range of 430-720 *nm* - represented by 1061 individual data points - was selected in order to include all the emission bands observed in analysed dataset and to exclude marginal regions with no apparent bands, high noise-to-signal ratio, and low system response.

Based on our observations from spectra of all studied samples we identify following emission bands and

corresponding lanthanide activators (Fig. 10):

- wavelengths below 460 *nm* - broad emission band with increasing intensity towards the lower wavelengths extending beyond the lower limit of analysed range where absorption effects of optical equipment becomes apparent. This emission band can be attributed to activation by Eu^{2+} with the possible interference from the tail of broad emission band produced by Ce^{3+} at lower wavelengths (Waychunas, 2002).

- 460-500 *nm* - this broad emission band with well defined maximum at around 485 *nm* presents characteristic band of Dy^{3+} ions. In some cases, this may be interfered by the emission of Pr^{3+} laying around the same wavelength range. Then, it is possible to distinguish interfered band by its shape. While band with the sole contribution from Dy^{3+} shows pseudo-Gaussian trend, interference from sharp band of Pr^{3+} changes its shape towards more Lorentzian-like trend.

-525-530 *nm* - weak emission band observed in this region may be attributed to Er^{3+} with the possible contribution of Ho^{3+} ions. Both of these activators show great similarities in their geochemical behaviour as well as the shape of cathodoluminescence spectra (Czaja et al., 2013). This makes determination of their relative contributions solely on the luminescence data very difficult.

- 538-555 *nm* - this spectral range is commonly attributed to luminescence from Tb^{3+} centres. While there exists little interference from other lanthanide ions - e.g. Er^{3+} - in this region, this band is in natural apatites commonly obscured by the broad band of Mn-activated luminescence similar to that in carbonates. In the case of interference from Er^{3+} ions, shape of the band is more asymmetric with maximum values occurring in lower wavelengths around 540 *nm*.

- 555-570 *nm* - one of the Sm^{3+} bands observed in this range is usually heavily overlapped by the combination of Tb^{3+} band described above, broad Mn^{2+} band present in variable proportions in all natural

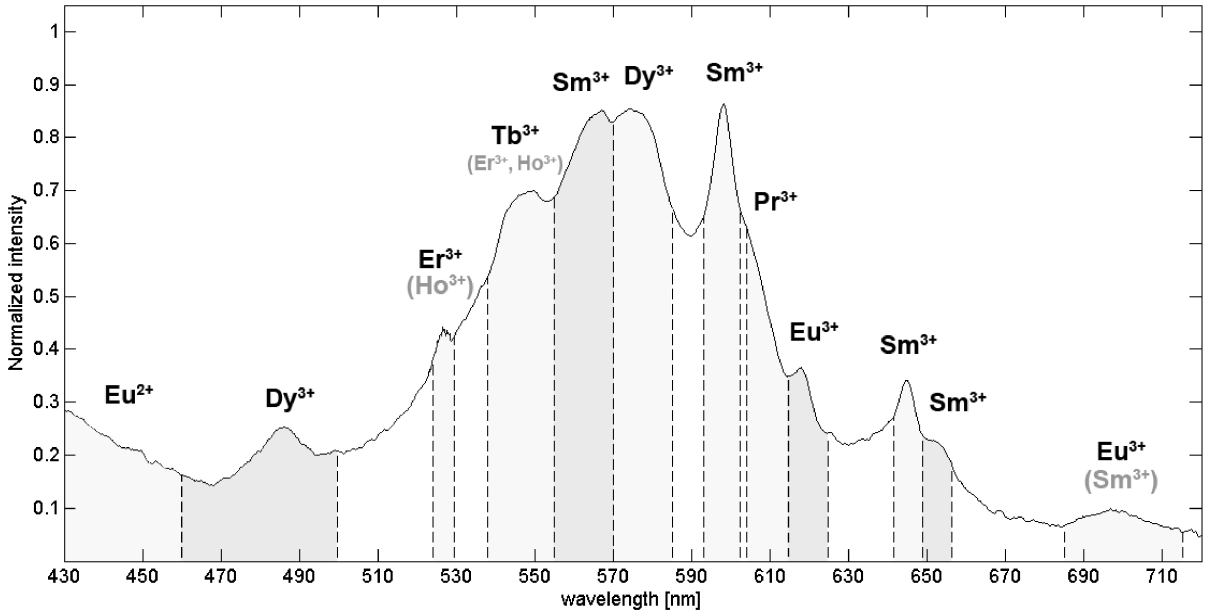

Fig. 10. Characteristic emission bands of lanthanide activators in cathodoluminescence spectra of apatites.

apatites, and additionally by Dy^{3+} band occurring at higher wavelengths. Therefore, it is often difficult to identify and quantify Sm^{3+} band in this range.

- 570-585 *nm* - as in the previous case, Dy^{3+} band that occurs in this region is usually overlapped by both Sm^{3+} and Mn^{2+} emission bands. One of the diagnostic features that may be utilized for identification of this band is common splitting that can be observed in its apical part, producing twin peaks with resulting M-shape of emission band.

- 593-602 *nm* - the strongest emission band from Sm^{3+} luminescence centres observed in this region is generally the most prominent and sharpest of all the emission bands occurring in this range, showing well-defined Lorentzian trend.

- 605-615 *nm* - band of Pr^{3+} with maximum intensity at around 607 *nm* is usually apparent only as a broadening of Sm^{3+} band whose right tail obscures shape of this emission band.

- 615-625 *nm* - Eu^{3+} shows in this region weak luminescence that is often obscured by stronger emissions by Mn^{2+}, Sm^{3+}, and Pr^{3+}.

- 642-649 *nm* - another sharp Lorentzian-shaped emission band of Sm^{3+} which shows variable degree of interference from weaker broad band of Dy^{3+} that lifts tails of this sharp band in the region between around 630 and 650 *nm*.

- 651-656 *nm* - another weaker band of Sm^{3+} occurring along the one described above and usually showing good correlation with the intensity of this stronger emission. In some cases, this can be obscured by luminescence of Er^{3+} which shows maxima of one of its emission bands in the same region.

- 685-715 *nm* - last emission band observed in the studied region represented by a broad band of low intensity in this range can be attributed to the combination of bands from Eu^{3+} and Sm^{3+}. Contribution of each of these components may be assessed by analysing relative intensities of other emission bands of these elements described above.

Once we identified all the characteristic emission bands that occur in obtained spectra, it is possible to proceed with their analysis. As we discussed in section 1.3.2 it is possible to distinguish two major types of apatite spectra - those dominated by the activation from Mn^{2+} centres with characteristic pseudo-Gaussian shape and those where contribution of Mn is lower and dominant type of luminescence is that from lanthanide luminescence centres. This trend can be linked directly to the chemistry of hosting rock as shown by Kempe & Götze (2002), with Mn^{2+} being the dominant activator in granites, pegmatites, and other felsic rocks, while in alkaline rocks, lanthanides are the dominant activator of luminescence in apatites. Our data agree with these observations with all samples of granites (MM1-MM7 and CE1-CE3) as well as those of paragneisses (PMM1-PMM4, PCB1, and PCE1) falling into the group with Mn-dominated apatite luminescence. Additionally, one group of spectra representing gabbro from Mařiž (MA2) also shows Mn-dominated luminescence dissimilar to that from the other group of spectra (MA1) from the same locality that shows activation by lanthanides. Reasons for this dichotomy will be discussed in section 5.2.

All the remaining luminescence spectra - i.e. those from durbachite, rhyolite, quartzite, granulite, and

biogenic materials were classified as lanthanide-dominated. Even though some of these spectra - e.g. those of quartzites or granulites - show substantial contribution from the Mn-component, emission bands of lanthanides are not obscured by this luminescence and are easily discernable and identifiable.

For Mn-dominated spectra where lanthanide emission bands are undistinguishable, we employ identical method of least-squares fitting of Gaussian curve as described for carbonates in section 4.1.1. However, analysis of variability among the centroids - i.e. values of *b* coefficients - of curves obtained in this way shows great degree of overlap between the different localities and rock types (Fig. 11) and thus it is not possible to utilize these values for preliminary partial classification or dataset reduction. Therefore, further analysis of these spectra will be employed on the residual data that are obtained by the subtraction of fitted Gaussian curve from the original spectrum and subsequent normalization of obtained values by the multiplication of each individual data point and corresponding value of fitted curve. This method ensures suppression of marginal regions with high noise-to-signal ratios and thus amplifies information from the central part of analysed range in a same way as described for carbonate samples in section 4.1.1. Normalized residual spectra obtained in this way, as well as spectra from the second group dominated by lanthanide emission will be subsequently analysed and following features will be assessed:

- presence or absence of specific emission lines in cathodoluminescence spectra,
- relative contributions of individual activators to overall luminescence emission and characteristics of this luminescence for various rock types, and
- effect of crystallographic orientation of apatite crystals on the final shape of spectrum.

Last of the three points presents an important factor influencing luminescence of apatites which is usually neglected in spectroscopic studies of these minerals. Various workers studied this phenomenon and

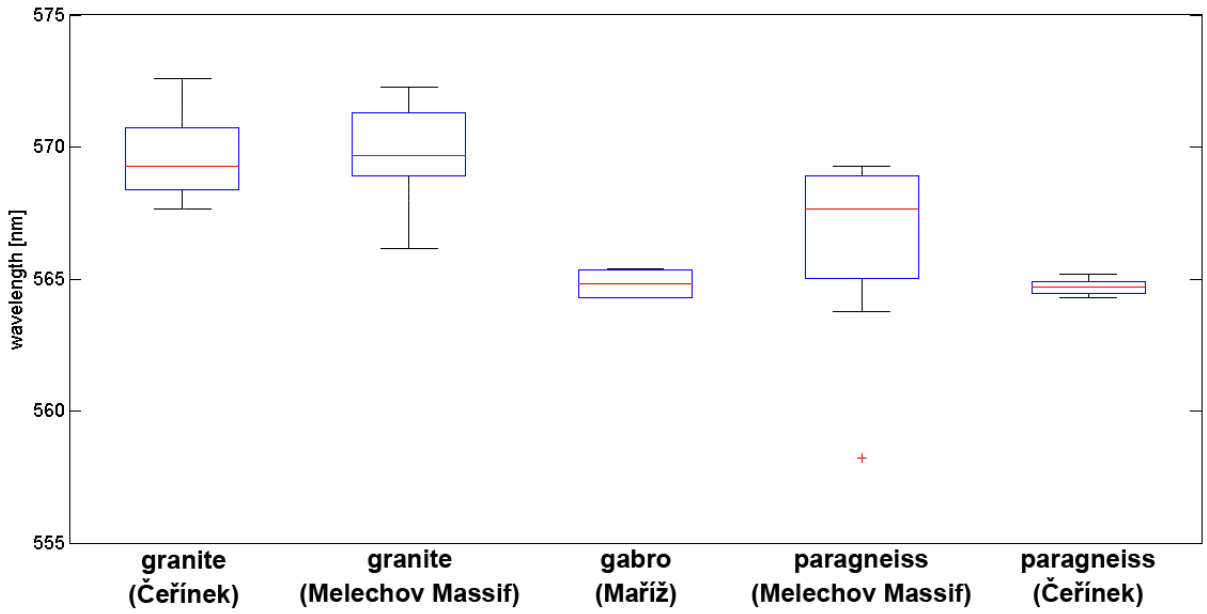

Fig. 11. Variability of centroids in different rock types and localities. Whiskers represent 1.5 interquartile range.

report following observations:

Murray and Oreskes (1997) examined sections of apatite crystals perpendicular and parallel to crystallographic axis *c* and observed that emission band intensity of some activators - such as Sm^{3+} - is stronger in perpendicular sections, while those of others - such as Dy^{3+} - are more pronounced in parallel sections.

Barbarand and Pagel (2001) report that shapes of Mn-dominated luminescence spectra are the same for both basal and prismatic sections but conclude that only the latter should be employed for the analysis of luminescence as these show higher overall intensities and thus lower noise-to-signal ratio. These authors explain differences in observed intensities by the effect of preferential diffusion of activator ions along the *c*-axis of apatite crystals.

More recently, Lenz et al., (2013) examined effect of crystallographic orientation on the lanthanide-activated luminescence of some phosphate and silicate minerals. They report considerable variations in the relative intensities of individual emission bands as a function of this orientation and propose explanation based on the crystal field theory where difference in observed spectra may be explained by the variations in charge distribution around the lanthanide luminescence centres in different sections of a crystal.

Thus, it is apparent that crystallographic orientation of analysed apatite crystals may have great impact on the characteristics of obtained spectroscopic data. Therefore, we will attempt to evaluate extent of this phenomenon in our spectra and subsequently, to assess how this relates to the potential of apatite luminescence spectroscopy as a tool for provenance determination.

5.1 Results of carbonate analysis

Dataset selection: Selection of spectra from the database that are matched against the analysed unknown sample is one of the crucial steps of analysis as it determines the overall success of our matching method. Therefore, it is necessary to assess whether the values of *b* coefficients - i.e. centroids - obtained by the curve fitting method present groups and ranges specific for each given locality and further, whether overlap of their variability between individual localities is sufficiently low to permit efficient selection of spectra from the database.

Fig. 12 shows variability of *b* coefficients for all five localities studied in this work. For localities Čertovy Schody (CS) and Bohdaneč (227) variability of centroids for both calcitic and dolomitic samples is shown. These results demonstrate that variability of dolomitic samples is considerably higher than that of calcitic samples from the same locality. Whether this is a general feature of dolomitic samples is uncertain as only two of the studied localities in our dataset include this type of spectra.

Box plots of centroid variability for calcitic spectra show relatively compact ranges for each locality. While some of these are completely or almost completely free of mutual overlap, others overlap substantially. More compact nature of within-locality centroid variation should in theory provide generally better results of selection from the database. However, actual results of this selection will be determined by the combination of following factors:

- *position of analysed unknown spectrum* - i.e. of its *b* coefficient - relative to each cluster of coefficients

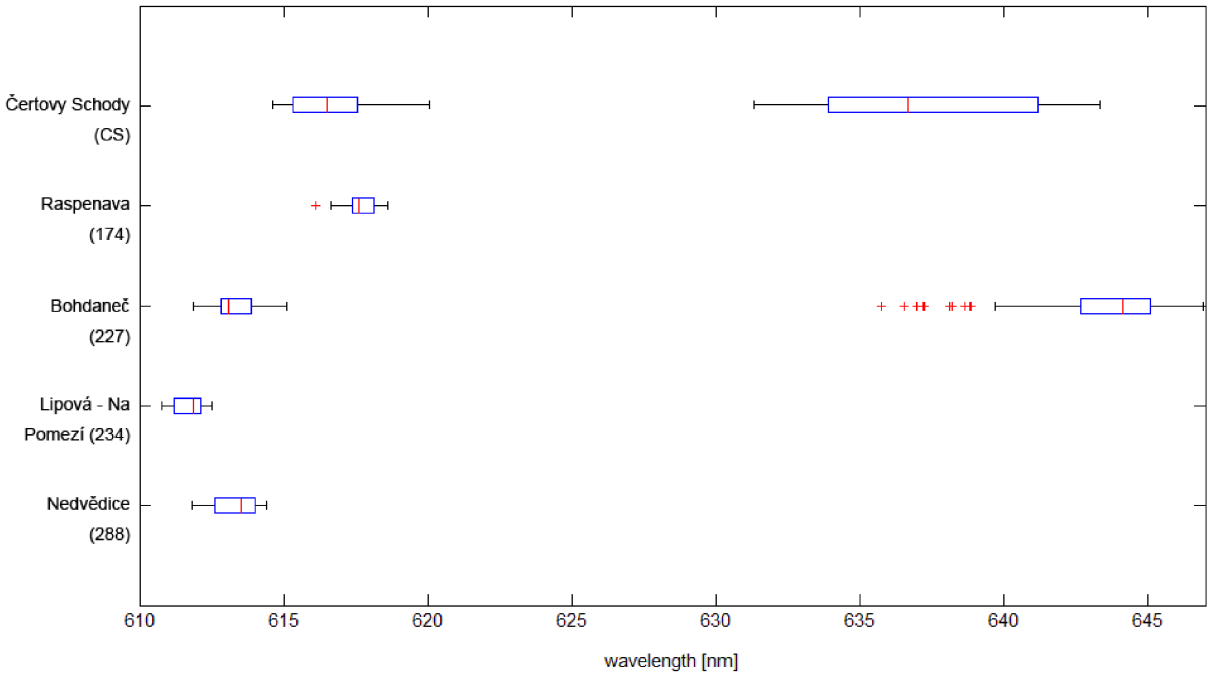

Fig. 12. Variability of centroids in calcitic and dolomitic samples from different localities. Whiskers represent 1.5 interquartile range.

from individual localities. If *b* coefficient of analysed spectrum represents one of the marginal members of cluster belonging to database entries from its correct locality and this region of cluster is overlapped by values of some other neighbouring group, results of dataset selection will contain higher proportion of spectra belonging to this other - possibly unrelated - group of samples.

- *degree of overlap between the individual groups* - previous point implies that the portion of correctly selected spectra will decrease with increasing number of clusters that overlap as well as with increasing degree of this overlap.

- *symmetry of database coefficient distribution around the coefficient of analysed spectrum* - effect of asymmetry may be observed when there exists a considerable difference in spacing between the values of two or more clusters that overlap range around the value of analysed coefficient. While cluster with wider spacing between its values may contain value that is closest to analysed coefficient, its next value may lay much further away and thus, several values of another cluster with more narrow distribution are likely to occur in the region between the two values of the first cluster. In this way, more samples will be generally selected from groups showing higher density of coefficient distribution in the range around the value of coefficient belonging to analysed unknown sample.

Effects described above as observed in our dataset are illustrated on examples in Tab. 2. Random spectrum was selected from spectra of each thin section of calcitic samples. In order to suppress possible effects of preference for spectra from the same thin section, average spectrum was calculated by combining one spectrum from each thin section from a given locality, thus obtaining average spectrum for each locality with random position of coefficient *b*. This method was employed as an alternative to simple averaging of all spectra from each locality which would provide resulting spectrum with centroid representing mean value of centroids in each cluster and thus would inevitably provide biassed results of dataset selection. Individual dataset selection was then performed for each spectrum obtained in this way and effect of variable size of the dataset - between 10 and 100 spectra - was assessed.

Results in Tab. 2 clearly show that method of dataset selection based on the similarity of centroids is very effective for all studied localities. By the examination of these data it can be seen that when size of selected dataset is too low, there may arise problem with representativeness of this set as majority of selected spectra may represent only one locality. While this is a good indication that the dominant group represents true provenance of an analysed sample, this may not always hold true in a more heavily overlapped database. Thus, for meaningful analysis of spectral similarity and provenance determination it is advisable to work with datasets of bigger size.

Another variable that needs to be considered is the number of spectra for each individual locality stored in the database. For localities represented by the lower amount of database entries it is generally preferable to select smaller dataset. This can be shown on an example of locality Raspenava (174) for which all of the database entries are included when the selection size reaches 30 spectra. Thus, no additional correct matches can be gained by further increase of dataset size.

As discussed above, another factor that will influence appropriate size of dataset selection is variability

Tab. 2. Number of selected correct spectra for analysed sample from each locality as a function of dataset size. Values in borders represent points at which maximum number of correct matches from the database is included in the dataset.

	Nedvědice (288)	**Lipová - Na Pomezí (234)**	**Bohdaneč (227)**	**Raspenava (174)**	**Čertovy Schody (CS)**
Spectra in DB	60	39	40	19	27
Size of dataset					
10	10	10	9	5	5
20	18	17	16	13	9
30	27	25	23	19	12
40	35	29	30		21
50	41	31	31		26
60	50	31	31		26
70	56	31	31		27
80	60	31	34		
90		31	35		
100		31	36		

of each group in the range around the coefficient value of analysed sample. It can be seen from Tab. 2 that for locality Nedvědice (288) having the most database entries, all of these are included when dataset contains 80 spectra. In contrast, entries corresponding to localities Lipová - Na Pomezí (234) and Bohdaneč (227) are not completely represented even when size of the dataset reaches 100 spectra. While from box plots in Fig. 12 it may seem that the degree of variability of these three groups is not that different, relative position of each analysed spectrum within the group must be also considered as described above. Results for each sample representing individual studied locality reported below were obtained by complete analysis of all entries in our current database.

Variability of original and residual spectra: Fig. 13a illustrates degree of variability between the normalized spectra obtained from the samples of all studied localities including both calcitic and dolomitic samples. Each spectrum represents average of all samples from a given locality. It can be noted that these spectra have very similar positions, widths, and share many of the minor features that occur along their pseudo-Gaussian trend. Difference in shape between the two localities of dolomitic samples is greater than that observed in calcitic group and thus these two localities can be distinguished without a difficulty.

Fig. 13b illustrates how variability from Fig. 13a is amplified after the transformation of normalized

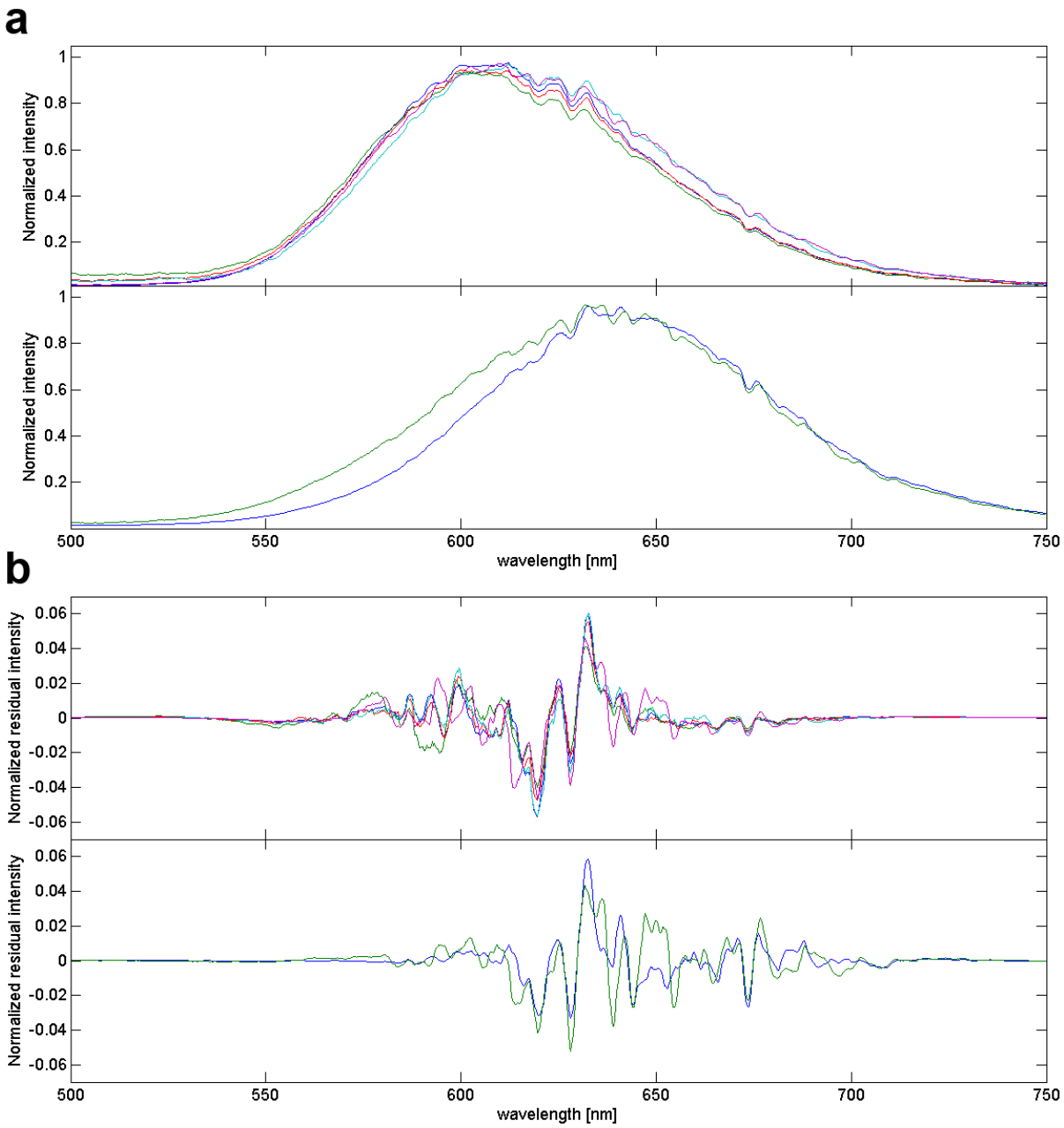

Fig. 13. a - average normalized cathodoluminescence spectra of calcitic (top) and dolomitic (bottom) samples from studied localities. b - corresponding average normalized residual spectra obtained by subtraction of Gaussian trend.

spectra to normalized residual spectra. Identification of two distinct groups of dolomitic samples is in this case even more straightforward, while for the calcitic samples it is still problematic to identify individual localities purely by visual examination. Thus, in the following paragraphs are reported only results for calcitic samples that present more difficult case of provenance determination when only the simplest measures of similarity are employed. Two types of data - normalized original data and normalized residual data - that are used for the analysis will be further referred to simply as *original data* and *residual data.*

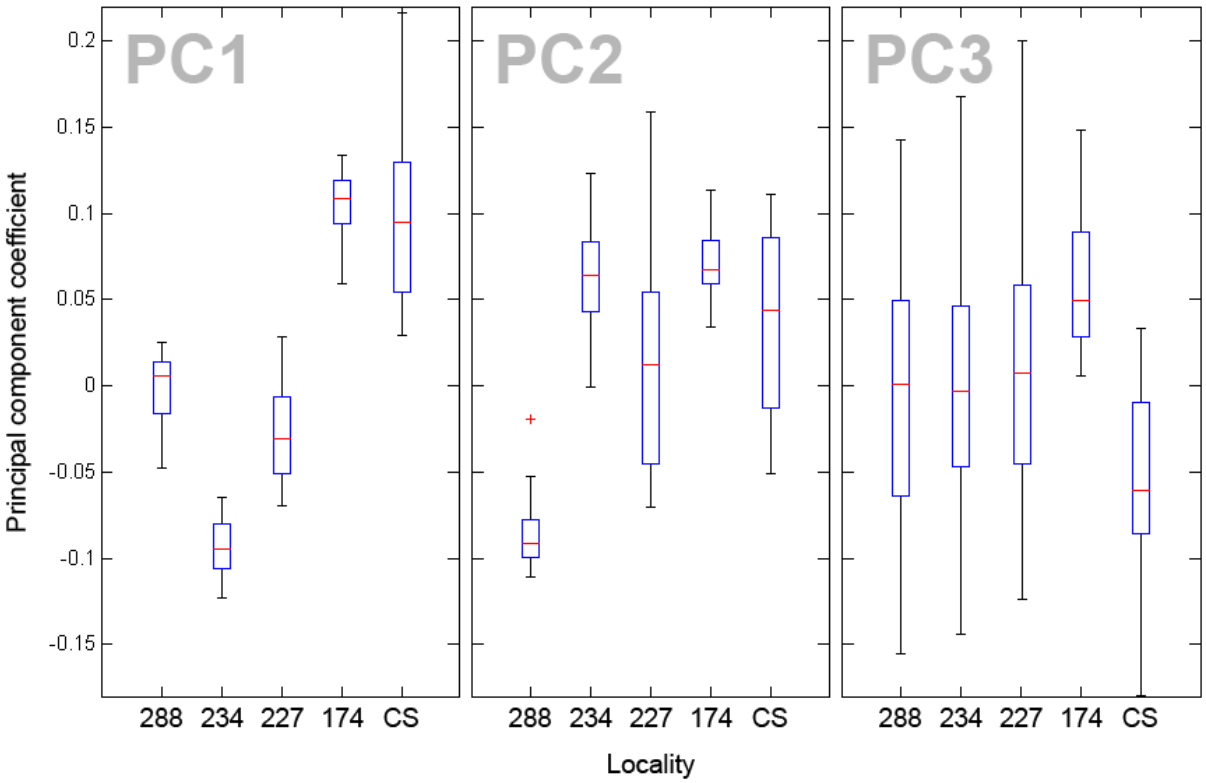

Fig. 14. Variability of principal component coefficients (loadings) between the studied localities for the first three principal components. Whiskers represent 1.5 interquartile range.

Principal component analysis: Before we proceed with our analysis it is necessary to evaluate results of modified principal component analysis - as proposed in section 4.1.2 - and determine which of the obtained principal components provides the best results when absolute differences of its coefficients are calculated. Fig. 14 shows variability of these coefficients between the studied localities for the first three principal components. It is apparent that only the first and second component produce results that may be utilized for determination of provenance, while variability of the third component - and components of higher order - is not sufficiently specific between the studied localities. By comparing results obtained from coefficients of first and second component for both original and residual data for each locality (Appendix A), it was determined that for the analysis of original spectra it is more appropriate to use the former, while for the residual spectra the latter provides better results.

Analysis and meta-analysis of spectral similarity: Results of spectral analysis for each of the studied localities are illustrated in Fig. 15. Two figures for each locality represent results obtained from the analysis of original spectra (left) and residual spectra (right) of selected dataset which is in this case comprised of all spectra in the database. Both figures contain five columns for individual studied localities and colour of each square represents value of correlation - ranging from 0 to 1 - between an unknown analysed spectrum and spectra of given localities. Value in each square is calculated as an arithmetic mean of correlation coefficients for all spectra representing this locality. Seven rows in these

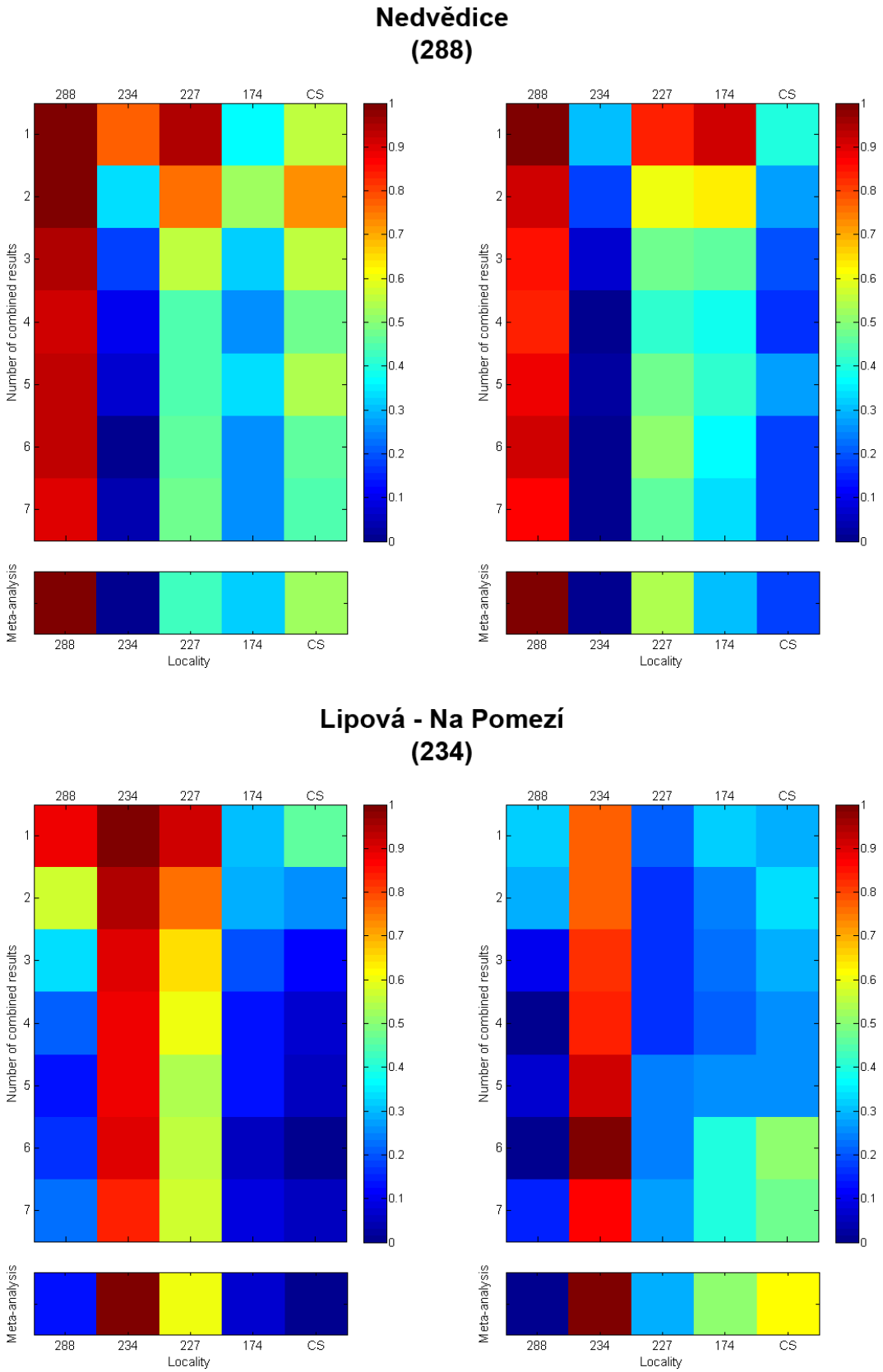

Fig. 15. Values of correlation coefficients in each step of analysis based on the original data (left) and residual data (right). Below are reported results of meta-analysis evaluating trend along the rows 1-7.

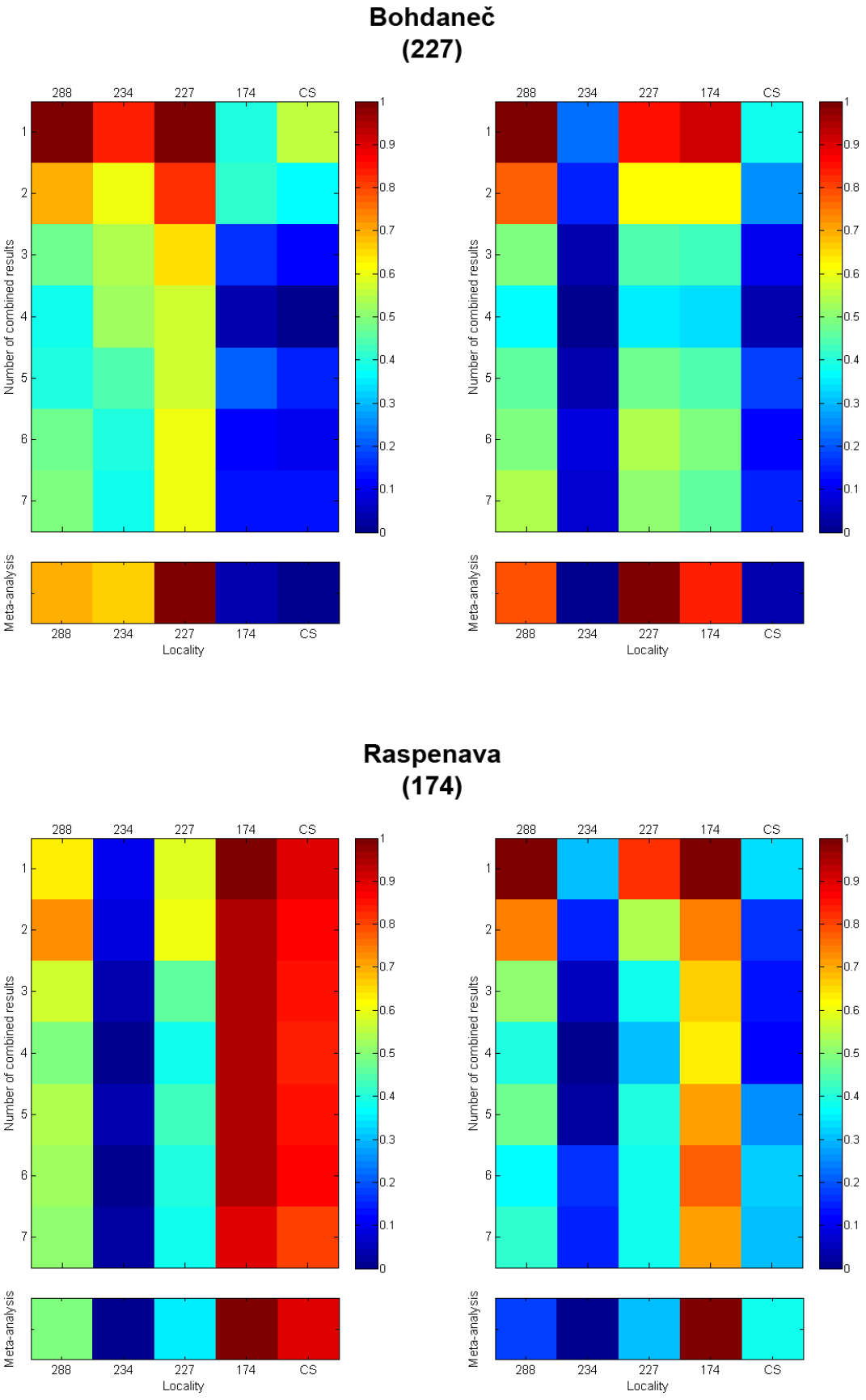

Fig. 15. (continued).

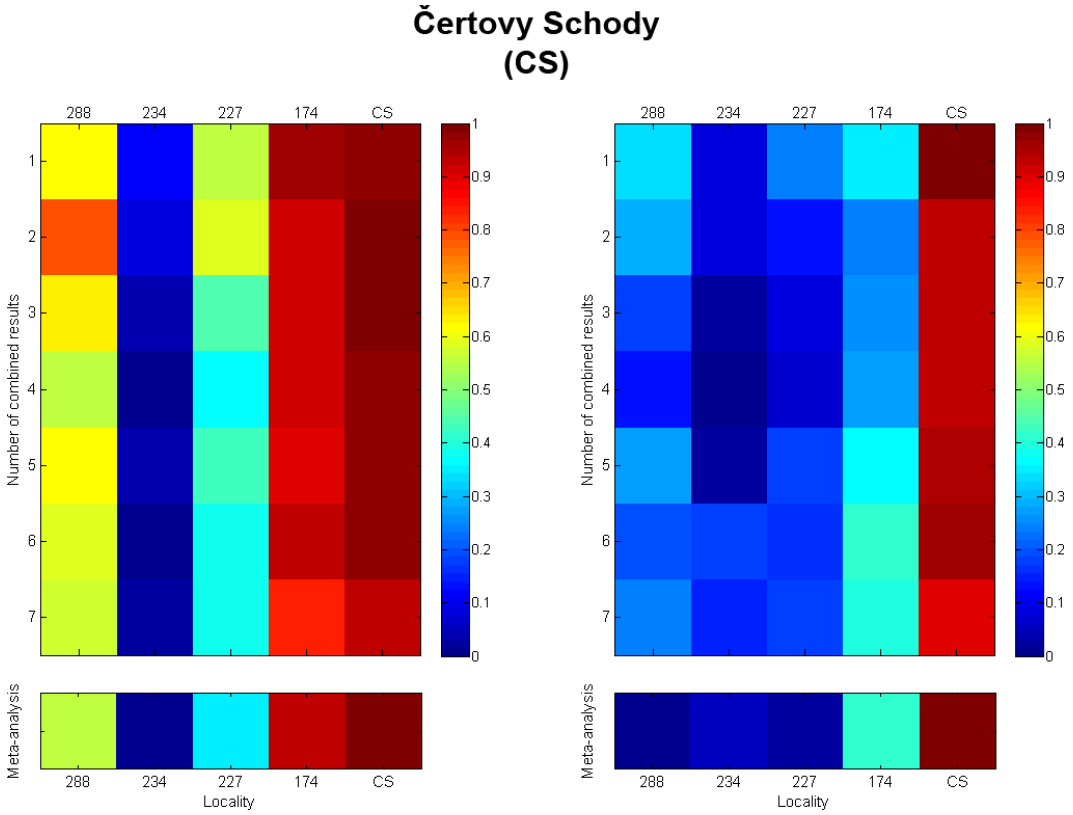

Fig. 15. (continued).

figures correspond to seven partial steps where values of correlation matrices A-G are combined as described in section 4.1.3. Sum in each step of addition is divided by the number of combined matrices in order to preserve relative scaling of results. Under the results of analysis for both original and residual data are presented results of meta-analysis which evaluates trend along the partial correlation coefficients in rows 1-7 - prior to their division - by the method described in section 4.1.4.

Brief description and assessment of obtained results for each locality are presented below.

Locality Nedvědice (288) - Identification of sample from this locality was straightforward from both original and residual data. While in the first and second step of analysis it is possible to observe high values of correlation with other localities, these are substantially lowered in the subsequent steps. In the last - seventh - step of analysis, only the samples from correctly identified locality Nedvědice (288) show value of average correlation above 0.8 for both types of data. By employing meta-analysis of these results, difference between the correct locality and the rest of the dataset is further amplified with value for Nedvědice (288) approaching 1 while those of other localities laying below the value of 0.6. In this particular case, analysis of original data would be sufficient for correct identification. Nevertheless, residual data further confirm results obtained by this analysis.

Locality Lipová - Na Pomezí (234) - In this case, identification based on the original data was not as straightforward as in the case discussed above. First two steps of analysis are again inconclusive as before, while the highest degree of correlation is in all steps correctly observed for locality 234.

However, persistence of higher values for locality 227 may be observed in the course of the analysis, even though these show gradually decreasing trend. Additionally, upon the meta-analysis of results this value is again increased to around 0.6. While this value is relatively low when compared with that for correct locality 234 which approaches 1, there may still remain some uncertainty of determination between the localities 234 and 227. This is resolved by examining results from residual data which show consistently low values of coefficients for incorrect locality 227. Upon the meta-analysis, however, value of coefficient corresponding to locality CS is increased to level comparable to that of locality 227 in the first case and thus there again arises doubt concerning identification of this locality. Clear identification of correct locality is obtained by combining results of meta-analysis from both types of data, whereupon values for both localities 227 and CS decrease as a result of averaging between the two types of results.

Locality Bohdaneč (227) - Spectra obtained from samples of this locality are characterized by very low intensities of cathodoluminescence emission. This is reflected in high contribution of noise to these spectra which makes their identification more difficult. While results from original data show consistently highest values of correlation for the correct locality 227, it is also possible to observe persistent trend of increased values for localities 288 and 234 which is preserved even in the results of meta-analysis. In a similar way, higher values are observed for localities 288 and 174 in analysis and meta-analysis of residual data. By the combination of these two types of data it is readily possible to exclude locality 234 - with consistently low values in analysis of residual data - as well as locality 174 - which shows consistently low correlation in the analysis of original data. Thus, only two possible localities remain - correctly identified locality 227 with the value of correlation coefficient approaching 1 and locality 288 which shows increased values between 0.7-0.8. Distinction between these two localities can be made by examining results of meta-analysis for individual spectra sorted in descending order (Appendix B). It can be seen that in results of meta-analysis based on the original data, 24 out of 30 highest values of correlation coefficient are represented by spectra from locality 227, while only 5 belong to locality 288. Results from meta-analysis of residual data show similar trend with 23 out of 30 highest correlation coefficients represented by locality 227 and only two by locality 288.

Locality Raspenava (174) - As in the previous cases, each step of analysis employing original data shows highest values of correlation for correct locality 174. However, in this case it is observed that values for locality CS are only slightly lower in the whole course of analysis as well as after meta-analysis of results. In contrast to this, identification based on the residual data is absolutely straightforward, once again demonstrating ability of residual spectra to amplify information contained in the original data.

Locality Čertovy Schody (CS) - This case is analogous to that described above, with the only difference being that results of residual data analysis obtained for this locality provide unequivocal identification of correct locality in every single step of analysis.

Thus, we have successfully demonstrated good performance of our combined analysis of original and residual data connected with meta-analysis of its results and confirmed its applicability for quick determination of provenance based on the cathodoluminescence signatures of carbonate samples from

various quarries in Bohemian Massif.

Hierarchical clustering: In order to identify most appropriate way of clustering for cathodoluminescence data used in this work, each of the twelve possible methods of hierarchical clustering was performed. These twelve methods present all possible combinations of three distance metrics - City block, Euclidean, and Minkowski - with four linkage methods - average, single, complete, and Ward's - as described in section 4.1.2. These were applied to six different datasets including original data of all spectra in the database, their corresponding residual spectra, overall results of analysis for both of these datasets, and additionally, data from the meta-analysis of these results. Thus, we obtained 72 different methods of hierarchical clustering. To assess which of these methods is the most appropriate for our data, *cophenetic correlation coefficient* was calculated for each of the 72 cluster trees. This is given as:

$$c = \frac{\sum_{i<j}(x_{ij} - \bar{x})(y_{ij} - \bar{y})}{\sqrt{\sum_{i<j}(x_{ij} - \bar{x})^2 \sum_{i<j}(y_{ij} - \bar{y})^2}} \tag{17}$$

where x_{ij} is the distance between spectra i and j calculated by one of the distance metrics, y_{ij} is the cophenetic distance between these spectra in the cluster tree calculated by one of the linkage methods, and $\bar{x}$, $\bar{y}$ represent average values of these distances for the whole dataset. Cophenetic correlation coefficient behaves in a similar way as classical correlation coefficients with values closer to 1 showing better correlation of distances between spectra in original dataset with those in the cluster tree, indicating that this represents good representation of dataset variability. Complete list of cophenetic correlation coefficients is presented in Table 3.

Most of the coefficients for original data show increase of values for overall results of analysis, and still further increase for results of meta-analysis. While this may indicate that results obtained from analysis and meta-analysis are more appropriate for hierarchical clustering than the original spectra, it will be shown below that this is not always the case when we are concerned with correct classification of spectra based on the provenance.

The trend observed for original data is not observed for the three datasets based on the residual data where most of the coefficients show highest values for hierarchical trees of residual spectra, lower for results of meta-analysis, and the lowest values for overall results of analysis. From each of these six datasets were selected two cluster trees representing two most efficient linkage methods along with the corresponding distance metric that provides the highest value of cophenetic correlation coefficient for this linkage methods. Due to variability of its coefficients, third combination was selected for residual data. Results for these selected cluster trees are briefly summarized below.

Original data:

- *Minkowski distance with average linkage* (c = 0.855) - Out of 185 spectra in the dataset 157 were classified correctly, representing 84.9 % of the dataset.

Tab. 3. Values of cophenetic correlation coefficient for all methods of hierarchical clustering based on the three distance metrics and four linkage methods employed. Values in bold borders represent selected methods for which performance was evaluated (see text).

Original data	average	single	complete	Ward's	**Residual data**	average	single	complete	Ward's
City block	0.844	0.688	0.830	0.830		0.899	0.897	0.925	0.794
Euclidean	0.850	0.717	0.868	0.830		0.918	0.918	0.902	0.800
Minkowski (p = 3)	0.855	0.731	0.853	0.844		0.934	0.924	0.888	0.818
Overall results of analysis					**Overall results of analysis**				
City block	0.908	0.860	0.883	0.899		0.821	0.574	0.870	0.818
Euclidean	0.904	0.853	0.878	0.899		0.858	0.648	0.868	0.815
Minkowski (p = 3)	0.901	0.837	0.777	0.895		0.869	0.719	0.844	0.815
Results of meta-analysis					**Results of meta-analysis**				
City block	0.909	0.876	0.894	0.918		0.893	0.619	0.889	0.878
Euclidean	0.911	0.857	0.914	0.917		0.887	0.657	0.856	0.810
Minkowski (p = 3)	0.922	0.777	0.874	0.910		0.880	0.670	0.883	0.824

- *Euclidean distance with complete linkage* (c = 0.868) - results of this combination show high degree of inconsistency on the lowest levels of obtained cluster tree. Only 100 of 185 spectra (54.1 %) were classified correctly.

Overall results from analysis of original data:

- *City block distance with average linkage* (c = 0.908) - 120 of 185 spectra (64.9 %) classified correctly.
- *City block distance with Ward's linkage* (c = 0.899) - 115 of 185 spectra (62.2 %) classified correctly.

Results from meta-analysis of normalized original data:

- *Minkowski distance with average linkage* (c = 0.922) - 126 of 185 spectra (68.1 %) classified correctly.
- *City block distance with Ward's linkage* (c = 0.918) - 117 of 185 spectra (63.2 %) classified correctly.

These results show that best method for hierarchical clustering of the three datasets presented above is that based on the analysis of original data utilizing Minkowski distance with the value of coefficient p = 3 and average method of linkage. Fact that this particular method shows the lowest value of cophenetic correlation coefficient of all six selected combinations demonstrates that choice of method for hierarchical clustering of a given dataset should not be based solely on the value of this coefficient. Results of remaining three datasets based on the residual spectra are as follows:

Residual data:

- *Minkowski distance with average linkage* (c = 0.934) - while value of cophenetic correlation coefficient indicates good correlation of distances in the cluster tree with those in the dataset of residual spectra, linkage in this tree shows high degree of inconsistency with resulting classification of 151 out of 185 spectra into the same cluster. This method is therefore inappropriate for the classification of these data based on their provenance.
- *Minkowski distance with single linkage* (c = 0.924) - as in the previous case, this method failed to produce meaningful results. 181 of 185 spectra were classified into the same cluster.
- *City block distance with complete linkage* (c = 0.925) - results of this method are similar to those described above with 129 of 185 spectra classified into the same cluster.

Overall results from analysis of residual data:

- *Minkowski distance with average linkage* (c = 0.869) - out of 185 spectra in the dataset 153 were classified correctly, representing 82.7 % of dataset.
- *City block distance with complete linkage* (c = 0.870) - 145 of 185 spectra (78.4 %) classified correctly.

Results from meta-analysis of residual data:

- *City block distance with average linkage* (c = 0.893) - 140 of 185 spectra (75.7 %) classified correctly.
- *City block distance with complete linkage* (c = 0.889) -130 of 185 spectra (70.3 %) classified correctly.

These results again show that best results are obtained for method with the lowest value of cophenetic correlation coefficient of all six selected combinations. Here, this is represented by the method based on overall results from analysis of residual data utilizing Minkowski distance with the value of coefficient p = 3 and average method of linkage.

Thus, it is concluded that when concerned with the provenance of samples, best method for hierarchical

clustering of their cathodoluminescence data is the one combining Minkowski distance with average linkage method for original spectra and overall results from the analysis of the residual spectra, providing in both cases correct classification of more than 80 % of dataset studied in this work. Dendrograms constructed from results of both of these methods are illustrated in Appendix C.

5.2 Results of apatite analysis

Below are briefly presented results obtained from the analysis of apatite spectroscopic data. As lanthanide-dominated and Mn-dominated spectra were analysed by different approaches, results for each of these groups are presented separately. For further discussion of these results see section 6.

5.2.1 Lanthanide-dominated luminescence spectra of apatites

Durbachite: Cathodoluminescence data of durbachites from both studied localities - Kamenné Doly (DU1) and Vepice (DU2) - reveal very similar shapes of spectra containing identical emission bands as well as very close relative proportions of these bands (Fig. 16).

Wavelength range below 460 *nm* is dominated by the prominent broad emission band of Eu^{2+} with gradually increasing intensity towards the lower limit of analysed range. Interestingly, emission bands that would indicate presence of trivalent Eu - e.g. that commonly occurring at 610-625 *nm* - are absent in all durbachite spectra. This could either indicate that trivalent Eu produces considerably less effective luminescence in comparison to its divalent form or alternatively, this may indicate higher proportions of divalent Eu in these apatites as a consequence of crystallization under reducing conditions. Some indications that may possibly point to the latter scenario will be discussed in the results reported for other

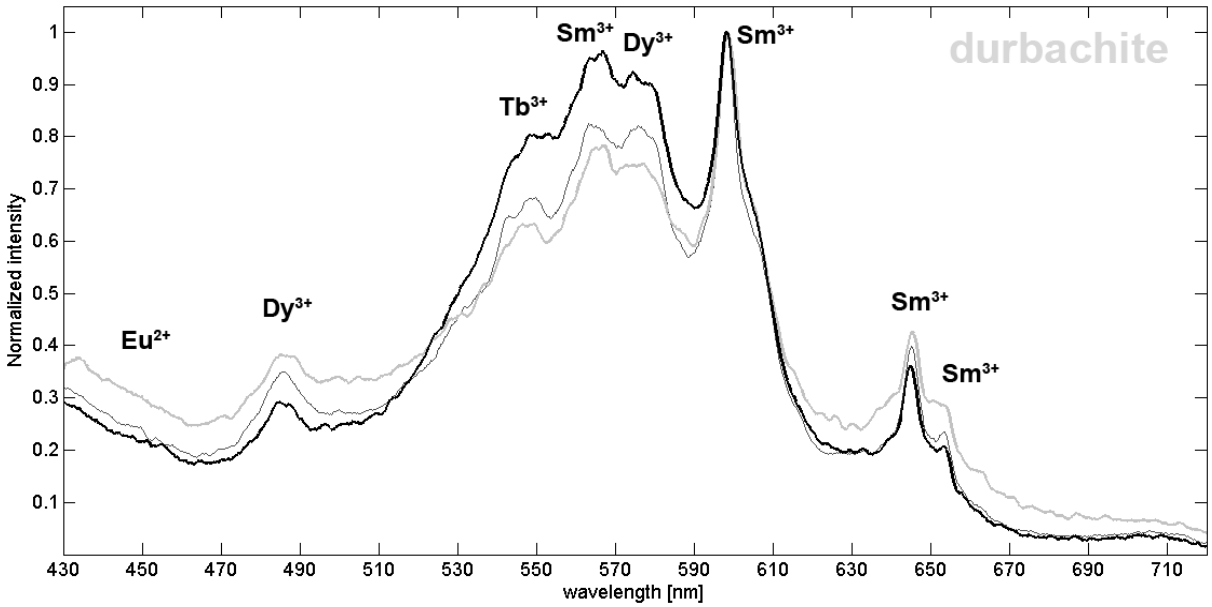

Fig. 16. Average cathodoluminescence spectra of apatites from samples of durbachite (DU1, DU2) with characteristic emission bands of lanthanide activators. For explanation of observed trend see text.

rock types below.

Continuing to the higher wavelengths, next emission band observed between 460 and 500 *nm* with maximum around 484 *nm* is that of Dy^{3+} . This band is accompanied by the other two Dy^{3+} emission bands at 570-585 and 630-650 *nm*. Peculiar trend observed in our durbachite samples is that increasing intensity of Tb^{3+}-Sm^{3+}-Dy^{3+} band triplet at 538-585 *nm* is connected with corresponding decrease of intensities for both Dy^{3+} (at 484 *nm*) and Sm^{3+} (at 640-655 *nm*) bands in the peripheral regions. We propose that this effect may be attributed to variable contribution from Mn^{2+} luminescence component and support this notion by the following observations:

1. In data without normalization, spectrum with the highest relative intensities of Tb^{3+}-Sm^{3+}-Dy^{3+} band triplet (black) shows the lowest intensities of luminescence, while spectrum with the lowest intensity of this triplet (light grey) shows the highest overall intensities. Thus, normalization of spectra induces reversal of observed trend for Mn-interfered bands in the middle of studied range, while preserving original trend in the marginal regions with little contribution of Mn-component.

2. Three bands within the triplet show little variation in their relative itensities - 1-1.1 for Sm^{3+}/Dy^{3+}, around 1.2 for Sm^{3+}/Tb^{3+}, and 1.1-1.2 for Dy^{3+}/Tb^{3+} - while ratios of two bands belonging to the same activator, where one is in the triplet and the other in the marginal region vary considerably - 2.1-2.7 for Sm^{3+}(555-570 *nm*)/Sm^{3+}(640-655 *nm*) and 2-3.2 for Dy^{3+}(570-585 *nm*)/Dy^{3+}(484 *nm*). Thus, it is apparent that intensities of bands in the Tb^{3+}-Sm^{3+}-Dy^{3+} band triplet are controlled by the same mechanism - i.e. convolution with Gaussian Mn^{2+} band of the same shape but variable intensity - while bands on the periphery remain mostly unaffected. This example of durbachite spectra clearly demonstrates importance of evaluating relative contribution from Mn luminescence component when analysing spectral trends and intensities of various lanthanide activators contributing to overall cathodoluminescence emission.

Gabbro: Spectra obtained from samples of gabbro from locality Mařiž (MA1, MA2) present a unique case in our dataset as they contain both Mn-dominated group with pseudo-Gaussian shape and maxima around 560-570 *nm* as well as those dominated by emission bands of lanthanides (Fig. 17). The latter are very similar to spectra of durbachites, the only exception being lower intensity of Eu^{2+} emission band and bands of Dy^{3+} indicating their reduced contents in apatites of these gabbros. This results in different shape of band triplet Tb^{3+}-Sm^{3+}-Dy^{3+} at 538-585 *nm*, with the dominance of Sm^{3+} band in the middle and lower Tb^{3+} and Dy^{3+} bands on each side.

Striking dichotomy between the two types of observed spectra may be partly explained by considering processes by which gabbroic bodies in this area were created. Ulrych et al. (2010) report layering of these bodies observed on *cm* scales and describe these formations as cummulates that formed in crustal chambers trough the process of fractional crystallization connected with the contamination by surrounding crustal material which resulted in formation of layers enriched in olivine + pyroxene and those enriched in feldspar. It is then possible that this variation in composition induced during the consecutive stages of intrusion may be an explanation for observed variability of cathodoluminescence spectra.

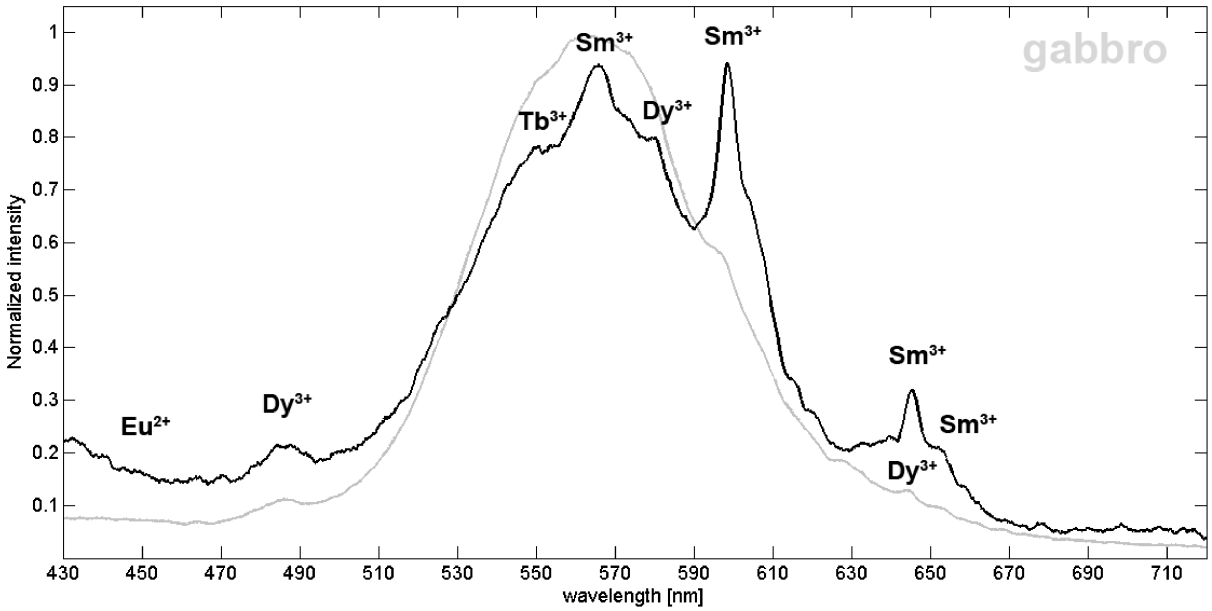

Fig. 17. Average cathodoluminescence spectra of apatites from samples of gabbro (MA1, MA2) showing both types of observed luminescence. For explanation of this dichotomy see text.

Rhyolite: Spectra of rhyolite from Fláje (RH1) in the Altenberg-Teplice Caldera show high degree of activation by lanthanides which is usually not expected in this type of acidic rocks (Fig. 18). This may be partially explained by examining specific geological evolution of these rhyolites.

Breiter et al. (2001) studied chemical properties of volcanic sequence in this area and describe trend of evolution from more acidic composition in basal units of rhyolites and dacites towards the less differentiated calc-alkaline Teplice rhyolite rich in potassium that forms younger units above. This shift of composition may be one of the factors that could explain observed characteristics of rhyolite cathodoluminescence spectra. Emission bands correspond to those observed in previous cases with the excepiton of Eu^{2+} band which is absent. This may present another indication that intensity of this band could be connected to the redox conditions during the apatite crystallization. As in the previous cases it is possible to identify four bands of Sm^{3+} (at 555-570 *nm*, 593-602 *nm*, 642-649 *nm*, and 651-656 *nm*), three bands of Dy^{3+} (at 460-500 *nm*, 570-585 *nm*, and 630-650 *nm*), and one band of Tb^{3+} (at 538-555 *nm*). While the most prominent emission band is that of Sm^{3+} at 593-602 *nm*, band of this ion in the middle of band triplet Tb^{3+}-Sm^{3+}-Dy^{3+} shows intensities slightly lower than those of Dy^{3+} band. This is in contrast with observations from durbachites and gabbros where this band shows higher intensities than that of Dy^{3+} even when its other band at 593-602 *nm* does not show such a degree of prominence as in the case of rhyolite. Size of our current dataset of rhyolite spectra is insufficient for assessment of trends between the relative band intensities in rhyolite samples. Thus, we can not exclude effect of variable crystallographic orientation on the shape of these luminescence spectra. Another possible cause of this phenomena may however stem directly from structural differences between apatites in plutonic and volcanic rocks. In theory, change of physico-chemical conditions in magma transported towards the areas

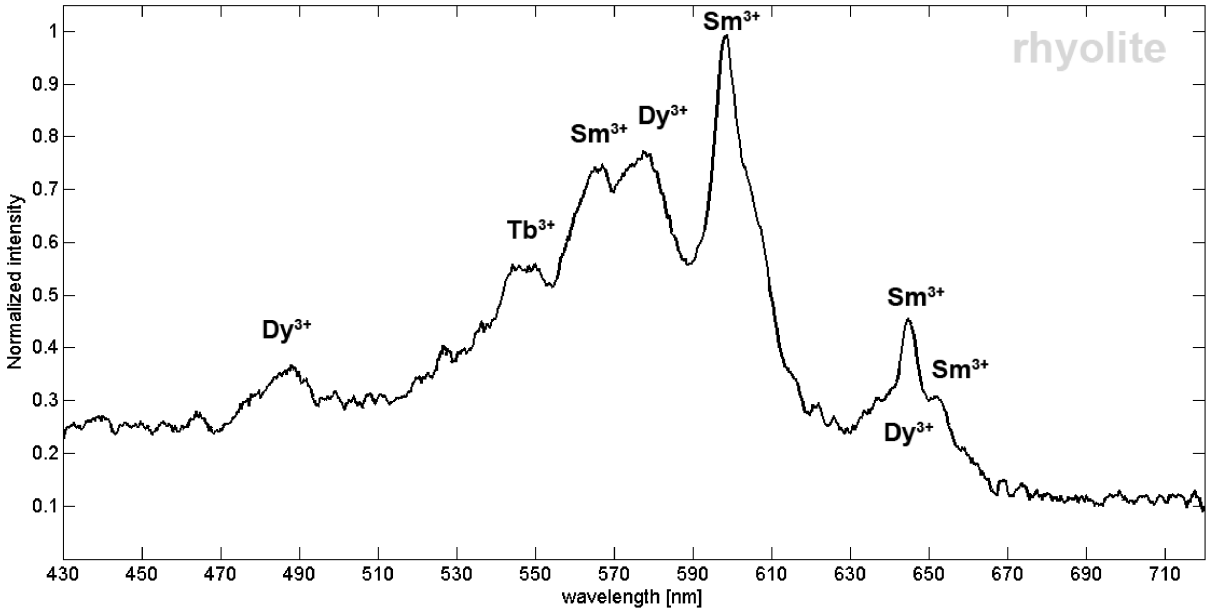

Fig. 18. Average cathodoluminescence spectrum of apatites from samples of rhyolite (RH1) with characteristic emission bands of lanthanide activators.

of lower pressure and temperature may produce site preference of Sm^{3+} between the two crystallographically different Ca-sites in apatite structure. This would then imply change in relative intensities of individual emission bands as a result of change in relative probabilities of individual emissive transitions producing these bands induced by the two different types of local crystal field.

Light lanthanides accommodated in apatite structure were found to prefer Ca2 sites over the Ca1 site due to the effects of charge equalization and strain minimization in the crystal lattice (Fleet & Pan, 1997a). However, degree of this site preference may be considerably influenced by the type of the dominant column anion (F, Cl, OH) which controls size of the Ca2 site, as well as by the concentrations of other cations competing for these crystallographic positions (Fleet & Pan, 1997b). Additionally, effects of elevated pressures and temperatures on the size and shape of coordination polyhedra should be also considered as an important factor controlling site preference of lanthanides in apatite structure.

Quartzites: Spectra of quartzites from the locality Rozkoš (Q1) and Těchobuz (Q2) show very dissimilar trends (Fig. 19). While both are characterized by high content of Mn luminescence component, bands corresponding to the lanthanide activators and their relative proportions are different.

Locality Rozkoš (Q1) is characterized by emission bands of very low intensity including those of Dy^{3+} (at 460-500 *nm* and 570-585 *nm*), Sm^{3+} (at 555-570 *nm*, 593-602 *nm*, and 642-649 *nm*), Tb^{3+} (at 538-555 *nm*), and additionally faint band of Eu^{3+} at approximately 625 *nm*. Luminescence of Dy^{3+} seems to be less effective than that of Sm^{3+} - probably due to their relative concentrations - and thus band triplet Tb^{3+}-Sm^{3+}-Dy^{3+} is dominated by Sm^{3+} band. Occurrence of Eu^{3+} band seems to be characteristic of this locality as it was not observed in any of the spectra described above.

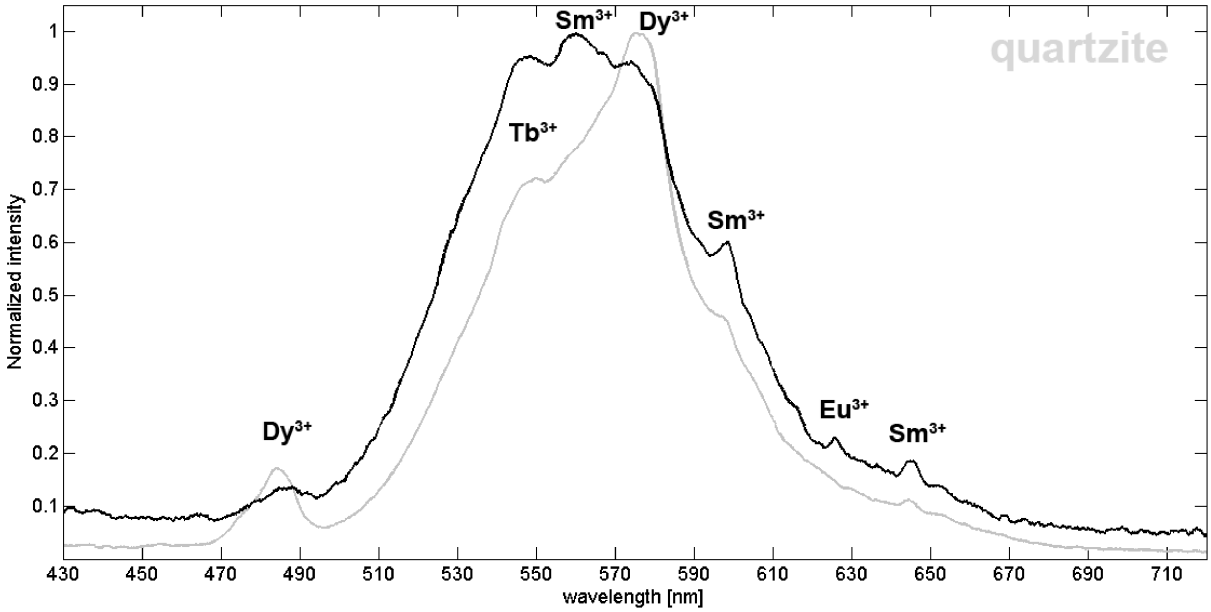

Fig. 19. Average cathodoluminescence spectra of apatites from samples of quartzite (Q1, Q2) with characteristic emission bands of lanthanide activators. For explanation of difference between these spectra see text.

Locality Těchobuz (Q2) shows striking dissimilarity of luminescence spectra with virtual absence of Sm^{3+} bands and dominance of well-defined bands of Dy^{3+} with smaller contribution from Tb^{3+}. Presence of Eu^{3+} emission band was not observed.

Difference in observed quartzite spectra are probably given by the fact that sedimentary protoliths of these rocks may contain apatites originating from all kinds of various rock types and geological settings. Thus, specificity of apatite luminescence signatures in sedimentary and meta-sedimentary rocks will depend on the homogeneity of apatite population in sedimentary material and this is in turn controlled by the number and variability of source areas from which this sedimentary material originated.

Granulites: Inhomogeneity of spectral data is characteristic also for granulites from Plešovice (PL1). In this case, however, continuous trend may be observed between the two types of lanthanide-dominated spectra identified (Fig. 20). First end-member of this trend is defined by the dominance of Dy^{3+} luminescence over that of Sm^{3+}, with dominant Dy^{3+} band at 570-585 *nm* and well defined band at 460-500 *nm*. Continuing along the proposed trend we observe gradual increase of intensity for emission bands of Sm^{3+} and decrease of those that belong to Dy^{3+}. Emission band of Tb^{3+} at 540-555 *nm* remains mostly unaffected along the whole trend.

Thus, question again arises whether this trend represents chemical variability of apatites in these rocks or whether this may be an effect of variable crystallographic orientations of analysed crystals. Our observations correspond to those of Murray and Oreskes (1997) that report attenuation of Sm^{3+} bands - along with the dominance of Dy^{3+} in Tb^{3+}-Sm^{3+}-Dy^{3+} band triplet - in apatite sections parallel to *c* axis and higher intensities of Sm^{3+} bands in sections perpendicular to *c*.

In our spectra, however, end-member with more pronounced Sm^{3+} bands shows an additional faint bands

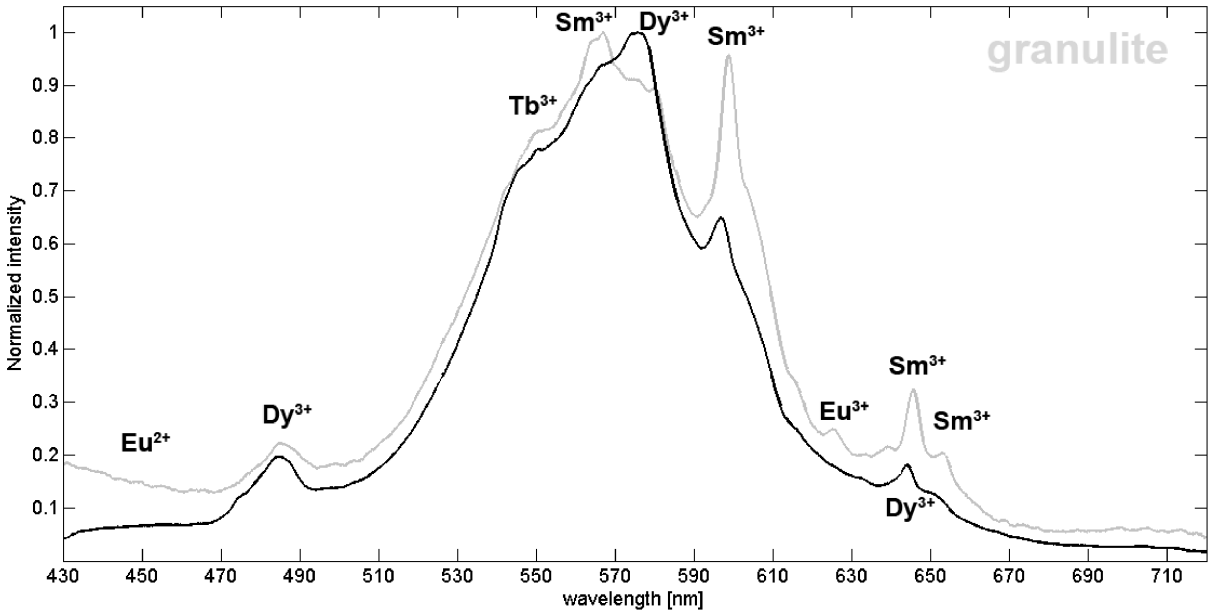

Fig. 20. Average cathodoluminescence spectra of apatites from samples of granulite (PL1) with characteristic emission bands of lanthanide activators. For explanation of observed trend see text.

at wavelengths below 460 *nm* and at around 625 *nm* which belong to Eu^{2+} and Eu^{3+}, respectively. As these are not present in spectra of end-member with more pronounce Dy^{3+} bands, this observation may point towards the scenario of chemical variability in the population of apatites in granulite samples. This may be further supported by the results of a complex analysis of these K-rich granulites by Janoušek et al. (2007). These authors conclude that fractional crystallization in the course of their evolution was controlled primarily by the apatite, garnet, and zircon present in the parent magma.

Biogenic apatites: Luminescence spectra of bioapatites from the shell (B1) - i. e. bone material - of Miocene turtle and the tooth of a fossil Pliocene rodent (B2) from Měňany are the most easily distinguishable as they contain several unique features (Fig. 21).

First, they show the lowest contributions from Mn^{2+}-activated luminescence which is a common feature of bioapatites as well as other biologically precipitated minerals such as carbonates as discussed in section 1.3.1. Spectra from both samples reach maximum intensity at around 600 *nm* where the strongest emission band of Sm^{3+} occurs. This is accompanied by other fainter band of this ion at 555-570 *nm*, well defined band at 642-649 *nm*, and an additional band of lower intensity at 651-656 *nm*. In spectra of shell (black), sharp band occurs in this last region. This, however, does not represent emission of Sm^{3+} but rather that of Pr^{3+} whose role as an activator in biologically precipitated apatites seems to be more important than in those from igneous and metamorphic rocks.

The most intense emission band of Pr^{3+} occurs at about 605-615 *nm* where it is often obscured by the tail of Sm^{3+} band. In spectra of shell, however, this band is clearly distinguishable from Sm^{3+} band. Third emission band of Pr^{3+} lies at around 485 *nm* where characteristic broad band of Dy^{3+} is observed. Contribution of Pr^{3+} emission to this band can be in this case distinguished by the shape of the band

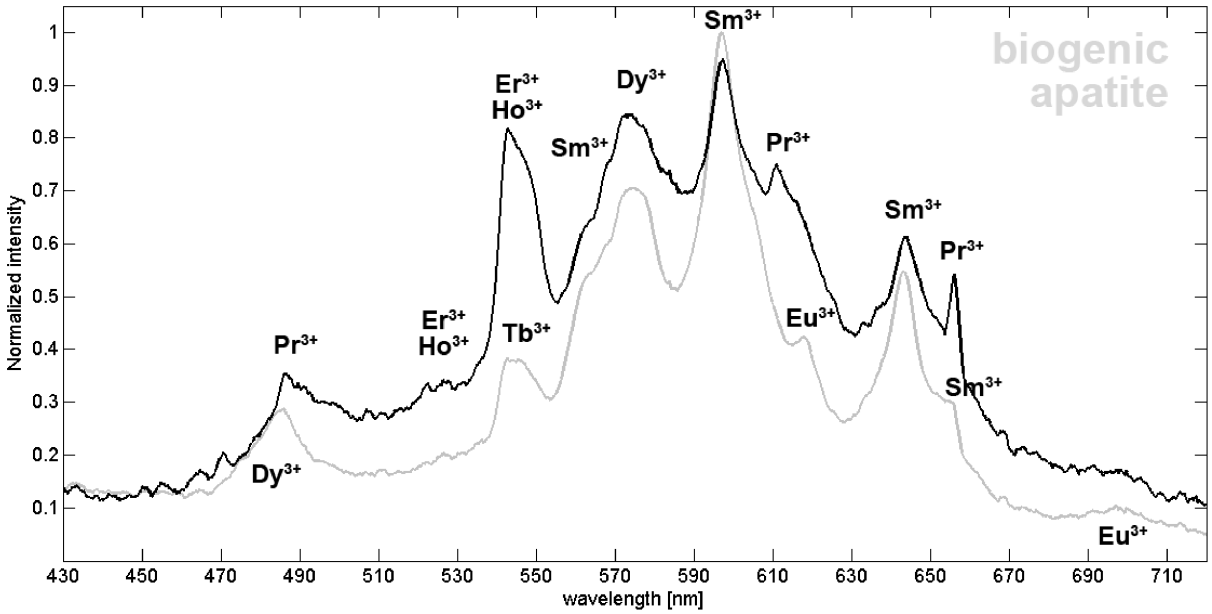

Fig. 21. Average cathodoluminescence spectra of apatites from samples of biogenic apatite (B1, B2) with characteristic emission bands of lanthanide activators.

which is sharper than that produced purely by Dy^{3+}.

In the case of spectra from fossil tooth it may seem that intensity of this band is unexpectedly high considering lower intensities of other Dy^{3+} and Pr^{3+} emission bands. This is given by the fact that the luminescence spectra are not interfered by the Mn-component and thus, intensities of bands in the central part of analysed wavelength range are not increased by the sum of the convolution with Mn^{2+} emission. Therefore, overall maximum intensities of biogenic apatites are generally considerably lower than those of igneous and metamorphic rocks. This implies that upon the normalization by lower values of maximum intensity, bands in the peripheral region that seem relatively smaller in rock samples will appear more prominent in biogenic samples as is the case illustrated in Fig. 21.

Another distinct emission band that occurs in these spectra is that at 540-555 *nm*. It may be induced from the preceding observations that this is the characteristic emission band of Tb^{3+}. On closer examination of its shape and by comparison with shapes and positions of Tb^{3+} bands reported above, however, it is shown that this is probably not the case. Highly asymmetric shape of this band in the shell samples showing maximum at around 542 *nm* indicates that this is an emission band of Er^{3+} and Ho^{3+}. These two activators produce very similar emission spectra and thus it is impossible to assess relative contribution of each of them based solely on the cathodoluminescence data. Indication of a faint emission band between 520 and 530 *nm* which is also characteristic for these activators further confirms assumption of their presence in studied samples.

Last type of emission bands that may be identified in bioapatites are those of Eu. These occur as a faint band at 615-625 *nm* along with a broad emission in the range 680-705 *nm* and belong to trivalent form

of this activator. In shell samples, band at 615-625 *nm* seems to be obscured by the presence of Pr^{3+} emission but can be distinguished as a broadening of right tail of this band. Absence of emission from Eu^{2+} at lower wavelengths corresponds with our assumption that Europium luminescence may reveal redox conditions that prevailed during the crystallization of apatite. In this case it would correctly indicate formation in an oxidizing environment.

5.2.2 Mn-dominated luminescence spectra of apatites

Cathodoluminescence spectra with the prevalence of Mn-component are characteristic for all analysed samples of granites, as well as paragneisses and additionally for one group of gabbros from locality Mařiž (MA2) as discussed above. Variability of spectra between these three types of rocks is very small as is apparent from Fig. 22 that shows average spectrum for each rock type. This is also reflected in the variability of centroids obtained by curve fitting - as discussed in section 4.2 - which is not specific for particular locality or rock type studied. Thus, it is not possible to perform preliminary dataset reduction based on these coefficients as in the case of carbonates where this step allowed substantial reduction in dataset size and therefore also in time necessary for the analysis.

Due to this low variability of original spectra we attempted to amplify variability of finer features contained in these spectra by the subtraction of fitted Gaussian curve and normalization as described in section 4.2. As was shown for the carbonate samples, residual spectra obtained in this way are more specific for each locality than the original spectra and thus provide more robust identification of the source area.

Residual data of apatite spectra obtained by identical algorithm, however, failed to produce satisfactory

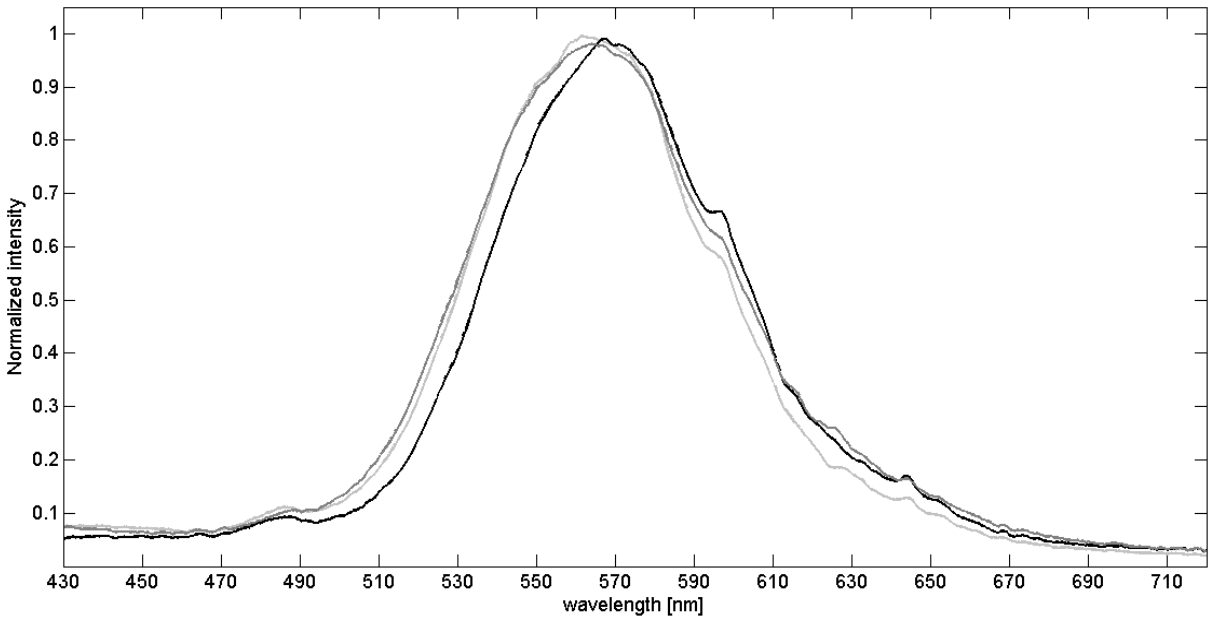

Fig. 22. Variability of average cathodoluminescence spectra of apatites from all samples of granite, gabbro, and paragneiss. Note low degree of variability between the different types of rocks.

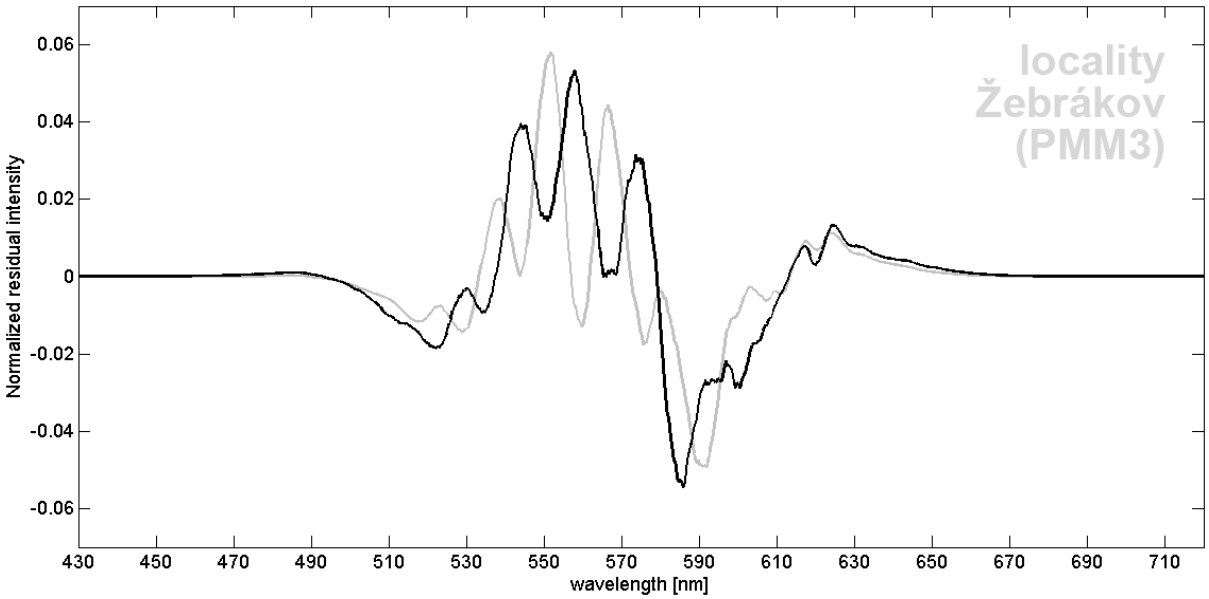

Fig. 23. Two residual spectra obtained from the same sample of paragneiss from locality Žebrákov (PMM3). Note high variability of relative intensities and positions of emission bands.

results. High variability of relative band intensities and their positions is observed even in spectra from the same sample. One of the extreme cases of this variability is illustrated in Fig. 23 on two spectra of paragneiss from the borehole in locality Žebrákov (PMM3) - it can be noted that intensities and positions of present emission bands show almost no correlation with each other. By analysing all of the obtained residual spectra we were able to identify continuous trend of change in intensities and positions of emission bands defined by four stages that will be described below. Fact that this trend is observed in all three rock types indicates that effects of crystallographic orientation that may have smaller effects on the high-intensity lanthanide-dominated spectra presented above are highly amplified in the low-intensity lanthanide bands obtained from Mn-dominated spectra. Individual stages of observed spectral variability are illustrated in Fig. 24 and are defined as follows:

- *stage 1* - band of Dy^{3+}at 570-585 *nm* is the most prominent and its other band at 460-500 *nm* is easily distinguishable. Band of Sm^{3+}at 555-570 is of lower intensity than that of $Dy^{3+}$and its other band at 593-602 *nm* is sharp and well defined. Additional bands of Sm^{3+}at 642-655 *nm* are distinguishable. Band of Tb^{3+}at 538-555 *nm* is of low intensity relative to other two bands in Tb^{3+}-Sm^{3+}-Dy^{3+} triplet. Troughs at 500-538 *nm* and 610-640 *nm* are the most prominent in this stage.
- *stage 2* - bands of Sm^{3+} and Dy^{3+} become less apparent, Dy^{3+} band at 460-500 *nm* is indistinguishable and relative intensities of Dy^{3+} and Sm^{3+} bands in triplet become more similar. Relative contribution of Tb^{3+} is increased and troughs become less pronounced.
- *stage 3* - intensity of Sm^{3+} band in the triplet overcomes that of Dy^{3+} band while at the same time intensity of other Sm^{3+} band at 593-602 *nm* decreases and bands at 642-655 *nm* become almost indistinguishable. Band of Tb^{3+} seems to be split into two bands at 538 and 551 *nm* and there is an

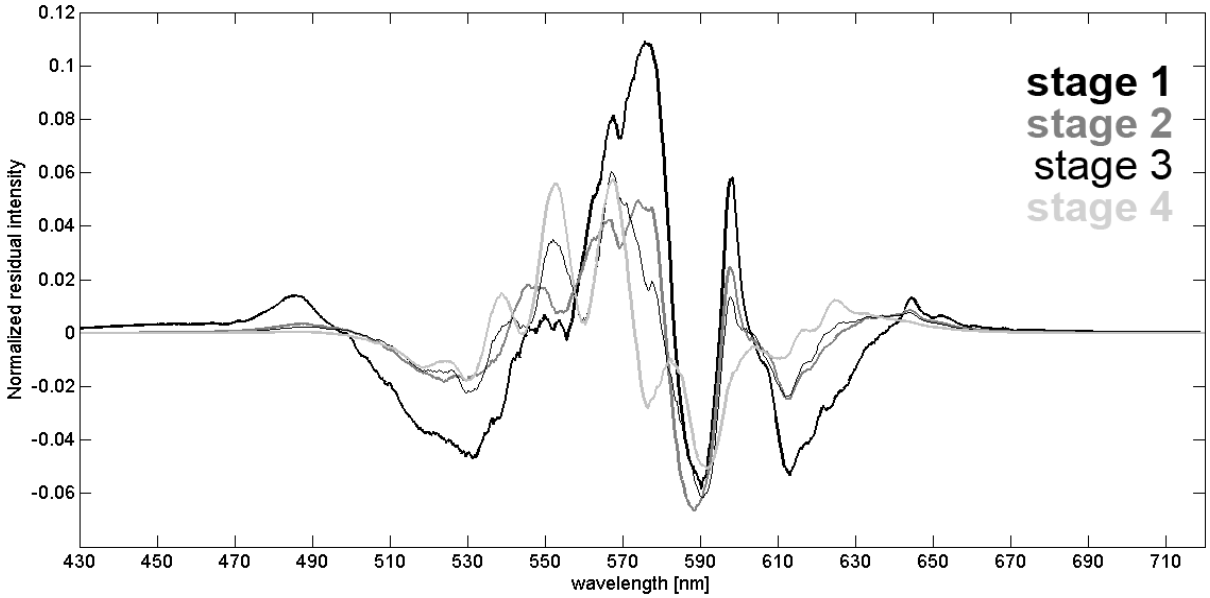

Fig. 24. Proposed trend of variability observed in residual spectra. For description of stages 1-4 see text.

indication of new additional bands at 518-526 *nm*, 616 *nm*, and 622-627 *nm*.

- *stage 4* - final stage is defined by the total loss of Dy^{3+} band at characteristic wavelengths 570-585 *nm* and appearance of low-intensity band in slightly shifted position at 575-585 *nm*. Sm^{3+} band at 555-570 *nm* is sharply defined while rest of its emission bands completely diminish. Intensity of bands produced by splitting of Tb^{3+} band in stage 3 and intensities of new bands appearing at 518-526 *nm*, 616 *nm*, and 622-627 *nm* continually increase.

As the crystallographic position of apatite crystals from which these spectra were obtained was not controlled and recorded during their collection, it is not possible to attribute each of these individual stages to some specific section of apatite crystals. However, it is important to note that this trend is similar to that observed in granulite samples in previous section and agrees with the observations of Murray and Oreskes (1997) whose results confirmed the following observations:

- Sm^{3+} bands are most prominent in sections that are perpendicular to crystallographic axis *c*.
- bands of Sm^{3+} are faint or absent in sections parallel to *c* axis and observed bands are smoother and steeper.

This means that trend from stage 1 to stage 4 could indicate variability of crystal orientation ranging from basal to prismatic sections. However, there is not a complete agreement of our data with those of Murray and Oreskes as in our spectra, band of Dy^{3+} at 570-580 *nm* is absent in stage 4 while these authors report its maximum intensity in the corresponding sections parallel to axis *c*.

Apart from the residual spectra described above we were able to identify two additional distinct groups of these spectra. These are illustrated in Fig. 25 and are reported separately because no gradual trend was found between them and the rest of the spectra in our current dataset.

First type shows troughs of similar prominence to those of stage 1 in Fig. 24 with the exception that in

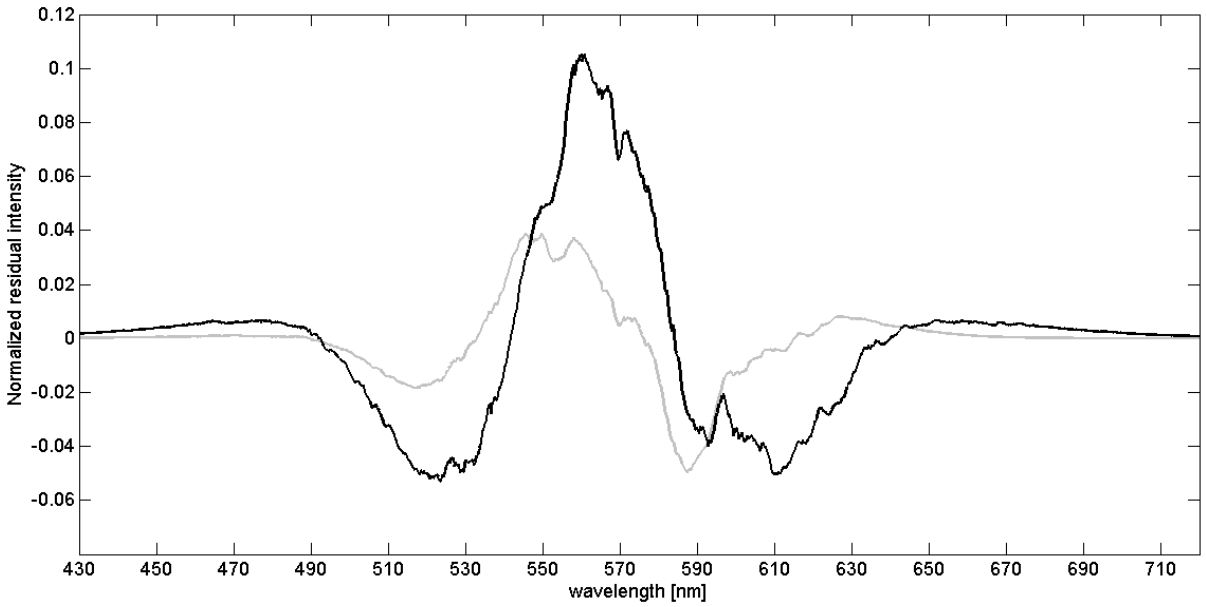

Fig. 25. Two additional types of residual spectra observed in the dataset. For description see text.

this case Sm^{3+} band is the most dominant in the triplet. This is contrasted by absence or very low intensities of its other bands. Whether this is an effect of crystallographic orientation or some other factors is inconclusive.

Second type of residual spectra is the most commonly observed in our dataset with approximately third of analysed spectra showing some variation of this type. It is characterized by triplet Tb^{3+}-Sm^{3+}-Dy^{3+} of lower intensities with variable relative proportions of these three bands, while all the other bands are usually very faint or completely absent. One of the spectra from locality Žebrákov (PMM3) illustrated in Fig. 23 presents extreme case of this type, while the other spectrum is representative of stage 4 in a trend described above. This could indicate that there is a connection between this type of spectra and those from the trend represented by stages 1 to 4. However, gradual change between this type and those of individual stages 1 to 4 was not observed in our current dataset.

6. DISCUSSION

6.1 Determination of provenance by analysis of carbonate spectra

Results of our provenance study based on the statistical analysis of cathodoluminescence spectra obtained from various carbonate samples demonstrate that when certain conditions are controlled during the collection of these spectra, it is possible to perform successful determination of provenance for samples they represent. However, there are many factors that must be considered in order to obtain satisfactory results of this analysis.

When collecting cathodoluminescence spectra of various samples that are meant to be compared with each other, it is important to perform this collection from the same structural features in all samples. This means that when spectra of one sample were collected e.g. from the fine-grained matrix between the larger crystals, spectra of all other samples for comparison should be also collected from the fine-grained matrices of these samples. Difficulties that may arise when this condition is not satisfied were demonstrated on spectra from locality Čertovy Schody (CS) where fine-grained matrix represents calcite-rich material, while large euhedral crystals enclosed in this matrix represent dolomite. Thus, spectra that were collected from the matrix cannot be matched with those from dolomite crystals even though they represent the same sample.

It should be noted that in some cases, even spectra of samples from different localities may be very similar due to the convergence of their chemical composition. This was demonstrated in our analysis where samples from localities Raspenava (174) and Čertovy Schody (CS) which are genetically unrelated provided very similar results that were distinguished only by analysis of their residual spectra.

Operational parameters during the data collection should be also considered as they influence final shape and intensities of cathodoluminescence spectra. Ideally, these should be kept constant during the acquisition of the whole dataset as in the case of carbonate spectra studied in this work. To further reduce possible effects of fluctuations or drift of system response it is advisable to analyse the whole dataset of possible matches for an unknown sample in a single session and perform regular subtraction of dark baseline in order to suppress contribution of noise. For our dataset, this was done before the measurement of each thin section and after acquisition of every four spectra. However, this is not always sufficient, especially when dealing with samples showing naturally low intensities of cathodo-luminescence emission. This was demonstrated on an example of samples from locality Bohdaneč (227) with very high noise-to-signal ratios that were reflected in the results of analysis as well as meta-analysis for both original and residual data. Even though in this case it was possible to determine correct provenance from the complete results of meta-analysis as presented in Appendix B, it is advisable to use longer acquisition times when collecting spectra from very faintly luminescing samples.

Further reduction of noise in cathodoluminescence spectra is possible by employing one of the smoothing methods such as that of recursive moving average used for our data. In this case it is important to select degree of smoothing in such a way that will suppress noise while preserving fine features in spectra that

carry the information allowing determination of their provenance. Moving average with the region of averaging 7 data points employed in this study seems to provide good results for our data with the resolution of 1 pixel - i.e. data point - per 0.27 *nm*. However, for data with lower or higher resolution, different region of averaging should be chosen.

As mentioned before, intensity of luminescence emission may greatly vary even among samples from the same locality. We have shown that when these are normalized to their maximum intensity, it is possible to match them against each other as their unique shape characteristics are mostly unaffected by the variations in intensity. Thus, it is recommended to perform all steps of analysis with normalized spectra.

When selecting dataset of possible matches for an unknown spectrum, it is advisable to choose fewer potential localities in order to minimize effects of *b* coefficient overlap in the database which may otherwise result in selection of unrepresentative dataset as discussed in section 5.1. Additionally, collection of spectra from smaller dataset may be performed in shorter sessions and thus, effects of fluctuation and drift of system response are reduced.

From the results of our analysis discussed in section 5.1 it is apparent that for various types of samples and datasets, different parts of analysis provide results of variable quality. For sample from locality Nedvědice (288), first part of analysis based on the original data is sufficient for correct identification of this sample and results from residual data and meta-analysis provide only additional confirmation of these results. For localities Lipová - Na Pomezí (234), Raspenava (174), and Čertovy Schody (CS), correct identification is possible only by employing second part of analysis based on the residual data. For locality Bohdaneč (227) which presented the most difficult case for identification, it was necessary to combine all the results including those from meta-analysis of both original and residual data. In this way, it was possible to exclude majority of possible matches with only two possibilities remaining which were distinguished as discussed in section 5.1.

Thus, it is not possible to assess which of the similarity measures should be included and which should not as performance of each of these will depend on the current dataset and sample being analysed. However, it should be noted that higher amount of employed similarity measures will generally provide more robust overall results of spectral analysis.

This applies also to meta-analysis of obtained results. As can be seen from Fig. 9 in section 4.1.4, divergence between the results of correct and incorrect localities will generally increase with the number of results combined in the analysis. While some of the employed methods may decrease overall value of correlation for the correct locality as can be seen in our results (Fig. 15), this decrease should be always connected with even higher relative decrease of values for incorrect localities. In this way, even if some of the methods show lower performance during the analysis, this will not have impact on the final results of meta-analysis if relative decrease for correct locality is lower than that for the rest of analysed dataset. Only methods that should be excluded from the analysis are those that provide contradictory results which may be tested on a selected dataset prior to analysis of an unknown sample.

When employing hierarchical clustering of spectroscopic data it must be kept in mind what is the purpose of this clustering. Classification of spectra based on their provenance is not analogous to classification based on the smallest differences of values between these spectra. For cases such as those of carbonate spectra where variability between the original data is extremely low, some spectra of unrelated samples may exhibit smaller differences than spectra of samples that belong to the same locality. This is confirmed by the results of hierarchical clustering evaluated in section 5.1 where best results were obtained from cluster trees showing the lowest values of cophenetic correlation coefficients. Thus, it is appropriate to always evaluate percentage of correctly classified spectra from the selected dataset when number of clusters is equal to number of localities included in this dataset.

6.2 Determination of provenance by analysis of apatite spectra

Results provided by the spectroscopic data of apatites studied in this work reveal some of the characteristic features of apatite cathodoluminescence in different types of rocks and indicate what precautions should be taken when employing these data as a tool for determination of provenance.

Mn-dominated cathodoluminescence spectra that are characteristic for all studied samples of granites, paragneiss, and one group of gabbros show shapes very similar to those of carbonate samples. When these are fitted with Gaussian curves , there is a great degree of overlap of centroid values between the individual localities, as well as rock types. This presents great difficulty for methods of dataset reduction as successfully employed for carbonate samples. However, even if it would be possible to perform dataset reduction for differently chosen dataset with lower degree of centroid overlap, evaluation of spectral similarity would be impossible due to effects of crystallographic orientation of analysed apatites. While no effect of this orientation on the final shape of spectra was observed in samples of carbonates, it appears to be greatly pronounced in apatites. This is given by the fact that crystal structure of studied carbonates is much simpler than that of apatites. This means that carbonates show smaller difference in physico-chemical properties in different crystallographic directions as compared with apatites. As discussed in section 4.2, more complex structures of apatites show preferential diffusion of activators along the *c*-axis and different sections of crystal reveal variable type of local crystal field and charge distribution. This results in variations of intensity and shape of cathodoluminescence spectra.

These effects were clearly observed in amplified variability of residual data obtained from the Mn-activated spectra of apatites. Gradual change of relative intensities and even positions of observed emission bands as a function of crystallographic orientation demonstrates that for successful application of cathodoluminescence spectroscopy of apatites for provenance studies, it is crucial to strictly control orientation of crystals in order to maintain identical geometry for all measurements. Without this precaution, it is impossible to match even spectra from the same sample as demonstrated on paragneiss from locality Žebrákov (PMM3) in Fig. 23. While trend of variability observed in our samples shows many similarities to those reported by previous workers, there exists only a small body of works concerned with this issue and in many cases it is completely overlooked. Therefore, future research

should attempt to examine this phenomenon more closely and assess what are the physico-chemical principles inducing variations observed in cathodoluminescence spectra.

For samples with lanthanide-dominated luminescence - i.e. durbachites, one group of gabbros, rhyolite, quartzite, granulite, and biogenic materials - effect of variable crystallographic orientation seems to be less pronounced, particularly because in this case we do not work with residual spectra. Variability similar to that characteristic for Mn-dominated spectra was observed for granulites (PL1). This may indicate that in some cases, effect of crystallographic orientation can be pronounced even in lanthanide-dominated spectra. In this case, however, one end-member of trend observed in granulites shows emission bands of Eu^{2+} and Eu^{3+} that are not present in the other end-member and this points towards the scenario of chemical variability. It is inconclusive whether this chemical variability is given by the variability of apatite population in this rock as a result of fractional crystallization as described in section 5.2 or whether it is an effect of preferential diffusion of activators in particular crystallographic directions in apatite crystals.

Chemical variability of analysed samples must be considered during the collection of spectra in a same way as described for carbonate samples. Effect of variable composition on resulting cathodo-luminescence emission was demonstrated on samples of gabbro from Mařiž (MA1, MA2) that forms layered cummulates with zones enriched in olivine with pyroxene and zones enriched in feldspar. This is reflected in the two types of obtained spectra - Mn-dominated for more acidic portions of rock (MA2) and lanthanide-dominated for more basic layers (MA1). Thus, it is evident that it would be impossible to match these two types of spectra against each other even though they represent the same sample.

Apart from chemical variability within the rock and that along certain crystallographic axes within the crystal, additional effect of chemical variability in apatites is given by their commonly observed zoning. Therefore, even after identification of appropriate portion of rock for analysis and identification of suitable apatite sections in this selected part of the rock, it is crucial to obtain cathodoluminescence spectra from the same zone of analysed apatites - which should be shared by the majority of crystals in a homogeneous population - in order to suppress any effects of chemical variability induced during the growth and later alterations.

Sometimes, however, observed variations in relative intensities of lanthanide emission bands do not reflect variability in concentrations of these elements but are produced as an artifact of normalization due to variable contribution from Mn-component. This was demonstrated on example of durbachites (DU1, DU2) where intensities of bands in the middle of studied range are strongly controlled by their convolution with underlaying emission band of Mn^{2+}, while bands in the marginal regions are mostly unaffected by this band. Thus, it is possible to observe strong correlation in trends of intensities for emission bands of different activators in this strongly interfered region, while two emission bands of the same activator - where one is in the interfered central region and the other in the marginal region - show much lower correlation of their relative intensities. Therefore, contribution of Mn-component should be always assessed prior to comparison of relative intensities between emission bands of lanthanide

activators.

Some of the variability in contributions of individual lanthanide activators in different rock types as described in section 5.2 may be attributed to physico-chemical conditions that prevailed during the crystallization and subsequent alteration of apatites in these rocks. Site preference of lanthanide activators between the two different Ca-sites in the structure of apatites is hard to evaluate as it is a result of complicated interplay between P-T conditions of crystallization or alteration (controlling the shapes and sizes of coordination polyhedra), type of prevalent column anion present in the structure (affecting the size of Ca2-site), and concentrations of other cations competing with lanthanides for these crystallographic positions.

One of the observed emission bands - that of Eu^{2+} - seems to be a good indicator of redox conditions during the crystallization and alteration. Highest intensities of this emission band are observed in samples of durbachites (DU1, DU2), lower in gabbros (MA1), and its contribution is apparent in some spectra of granulites (PL1). On the other hand, this band is completely absent in spectra of rhyolite and biogenic apatites, even though the latter contain apparent emission bands of Eu^{3+}. These results may indicate that greater prominence of Eu^{2+} emission band could be linked to more reducing conditions of crystallization.

Metasedimentary rocks seem to present a difficult group for provenance studies based on the luminescence of apatites due to the fact that their sedimentary protoliths may contain apatite populations from different source areas with possibly unrelated rock types and thus variable chemistry. Therefore, determination of provenance by cathodoluminescence of apatites from metasedimentary rocks will be possible only in cases where apatites form only one homogeneous population in protoliths containing material from a single source area or more source areas with very close chemistry.

Apatites of biogenic origin - bones and teeth of animals - present group of cathodoluminescence spectra very different from those of all studied rock types. As in the carbonates, biogenic origin of these apatites can be distinguished by unusually low contribution of Mn-component of luminescence, i.e. low concentrations of Mn in their structure which is characteristic for many biominerals. Absence of Mn^{2+} is connected with the higher concentrations of some lanthanide activators not observed in rock samples. These include Pr^{3+}, Er^{3+}, and Ho^{3+} which interfere some of the emission bands of activators typical for rock samples. Their contribution to these emission bands may be assessed from the different shapes of resulting interfered bands as described in section 5.2.1.

7. CONCLUSIONS

This work demonstrated that determination of geological provenance by cathodoluminescence spectroscopy is possible when operational parameters during the collection of spectral data are closely controlled. Spectra obtained from the carbonate samples show low degree of variability between the five studied localities. Therefore, it is necessary to amplify this variability by the subtraction of Gaussian trend characteristic for all carbonate samples. Residual spectra produced by this subtraction are then analysed - along with the original spectra - by the combination of statistical methods that evaluate similarity of spectra. In this way, analysed sample of an unknown provenance is matched against the spectroscopic data of selected localities in the database and result for each possible match is given by the average correlation coefficient obtained from seven different statistical methods. This provides more robust results than individual measures of similarity. By the combination of results from original and residual spectra it is possible to identify correct provenance even for samples where data from the original spectra are incapable to provide unambiguous identification on their own.

Additionally, employed method combining seven different similarity measures allows us to perform meta-analysis of results along the individual steps of analysis. Meta-analysis produces results that are not based on the original spectroscopic data but rather on the behaviour of these data during their analysis. These results provide additional information that is not present in the original spectroscopic data but is generated in the course of the analysis and thus allow still better identification of correct provenance.

The same method applied to Mn-dominated spectra of apatites - observed in all samples of granites and paragneiss - with shapes very similar to those of carbonates fails to provide correct results due to the effect of variable crystallographic orientation that produces high variability of residual spectra even in apatites from the same sample.

Second group of apatite spectra where Gaussian trend of Mn^{2+} component is concealed by sharp emission bands of lanthanide activators was observed in samples of durbachite, gabbro, rhyolite, quartzite, granulite, and biogenic apatites. Presence of various activators was assessed for spectra of different rock types along with the definition of trends observed in these spectra that may reveal certain physico-chemical conditions that prevailed during the crystallization and subsequent alteration of apatites in these samples.

References

Akridge, D. G., & Benoit, P. H. (2001). Luminescence properties of chert and some archaeological applications. *Journal of Archaeological Science*, 28(2), 143-151.

Augustsson, C., & Bahlburg, H. (2003). Cathodoluminescence spectra of detrital quartz as provenance indicators for Paleozoic metasediments in southern Andean Patagonia. *Journal of South American Earth Sciences*, 16(1), 15-26.

Augustsson, C., & Reker, A. (2012). Cathodolumenescence spectra of quartz as provenance indicators revisited. *Journal of Sedimentary Research*, 82(8), 559-570.

Bajnóczi, B., Schöll-Barna, G., Kalicz, N., Siklósi, Z., Hourmouziadis, G. H., Ifantidis, F., Kyparissi-Apostolika, A., Pappa, M., Veropoulidou, R., & Ziota, C. (2013). Tracing the source of Late Neolithic *Spondylus* shell ornaments by stable isotope geochemistry and cathodoluminescence microscopy. *Journal of Archaeological Science*, 40(2), 874-882.

Barbarand, J., & Pagel, M. (2001). Cathodoluminescence study of apatite crystals. *American Mineralogist*, 86(4), 473-484.

Bell, S. C., Nawrocki, H. D., & Morris, K. B. (2009). Forensic discrimination of glass using cathodoluminescence and CIE LAB color coordinates: a feasibility study. *Forensic Science International*, 189(1), 93-99.

Bernet, M., & Bassett, K. (2005). Provenance analysis by single-quartz-grain SEM-CL/optical microscopy. *Journal of Sedimentary Research*, 75(3), 492-500.

Boggs, S., Kwon, Y. I., Goles, G. G., Rusk, B. G., Krinsley, D., & Seyedolali, A. (2002). Is quartz cathodoluminescence color a reliable provenance tool? A quantitative examination. *Journal of Sedimentary Research*, 72(3), 408-415.

Boggs, S., & Krinsley, D. (2006). Application of cathodoluminescence imaging to the study of sedimentary rocks. *Cambridge University Press*, 176 pp.

Breiter, K., Novák, J. K., & Chlupáčová, M. (2001). Chemical evolution of volcanic rocks in the Altenberg-Teplice Caldera (Eastern Krušné hory Mts., Czech Republic, Germany). *Geolines*, 13, 17-22.

Burns, R. G. (1993). Mineralogical applications of crystal field theory, second ed. (Vol. 5). *Cambridge University Press*, 551 pp.

Cazenave, S., Chapoulie, R., & Villeneuve, G. (2003). Cathodoluminescence of synthetic and natural calcite: the effects of manganese and iron on orange emission. *Mineralogy and Petrology*, 78(3-4), 243-253.

Czaja, M. B., Bodyl-Gajowska, S., & Mazurak, Z. (2013). Steady-state luminescence measurement for qualitative identification of rare earth ions in minerals. *Journal of Mineralogical and Petrological Sciences*, 108(2), 47-54.

Dempster, T. J., Jolivet, M., Tubrett, M. N., & Braithwaite, C. J. R. (2003). Magmatic zoning in apatite: a monitor of porosity and permeability change in granites. *Contributions to Mineralogy and Petrology*,

145(5), 568-577.

Ebert, A., Gnos, E., Ramseyer, K., Spandler, C., Fleitmann, D., Bitzios, D., & Decrouez, D. (2010). Provenance of marbles from Naxos based on microstructural and geochemical characterization. *Archaeometry*, 52(2), 209-228.

Edwards, P. R., Jagadamma, L. K., Bruckbauer, J., Liu, C., Shields, P., Allsopp, D., Wang, T., & Martin, R. W. (2012). High-resolution cathodoluminescence hyperspectral imaging of nitride nanostructures. *Microscopy and Microanalysis*, 18(06), 1212-1219.

Elliott, J. C., Wilson, R. M., & Dowker, S. E. P. (2002). Apatite structures. *Advances in X-ray Analysis*, 45, 172-181.

England, J., Cusack, M., Paterson, N. W., Edwards, P., Lee, M. R., & Martin, R. (2006). Hyperspectral cathodoluminescence imaging of modern and fossil carbonate shells. *Journal of Geophysical Research: Biogeosciences*, 111(G03001), 1-8.

Fleet, M. E., & Pan, Y. (1997a). Rare earth elements in apatite: uptake from H_2O-bearing phosphate-fluoride melts and the role of volatile components. *Geochimica et Cosmochimica Acta*, 61(22), 4745-4760.

Fleet, M. E., & Pan, Y. (1997b). Site preference of rare earth elements in fluorapatite: Binary (LREE+ HREE)-substituted crystals. *American Mineralogist*, 82(9), 870-877.

Gaft, M., Reisfeld, R., Panczer, G., Blank, P., & Boulon, G. (1998). Laser-induced time-resolved luminescence of minerals. *Spectrochimica Acta Part A: Molecular and Biomolecular Spectroscopy*, 54(13), 2163-2175.

Gaft, M., Reisfeld, R., & Panczer, G. (2005). Modern luminescence spectroscopy of minerals and materials. *Springer*, 356 pp.

Gillhaus, A., Richter, D. K., Meijer, J., Neuser, R. D., & Stephan, A. (2001). Quantitative high resolution cathodoluminescence spectroscopy of diagenetic and hydrothermal dolomites. *Sedimentary Geology*, 140(3), 191-199.

Götte, T., & Richter, D. K. (2006). Cathodoluminescence characterization of quartz particles in mature arenites. *Sedimentology*, 53(6), 1347-1359.

Götte, T., & Richter, D. K. (2009). Quantitative aspects of Mn-activated cathodoluminescence of natural and synthetic aragonite. *Sedimentology*, 56(2), 483-492.

Götze, J., Heimann, R. B., Hildebrandt, H., & Gburek, U. (2001). Microstructural investigation into calcium phosphate biomaterials by spatially resolved cathodoluminescence. *Materialwissenschaft und Werkstofftechnik*, 32(2), 130-136.

Götze, J., Plötze, M., & Trautmann, T. (2005). Structure and luminescence characteristics of quartz from pegmatites. *American Mineralogist*, 90(1), 13-21.

Götze, J., & Kempe, U. (2008). A comparison of optical microscope-and scanning electron microscope-based cathodoluminescence (CL) imaging and spectroscopy applied to geosciences. *Mineralogical Magazine*, 72(4), 909-924.

Götze, J., & Kempe, U. (2009). Physical principles of cathodoluminescence (CL) and its applications in geosciences. In: Gucsik, A. (Ed.) *Cathodoluminescence and its Application in the Planetary Sciences*. Springer Berlin, pp. 1-22.

Götze, J. (2012). Application of cathodoluminescence microscopy and spectroscopy in geosciences. *Microscopy and Microanalysis*, 18(06), 1270-1284.

Habermann, D., Neuser, R. D., & Richter, D. K. (1998). Low limit of Mn^{2+}-activated cathodoluminescence of calcite: state of the art. *Sedimentary Geology*, 116(1), 13-24.

Habermann, D., Neuser, R. D., & Richter, D. K. (2000). Quantitative high resolution spectral analysis of Mn^{2+} in sedimentary calcite. In: Pagel, M., Barbin, V., Blanc, P., & Ohnenstetter, D. (Eds.) *Cathodoluminescence in Geosciences.* Springer Berlin, pp. 331-358.

Habermann, D. (2002). Quantitative cathodoluminescence (CL) spectroscopy of minerals: possibilities and limitations. *Mineralogy and Petrology*, 76(3-4), 247-259.

Harlov, D. E., Procházka, V., Förster, H. J., & Matějka, D. (2008). Origin of monazite–xenotime–zircon–fluorapatite assemblages in the peraluminous Melechov granite massif, Czech Republic. *Mineralogy and Petrology*, 94(1-2), 9-26.

Holub, F. V. (1997). Ultrapotassic plutonic rocks of the durbachite series in the Bohemian Massif: petrology, geochemistry and petrogenetic interpretation. *Sborník Geologických Věd*, 31, 5-26.

Houzar, S., Litochleb, J., Sejkora, J., Cempírek, J., & Cícha, J. (2008). Unusual mineralization with niobian titanite and Bi-tellurides in scheelite skarn from Kamenné doly quarry near Písek, Moldanubian Zone, Bohemian Massif. *Journal of Geosciences*, 53(1), 1-16.

Hughes, J. M., & Rakovan, J. (2002). The crystal structure of apatite, $Ca_5(PO_4)_3(F, OH, Cl)$. *Reviews in Mineralogy and Geochemistry*, 48(1), 1-12.

Hunt, A. M. (2013). Development of quartz cathodoluminescence for the geological grouping of archaeological ceramics: firing effects and data analysis. *Journal of Archaeological Science*, 40(7), 2902-2912.

Janoušek, V., Bowes, D. R., Rogers, G., Farrow, C. M., & Jelínek, E. (2000). Modelling diverse processes in the petrogenesis of a composite batholith: the Central Bohemian Pluton, Central European Hercynides. *Journal of Petrology*, 41(4), 511-543.

Janoušek, V., Krenn, E., Finger, F., Míková, J., & Frýda, J. (2007). Hyperpotassic granulites from Blanský les (Moldanubian Zone, Bohemian Massif) revisited. *Journal of Geosciences*, 52(1-2), 73-112.

Julig, P. J., Long, D. G. F., & Hancock, R. G. V. (1998). Cathodoluminescence and petrographic techniques for positive identification of quartz-rich artifacts from Late Paleo-Indian sites in the Great Lakes Region. *Wisconsin Archeologist*, 19(1), 68-88.

Kempe, U., & Götze, J. (2002). Cathodoluminescence (CL) behaviour and crystal chemistry of apatite from rare-metal deposits. *Mineralogical Magazine*, 66(1), 151-172.

Lapuente, M. P., Turi, B., & Blanc, P. (2000). Marbles from Roman Hispania: stable isotope and cathodoluminescence characterization. *Applied Geochemistry*, 15(10), 1469-1493.

Lapuente, P., Nogales-Basarrate, T., Royo, H., & Brilli, M. (2014). White marble sculptures from the National Museum of Roman Art (Mérida, Spain): sources of local and imported marbles. *European Journal of Mineralogy*, 26(2), 333-354.

Lenz, C., Talla, D., Ruschel, K., Škoda, R., Götze, J., & Nasdala, L. (2013). Factors affecting the Nd^{3+} (REE^{3+}) luminescence of minerals. *Mineralogy and Petrology*, 107(3), 415-428.

Lisitsyn, V. M., Polisadova, E. F., & Valiev, D. T. (2012). Pulsed cathodoluminescence of calcite crystals of various origins. *Inorganic Materials*, 48(7), 738-744.

MacRae, C. M., Wilson, N. C., & Torpy, A. (2013). Hyperspectral cathodoluminescence. *Mineralogy and Petrology*, 107(3), 429-440.

Mariano, A. N., & King, P. J. (1975). Europium-activated cathodoluminescence in minerals. *Geochimica et Cosmochimica Acta*, 39(5), 649-660.

Marshall, D. J., & Mariano, A. N. (1988). Cathodoluminescence of geological materials. *Unwyn Hyman, Boston,* 146 pp.

Mason, R., Clouter, M., & Goulding, R. (2005). The luminescence decay-time of Mn^{2+} activated calcite. *Physics and Chemistry of Minerals*, 32(7), 451-459.

Matějka, D., & Janoušek, V. (1998). Whole-rock geochemistry and petrogenesis of granites from the northern part of the Moldanubian Batholith (Czech Republic). *Acta Universitatis Carolinae: Geologica*, 42, 73-79.

Mitchell, R.H., Xiong, J., Mariano, A.N. and Fleet, M.E. (1997). Rare-earth-element-activated cathodoluminescence in apatite. *Canadian Mineralogist*, 35, 979–998.

Mlčoch, B., & Skácelová, Z. (2010). Geometry of the Altenberg-Teplice Caldera revealed by the borehole and seismic data in its Czech part. *Journal of Geosciences*, 55(3), 217-229.

Murray, J. R., & Oreskes, N. (1997). Uses and limitations of cathodoluminescence in the study of apatite paragenesis. *Economic Geology*, 92(3), 368-376.

Noda, I., & Ozaki, Y. (2005). Two-dimensional correlation spectroscopy: applications in vibrational and optical spectroscopy. *John Wiley & Sons*, 310 pp.

Palenik, C. S., & Buscaglia, J. (2007). Applications of cathodoluminescence in forensic science. In: Blackledge, R. D. (Ed.) *Forensic Analysis on the Cutting Edge: New Methods for Trace Evidence Analysis*, John Wiley & Sons, pp. 141-173.

Perseil, E. A., Blanc, P., & Ohnenstetter, D. (2000). As-bearing fluorapatite in manganiferous deposits from St. Marcel–Praborna, Val d'Aosta, Italy. *The Canadian Mineralogist*, 38(1), 101-117.

Picouet, P., Maggetti, M., Piponnier, D., & Schvoerer, M. (1999). Cathodoluminescence spectroscopy of quartz grains as a tool for ceramic provenance. *Journal of Archaeological Science*, 26(8), 943-949.

Polikreti, K., & Maniatis, Y. (2002). A new methodology for the provenance of marble based on EPR spectroscopy. *Archaeometry*, 44(1), 1-21.

Portnov, A. M., & Gorobets, B. S. (1969). Luminescence of apatite from different rock types. *Doklady Akademii Nauk SSSR*, 184, 110-13.

Procházka, V., & Matějka, D. (2006). Rock-forming Accessory Minerals in the Granites of the Melechov Massif (Moldanubian Batholith, Bohemian Massif). *Acta Universitatis Carolinae: Geologica*, 48, 71-79.

Procházka, V. (2010a). Phosphates and accessory oxides in selected granitoids and paragneisses of the Moldanubian area in southeastern and southern Bohemia. *MS PhD thesis, Institute of Geochemistry, Mineralogy and Mineral Resources, Faculty of Science, Charles University, Prague*, 87 pp.

Procházka, V., Chlupáčová, M., Nižňanský, D., Hrouda, F., Uher, P., & Rajlich, P. (2010b). Magnetomineralogy of the cordierite gneiss from the magnetic anomaly at Humpolec, Bohemian Moldanubicum (Czech Republic). *Studia Geophysica et Geodaetica*, 54(1), 95-120.

Procházka, V., Seydoux-Guillaume, A. M., Trojek, T., Goliáš, V., Korbelová, Z., Matějka, D., & Novotná, P. (2011). Alteration halos around radioactive minerals in plutonic and metamorphic rocks of the northern Moldanubian area, Bohemian massif. *European Journal of Mineralogy*, 23(4), 551-566.

Putnis, A. (1992). An introduction to mineral sciences. *Cambridge University Press*, 480 pp.

Reed, S. J. B. (2005). Electron microprobe analysis and scanning electron microscopy in geology. *Cambridge University Press*, 232 pp.

Richter, D. K., Götte, T., Götze, J., & Neuser, R. D. (2003). Progress in application of cathodoluminescence (CL) in sedimentary petrology. *Mineralogy and Petrology*, 79(3-4), 127-166.

Roeder, P. L., MacArthur, D., Ma, X. P., Palmer, G. R., & Mariano, A. N. (1987). Cathodoluminescence and microprobe study of rare-earth elements in apatite. *American Mineralogist*, 72(7-8), 801-811.

Sippel, R. F. (1965). Simple device for luminescence petrography. *Review of Scientific Instruments*, 36(11), 1556-1558.

Šašić, S., Muszynski, A., & Ozaki, Y. (2000). A new possibility of the generalized two-dimensional correlation spectroscopy. 1. Sample-sample correlation spectroscopy. *The Journal of Physical Chemistry A*, 104(27), 6380-6387.

Šašić, S., & Ozaki, Y. (2001). Statistical two-dimensional correlation spectroscopy: Its theory and applications to sets of vibrational spectra. *Analytical Chemistry*, 73(10), 2294-2301.

Šťastná, A., & Přikryl, R. (2009). Decorative marbles from the Krkonoše-Jizera Terrane (Bohemian Massif, Czech Republic): provenance criteria. *International Journal of Earth Sciences*, 98(2), 357-366.

Šťastná, A., Přikryl, R., & Jehlička, J. (2009). Methodology of analytical study for provenance determination of calcitic, calcite-dolomitic and impure marbles from historical quarries in the Czech Republic. *Journal of Cultural Heritage*, 10, 82-93.

Šťastná, A., & Přikryl, R. (2010). Determination of source areas of natural stones: a methodology approach applied to impure crystalline limestones. In: Bostenaru Dan M., Přikryl, R., Török, Á. (Eds.) *Materials, Technologies and Practice in Historic Heritage Structures*. Springer, Berlin, pp. 157-175.

Šťastná, A., Přikryl, R., & Černíková, A. (2011). Comparison of quantitative petrographic, stable isotope and cathodoluminescence data for fingerprinting Czech marbles. *Environmental Earth Sciences*, 63(7-8), 1651-1663.

Šťastná, A., Šachlová, Š., Pertold, Z., & Přikryl, R. (2014). Factors affecting alkali-reactivity of quartz-rich metamorphic rocks: qualitative vs. quantitative microscopy. *Engineering Geology*, 187, 1-9.

Štemprok, M., Holub, F. V., & Novák, J. K. (2003). Multiple magmatic pulses of the Eastern Volcano-Plutonic Complex, Krušné hory/Erzgebirge batholith, and their phosphorus contents. *Bulletin of Geosciences*, 78(3), 277-296.

Ulrych, J., Ackerman, L., Kachlík, V., Hegner, E., Balogh, K., Langrová, A., Luna, J., Fediuk, F., Lang, M., & Filip, J. (2010). Constraints on the origin of gabbroic rocks from the Moldanubian-Moravian units boundary (Bohemian Massif, Czech Republic and Austria). *Geologica Carpathica*, 61(3), 175-191.

Walderhaug, O., & Rykkje, J. (2000). Some examples of the effect of crystallographic orientation on the cathodoluminescence colors of quartz. *Journal of Sedimentary Research*, 70(3), 545-548.

Waychunas, G. A. (2002). Apatite luminescence. *Reviews in Mineralogy and Geochemistry*, 48(1), 701-742.

Waychunas, G. A. (2014). Luminescence Spectroscopy. *Reviews in Mineralogy and Geochemistry*, 78(1), 175-217.